BUDAPEST UNIVERSITY OF TECHNOLOGY AND ECONOMICS
DEPT. OF TELECOMMUNICATIONS AND TELEMATICS

# NEW RESULTS IN MULTIFRACTAL TRAFFIC ANALYSIS AND MODELING

Trang Dinh Dang

Ph.D. Dissertation

Supervised by

Dr. Sándor Molnár
High Speed Networks Laboratory
Dept. of Telecommunications and Telematics
Budapest University of Technology and Economics

Budapest, Hungary
2002

---

[1]The reviews and the minutes of the Ph.D. Defense are available from the Dean's Office.

*To my family*

# Table of Contents

# List of Tables

# List of Figures

x

# Abstract

An alternative but very promising approach of traffic modeling is the use of fractal characterization to describe the high variability and bursty nature of network traffic. The aim of this dissertation is to contribute to this research approach, more precisely, to solve some problems in statistical testing, traffic characterization, modeling, and performance evaluation. First, the implications of non-stationarity on long-range dependence tests are presented. Next, the effects of traffic components in the aggregation are investigated in a comprehensive characterization study. In addition, an investigation of multifractal queuing performance is presented. Finally, a new traffic model is proposed which is able to capture the complete multifractal characteristics of network traffic.

# Acknowledgements

Dr. Sándor Molnár has been my research advisor from my university years. First of all I would like express to my deepest gratitude for his kind encouraging guidance and support. Without his help this dissertation would have never been established.

All my research work has been done in the framework of teletraffic research at High Speed Networks Laboratory (HsnLab), Dept. of Telecommunications and Telematics, Budapest University of Technology and Economics (DTT/BUTE). I would like to thank Dr. Tamás Henk, head of the laboratory, for his support. I also wish to acknowledge the help that I received from those people at DTT/BUTE during the years. It was my pleasure working together with them.

My special thanks are due to Dr. Attila Vidács and István Maricza for their helpfulness and fruitful advice contributing to my research work. I owe them a dept of gratitude.

Last but not at least, I am very thankful to my family for the stable background and the inspiration they have provided for me to begin and more importantly to accomplish this research work.

Budapest,                                                                                    Trang Dinh Dang
December 2002

# Introduction

In the last decade a number of teletraffic research papers have reported the high variability and bursty nature of LAN/WAN traffic in a wide range of network environments [57, 51, 46, 19, 18, 22, 45, 47, 39]. From the modeling point of view this phenomenon is difficult to characterize by the well-known Markovian models. An alternative but not very well elaborated type of modeling approach is to use the notion of fractals to characterize the complex "burst within burst" traffic structure. This is in close relationship to traffic burstiness because bursts should be defined in terms of time scales over which clustering activities occur. The surprising scaling phenomenon observed in data traffic is that these clustering activities are present over several time scales [57].

Fractal traffic modeling introduced the notion of long-range dependence (LRD), self-similarity, and recently multifractals to teletraffic theory. Historically first long-range dependence and self-similarity were detected in the statistical analysis of a large number of traffic traces and a group of studies is concentrated on the detection of these properties and their engineering impacts in network performance and operation. However, it was also discovered that LAN/WAN traffic reveals a highly irregular local structure with a more complex scaling behavior which cannot be explained in a self-similar framework [51, 19, 18]. Therefore multifractal traffic models with much more flexible scaling laws seem to be needed, especially for some WAN environments [46, 18, 47].

Since understanding traffic behavior and characteristics is very important in network dimensioning and performance prediction there is a basic need for a comprehensive and detailed study of fractal traffic theory. Although many significant results have been obtained in a number of approaches published in this field, there are still many open questions to be answered. The objective of this work is to contribute to this research approach, more precisely, to solve some problems in statistical testing, traffic characterization, modeling, and performance evaluation.

An important practical issue is the identification of LRD phenomena and the estimation of LRD parameters, especially the estimation of the Hurst parameter. Unfortunately, testing of measured data for LRD is not possible by simply checking the definitions. Instead, we can use some methods for testing the presence of some characteristics of the data which can or cannot support the LRD property and also can or cannot give a reliable estimate of the Hurst parameter. Moreover, if all methods support the assumption of the presence of LRD with some parameter $H$ it is still possible that this observation is caused by non-stationarities present in the data and is not due to LRD (since LRD is only defined for

stationary processes). In this case it is possible to end up with wrong conclusions and build wrong models. Therefore it is of interest to reveal the implications of the most important non-stationarity effects, which often occur in practice in the most frequently used LRD tests. This could support teletraffic engineers with guidelines so as not to mistake actual non-stationarities for stationary fractal behavior.

Scaling and multiscaling phenomena are often observed in WAN environments, especially in characterization studies of IP traffic. However, a few papers have examined the nature of IP traffic components. We know that understanding the characteristics of the individual components in the aggregation, i.e., a comprehensive analysis of different protocol layers with distinct traffic components is vital for establishing a correct physical understanding and modeling methodology. Such a study may give a deeper look into the nature of this typical WAN traffic and it can also show how components influence the aggregated traffic.

From a practical point of view queuing analysis of fractal traffic is a very important issue for network dimensioning and management. Therefore the study of queuing systems with fractal traffic input is a challenge in queuing theory. Recent traffic research has deeply analyzed the performance of queues with LRD or self-similar input [57, 53, 23, 35]. A collection of studies has proven that the fractional Brownian motion (fBm) based models have a tail queue distribution that decays asymptotically like a Weibullian law. However, there is a lack of queuing results available in the cases when the input traffic has a more complex scaling behavior. Especially, queuing systems with multifractal input are an undiscovered field with only a few results published in the literature [45]. An analytical study of multifractal queues is necessary for further applications of multifractal models. It is also of particular interest how the impact of multifractal traffic differs from the monofractal case. A simple and effective estimation method for queue tail probabilities could be very important for performance predictions of such queuing models.

One of the most important tasks of network research is to construct adequate models for the concerned traffic flows. There are different processes which are candidates for traffic with multifractal scaling property. These models are mainly based on the simplest multifractal processes, i.e. multiplicative cascades, and always concentrated in modeling of the scaling property. They do not aim to capture the complete multifractal characteristics, which also includes other factors apart from the scaling law, and/or use many parameters [45, 22, 10, 21, 34]. A simple and complete multifractal model with a few parameters is indispensable for further analysis of the model, i.e. in performance evaluation of the network traffic. Once a model is presented its statistical properties should be derived by comparing them to the real traffic characteristics and it also should be, for instance, validated in a queuing analysis study. This shows the applicability of the model in modeling multifractal traffic streams.

## Outline of the dissertation

First a brief summary of the mathematical background of the fractal theory is introduced in Chapter 1. In this chapter the main definitions and some typical properties of the fractal concepts are presented.

Next, the findings and results of this dissertation can be divided into four groups:

- In the first part the implications of some typical non-stationary effects, which can be observed in measured network traffic, were investigated in several long-range dependence tests.

Chapter 2 contains the investigations on this topic. In Section 2.1 and 2.2 long-range dependence testing methods and the non-stationary effects under investigation are described. Next, some analytical results are given in Section 2.3. The study is also completed with a detailed simulation of some example data series which is presented in Section 2.4. Section 2.5 concludes the main findings of the investigation and provides some guidelines to avoid some pitfalls in long-range dependence testing of the actual measured network traffic.

- The second part focuses on the correlation and scaling behavior of IP traffic components on both transport and application layers and shows how components influence the characteristics of the aggregated traffic.

The study is based on real IP traffic measurements which are described in Chapter 3. A global view about the structure of the measured IP traffic concerning the bandwidth share of transport and application layer protocols is presented in Section 3.1. The characteristics of the chosen interval to be analyzed based on a stationary and trend analysis study are also described in this section. In Section 3.2 the results of the scaling analysis are shown based on long-range dependence tests and scaling analysis tools. Finally, Section 3.3 summarizes the chapter.

- In the third part an approximation for the tail asymptotics of a simple queuing system, which is driven by general multifractal input process, is presented. The approximation reveals some highlights on how multifractal traffic impacts differ from monofractal cases. A new practical method for queuing performance estimation of multifractal traffic is also given.

Section 4.1 introduces the queuing system under investigation. The approximation for the queue tail probabilities with the proofs is shown in Section 4.2. Section 4.3 considers the important applications and the simulation validation of the suggested queue tail estimation method on some synthetic multifractal data series. In addition, this section also shows the impacts of multifractal characteristic functions. The applicability of the estimation method is verified in queuing simulation of measured network traffic and is presented in Section 4.4.

- In the fourth part a new multifractal traffic model is proposed. The aim is to find an alternative multifractal model which is simple enough but still able to capture the complete multifractal characteristics of data traffic. It is shown that the model has all the important properties observed in data traffic including long-range dependence, multifractality, and lognormality.

This part of the dissertation is shown in Chapter 5. Section 5.1 overviews the basics of the model, the multiplicative cascades. Section 5.2 presents the new multifractal model including the construction of the model, its parameters, and the main statistical properties. Section 5.3 shows the application of the model for measured data traffic with validation based on a queuing analysis study. Last, Section 5.4 concludes the chapter and suggests some opportunities for further developments of the model.

Chapter 6 summarizes the main results of the dissertation.

# Chapter 1

# Fractal Traffic Theory

The fractal concepts[1] are not new in mathematics. However, they were only introduced in network traffic modeling since the first findings of fractal properties in the LAN packet traffic study of Leland *et al.* in [31]. The fractal theory involves a large class of stochastic processes from long-range dependence (LRD), self-similarity, to multifractals. The following summary, mainly based on [50, 4, 44], provides a brief discussion of these topics and their related concepts.

## 1.1   Long-range dependence

LRD describes those processes which have the covariances decaying very slowly to the zero, like a power function [50]. Among the sets of processes with LRD self-similar and their related processes are important in probability and modeling because of their connection to limit theorems [30] and their simple structure.

Consider a stationary process $X = \{X_i, i \in \mathbb{Z}\}$ with autocovariance function

$$\gamma(k) = \text{Cov}\left[X_i, X_{i+k}\right], \qquad k \in \mathbb{Z}, \tag{1.1}$$

autocorrelation function given by $\rho(k) = \gamma(k)/\gamma(0)$, and power spectral density function defined by

$$f(\lambda) = \frac{1}{2\pi} \sum_{k=-\infty}^{\infty} \gamma(k) e^{ik\lambda}, \qquad \lambda \in [-\pi, \pi]. \tag{1.2}$$

**Definition 1.1.1.** *[4] The process $\{X_t, t \in \mathbb{Z}\}$ is called a stationary process with long-range dependence (or long memory) if there exists a real number $H \in (0.5, 1)$ and a constant*

---

[1]The term *fractal* is also used in the context of the scaling of non-random objects. In this document this notion is only mentioned regarding the stochastic processes.

$c_\rho > 0$ *such that*

$$\lim_{k \to \infty} \frac{\rho(k)}{c_\rho k^{2H-2}} = 1, \tag{1.3}$$

*where H is called the Hurst parameter which measures the degree of long-range dependence.*

The autocorrelation function and the power spectral density function are equivalent specifications of a stochastic process second-order properties, thus the following definition of LRD is also equivalent to the above:

**Definition 1.1.2.** *[4] Let X be a stationary process for which the following holds: There exists a real number $H \in (0.5, 1)$ and a constant $c_f > 0$ such that*

$$\lim_{\lambda \to 0} \frac{f(\lambda)}{c_f |\lambda|^{1-2H}} = 1. \tag{1.4}$$

*Then X is called a stationary process with long-range dependence.*

The connection between $c_f$ and $c_\rho$ is derived by the Tauberian theorem, i.e., $c_f = c_\rho \mathrm{Var}\,[X_t]\,\Gamma(2H-1)\sin(\pi - \pi H)$ where $\Gamma(\cdot)$ denotes the Gamma function,

$$\Gamma(z) = \int_0^{+\infty} x^{z-1} e^{-x} \mathrm{d}x, \qquad z > 0. \tag{1.5}$$

It directly follows from the definition of LRD that the sum of the autocorrelations is divergent, i.e., $\sum_k \rho(k) = \infty$. In contrast, for *short-range dependent* (SRD or *short memory*) processes the autocorrelation function is geometrically bounded, i.e., $\lim_{k \to \infty} \rho(k)/c^k = 1, 0 < c < 1$ and thus $\sum_k \rho(k) < \infty$. The processes for which Eq. (1.3) holds with $0 < H < 0.5$ and $\sum_k \rho(k) < \infty$ are called *intermediate memory* processes [4].

It is important to note that the definition of LRD only determines the asymptotic behavior of the process second-order specifications. It only tells something about the ultimate behavior of the correlations as the lag tends to infinity. In this generality, it does not specify the correlations for any fixed finite lag. Moreover, it determines only the rate of convergence, not the absolute size. Each individual correlation can be arbitrary small. Only the decay of the correlations is slow. This makes the detection of LRD more difficult [4]. Statistical methods for LRD detection and for estimation of Hurst parameter are described in the next chapter, section 2.1.

Examples for LRD processes are fractional Gaussian noise (fGn) and F-ARIMA processes, while all Markovian, ARMA, and finite memory processes are SRD.

## 1.2 Self-similarity

A stochastic process is self-similar if it is invariant in distribution under the scaling of time or space. For an exact self-similar process there is a rigorous scaling rule determined by

a parameter ($H$) over all available time scales. The only self-similar Gaussian process is called fractional Brownian motion (fBm).

**Definition 1.2.1.** *[50] The real-valued process $\{X(t), t \in \mathbb{R}\}$ is self-similar with index $H > 0$ (H-ss) if for all $a > 0$, the finite-dimensional distributions of $\{X(at), t \in \mathbb{R}\}$ are identical to the finite-dimensional distributions of $\{a^H X(t), t \in \mathbb{R}\}$, i.e., if for any $k \geq 1$, $t_1, t_2, \ldots, t_k \in \mathbb{R}$ and any $a > 0$,*

$$(X(at_1), X(at_2), \ldots, X(at_k)) \overset{d}{=} \left( a^H X(t_1), a^H X(t_2), \ldots, a^H X(t_k) \right). \tag{1.6}$$

The relation in Eq. (1.6) can be expressed in a more concise way:

$$X(at) \overset{d}{=} a^H X(t). \tag{1.7}$$

A non-degenerate $H$-ss process cannot be stationary because if it were, we would have for any $a > 0$ and $t > 0$, $X(t) \overset{d}{=} X(at) \overset{d}{=} a^H X(t)$ and we would obtain a contradiction because $a^H X(t) \to \infty$ as $a \to \infty$ [50]. There is, nevertheless, an important one to one correspondence between self-similar and stationary processes.

**Proposition 1.2.2.** *[50] If $\{X(t), 0 < t < \infty\}$ is H-ss, then*

$$Y(t) = e^{-tH} X(e^t), \quad -\infty < t < \infty, \tag{1.8}$$

*is stationary. Conversely, if $\{Y(t), -\infty < t < \infty\}$ is stationary, then*

$$X(t) = t^H Y(\ln t), \quad 0 < t < \infty, \tag{1.9}$$

*is H-ss.*

However a non-degenerate $H$-ss process can have stationary increments.

**Definition 1.2.3.** *The process $\{X(t), t \in \mathbb{R}\}$ is H-sssi if it is self-similar with index $H$ and has stationary increments.*

The definition of $H$-sssi process determines the possible vales of index $H$.

**Lemma 1.2.4.** *[50] Suppose that $\{X(t), t \in \mathbb{R}\}$ is a (non-degenerate) H-sssi finite variance process. Then*

$$0 < H \leq 1,$$

$$X(0) = 0 \quad a.s.,$$

*and*

$$\text{Cov}\left[X(t_1), X(t_2)\right] = \frac{1}{2}\left\{|t_1|^{2H} + |t_2|^{2H} - |t_1 - t_2|^{2H}\right\}\text{Var}\left[X(1)\right]. \qquad (1.10)$$

*Moreover, for all $t \in \mathbb{R}$*

$$\text{E}\left[X(t)\right] = 0 \quad \text{if} \ \ 0 < H < 1,$$

$$X(t) = tX(1) \quad a.s. \quad \text{if} \ \ H = 1.$$

If $X(t)$ is a (non-degenerate) $H$-sssi finite variance process, then $0 < H \leq 1$. The interesting range of H is $0.5 < H < 1$ for traffic modeling because $H$-sssi $X(t)$ processes with $H < 0$ are not measurable and represent pathological cases while for the $H > 1$ case the autocorrelation of the incremental process does not exist. The range of $0 < H < 0.5$ can also be excluded from our practice because in this case the incremental process is SRD. For practical purposes the range of $0.5 < H < 1$ is only important. In this range the autocorrelation function of the *incremental process* of $X(t)$, which can be defined in discrete time as

$$Z_k = X(k) - X(k-1), \qquad k \in \mathbb{Z}, \qquad (1.11)$$

have the following form:

$$\rho(k) = \frac{1}{2}\left[(k+1)^{2H} - 2k^{2H} + (k-1)^{2H}\right]. \qquad (1.12)$$

This incremental process is LRD which shows the connection between self-similar and LRD processes.

Self-similarity is also extended to discrete processes to fit the theory of time series. Let $X = \{X_i, i \in \mathbb{Z}\}$ be a stationary process with the autocorrelation function $\rho(\cdot)$. Define the $m$-aggregated time series $X^{(m)}$ by averaging the original series in non-overlapping blocks of $m$, replacing each block by its mean, i.e.,

$$X_i^{(m)} = \frac{1}{m}\left(X_{im-m+1} + X_{im-m+2} + \ldots + X_{im}\right) \qquad m = 1, 2, \ldots \qquad (1.13)$$

and denote its corresponding autocorrelation function by $\rho^{(m)}(\cdot)$.

**Definition 1.2.5.** *[51] A stationary process* $X = \{X_k, k \in \mathbb{Z}\}$ *is called exactly self-similar if it is satisfies*

$$X^{(m)} \stackrel{d}{=} m^{H-1} X \tag{1.14}$$

*for all aggregation levels* $m$.

The process $X$ is called *second-order self-similar* if

$$\mathrm{Var}\left[X^{(m)}\right] = \frac{1}{m^{2-2H}} \mathrm{Var}\left[X\right], \tag{1.15}$$

$$\text{or} \quad \rho^{(m)}(k) = \rho(k) \tag{1.16}$$

for any aggregation $m$. A weaker condition is the following: a process $X$ is said to be *asymptotically second-order self-similar* if

$$\lim_{m \to \infty} \rho^{(m)}(k) = \rho(k). \tag{1.17}$$

The only Gaussian process that is self-similar and has stationary increments is called fractional Brownian motion.

**Definition 1.2.6.** *[50] A Gaussian $H$-sssi process, $0 < H < 1$, is called fractional Brownian motion (fBm) and is denoted $\{B_H(t), t \in \mathrm{R}\}$. It is called standard fractional Brownian motion if $\sigma_0^2 \equiv \mathrm{Var}\left[B_H(1)\right] = 1$.*

The fBm has the following important properties:

(i) $B_H(t)$ has normal distribution with mean 0 and variance $\sigma_0^2 t^{2H}$,

(ii) $\mathrm{Cov}\left[B_H(t_1), B_H(t_2)\right] = \frac{1}{2}\left(|t_1|^{2H} + |t_2|^{2H} - |t_1 - t_2|^{2H}\right)$, $\quad H \in (0,1)$,

(iii) $B_H(t)$ has continuous sample paths.

The incremental process of the fBm is referred to as fractional Gaussian noise (fGn). In the special case of $H = 0.5$ the fBm is called Brownian motion.

## 1.3 Multifractals

In contrast to self-similar processes, multiscaling or multifractal processes allow a more flexible law of the scaling behavior. The class of multifractal processes involve all the processes with scaling property including self-similar, monoscaling, and multiscaling processes. The most obvious examples of the multiscaling processes are the multiplicative cascades.

**Definition 1.3.1.** *[8] A stochastic process $X(t)$ is called multifractal if it has stationary increments and satisfies*

$$\mathrm{E}\left[|X(t)|^q\right] = c(q)t^{\tau(q)+1} \tag{1.18}$$

*for some positive $q \in \mathrm{Q}, [0,1] \subset \mathrm{Q}$, where $\tau(q)$ is called the scaling function and the moment factor $c(q)$ is independent of $t$.*

An easy consequence of the definition is that $\tau(q)$ is a concave function. If $\tau(q)$ is linear in $q$ the process is called uniscaling or monofractal, otherwise it is multifractal. It can be show that in the special case of self-similar process with index $H$ we get $\tau(q) = qH - 1$ and $c(q) = \mathrm{E}\left[|X(1)|^q\right]$. The class of multifractal processes involve both monofractal and self-similar cases.

The definition above describes multifractality in terms of process moments and it may lead to a more intuitive understanding of multifractality. However, there is an alternative approach to multifractals which is based on the study of the local erratic behavior of the process by means of its local Hölder exponents.

### 1.3.1 Large deviation spectrum

Without loss of generality consider a process $X(t)$ defined on $I = [0,1]$. For any $n$ this interval can be decomposed as the disjoint union of $2^n$ dyadic subintervals $I_n^k = [k2^{-n}, (k+1)2^{-n})$, where $k = 0, 1, \ldots, 2^n - 1$. The *coarse Hölder exponents* at resolution $n$ are defined as the rescaled logarithmic increments of the process on $I_n^k$, i.e., $\alpha_n^k = -\frac{1}{n}\log_2 |X\left((k+1)2^{-n}\right) - X\left(k2^{-n}\right)|$. Define $k_n(t)$ such that $I_n^{k_n(t)}$ is the unique interval which contains $t$. The *local Hölder exponent* of $X$ at $t$ is defined as

$$\alpha(t) = \liminf_{n\to\infty} \alpha_n^{k_n(t)} \tag{1.19}$$

The *grained* or *large deviation spectrum* measures, loosely speaking, how fast the probability of observing a coarse Hölder exponent different from the expected value tends to zero as the resolution tends to infinity [32].

Let $N_n^\varepsilon(\alpha)$ be of the form

$$N_n^\varepsilon(\alpha) = \#\{k = 0, 1, \ldots, (2^n - 1) : \alpha_n^k \in [\alpha - \varepsilon, \alpha + \varepsilon]\}, \tag{1.20}$$

where $\varepsilon > 0$ is the scale of measurement. Then the large deviation spectrum, denoted by $f_g$, can be defined by

$$f_g(\alpha) = \lim_{\varepsilon\to 0} \limsup_{n\to\infty} \frac{\log N_n^\varepsilon(\alpha)}{n}. \tag{1.21}$$

The large deviation spectrum describes the distribution of the local singularities, since the number of dyadic intervals of size $2^{-n}$ with coarse Hölder exponent $\approx \alpha$ varies roughly as

$2^{nf_g(\alpha)}$ for large $n$. Equivalently:

$$P_n\left[\alpha_n^k \approx \alpha\right] \sim 2^{-n(1-f_g(\alpha))}, \tag{1.22}$$

where the probability is related to a random choice of $k$ uniformly in $\{0, 1, \dots, (2^n - 1)\}$, i.e., $P_n$ is the uniform distribution on the set of all dyadic intervals $I_n^k$ of size $2^{-n}$ [32].

### 1.3.2 Legendre spectrum

Legendre spectrum provides a robust estimation of the large deviation spectrum while data satisfies some necessary conditions.

Let $Y_n = \{Y_n^k : Y_n^k = |X((k+1)2^{-n}) - X(k2^{-n})|, k = 0, 1, \dots, 2^n - 1\}$ denote the discrete increment process of $X$. Define the partition sum $S_n(q)$ with $q \in \mathbb{R}$:

$$
\begin{aligned}
S_n(q) &= \sum_{k=0}^{2^n-1} \left|X((k+1)2^{-n}) - X(k2^{-n})\right|^q \\
&= \sum_{k=0}^{2^n-1} \left(Y_n^k\right)^q = 2^n E_n\left[e^{q\log Y_n}\right],
\end{aligned} \tag{1.23}
$$

where $E_n[\cdot]$ denotes the average operation. Then the scaling function can also be given by

$$\tau(q) = \liminf_{n\to\infty} \frac{\log S_n(q)}{-n\log 2} \tag{1.24}$$

and thus the *Legendre spectrum* of the process $X$ is defined by the following

$$f_l(\alpha) = \tau^*(\alpha) = \inf_{q\in\mathbb{R}}(\alpha q - \tau(q)). \tag{1.25}$$

Consider the moment generating function of the random variable $Z_n = \log Y_n^k$ where $k$ is distributed with $P_n$ as before

$$c_n(q) = -\frac{1}{n}\log E_n\left[e^{qZ_n}\right] = -\frac{1}{n}\log\left(2^{-n}S_n(q)\right). \tag{1.26}$$

The Gärtnet-Ellis theorem [15] shows that if $\lim c_n(q)$ exists (in which case $c_n(q) = \tau(q)+1$) and differentiable, then the following relation holds

$$f_l(\alpha) = f_g(\alpha), \tag{1.27}$$

which is also referred to as *multifractal formalism* [32].

Thus the Legendre spectrum provides a visualizing method for detection and delineation of multifractal property. Moreover, it is favorable since its computation is much easier than the direct computation of the large deviation spectrum which requires the evaluation of local quantities and of a double limit [32].

# Chapter 2

# Effects of Non-Stationarity in Long-Range Dependence Tests

Careful statistical analyses indicate that the measured traffic traces from live packet networks often contain non-stationary effects like level shifts or polynomial trends. In these cases several popular tests for long-range dependence can result in wrong conclusions and unreliable estimate of the Hurst parameter. The aim of this study is to reveal the implications of the most important non-stationary effects which occur in practice on the most frequently used LRD tests in order to have a good understanding of these phenomena and to investigate the robustness of these tests against non-stationarity effects.

The issue is not new and was also addressed in the hydrology literature (e.g. [28]) after the application of LRD processes in the modeling of natural storage systems [25, 36]. Some aspects of the problem were also presented and addressed in the recent teletraffic literature [12, 17, 24, 41, 52, 48]. Important results are shown in [52] where the variance-type estimator is investigated under several non-stationary conditions. The robustness of the A-V wavelet estimator against non-stationary effects is presented in [48]. However, the understanding of these phenomena is far from being complete, the stationarity tests and the validation techniques of fractal models have not widely been applied in today's teletraffic practice.

Note that this topic is somewhat philosophical from the application point of view. Theoretically, the measured data traces with finite length can be originated both from stationary or non-stationary traffic source. Therefore, from modeling point of view the traffic can also be considered to be stationary or non-stationary. One practical solution is based on the notion of *local stationarity*, where stationarity is only assumed over some short periods of time. Local stationarity with traditional models can also be used to capture the observed characteristics [55]. An alternative but rather difficult solution is to use *non-stationary models*, e.g. [13].

In this study both analytical and simulation investigations of the implications of non-stationary effects on several tests are presented contributing to this research approach. The results are also demonstrated with examples based on measured ATM traces. The main use of these results can be utilized to avoid pitfalls in LRD traffic modeling.

## 2.1 Long-range dependence tests

The task of testing LRD and the estimation of the Hurst parameter are not simple in practice. The main problem is that it is rather difficult to distinguish between non-stationary processes and stationary LRD processes due to the fact that LRD processes appear to have local trends, cycles, etc., many of the characteristics of non-stationary processes. Choosing a finite and sometimes also short data set may avoid the appearance of non-stationarities but it also makes the identification of LRD almost impossible. Having a longer data set this identification becomes easier but we know for sure that in a long measured data non-stationary effects are present due to the daily cycles of traffic characteristics. The assumption about stationarity with high reliability may only be supported in the *busy periods* of the traffic. However, in some cases (e.g. IP traffic in a LAN) the notion of busy period cannot be applied [5].

There are methods developed to test stationarity (e.g. [54, 16, 40]) and to distinguish between LRD and non-stationarities (e.g. [29, 4, 48]) but application of these tests is not easy in practice. Moreover, such tests can seldom support their results with high reliability. Four widely used LRD tests are briefly reviewed here: the variance-time plot, the R/S analysis, the periodogram, and the wavelet based $H$-estimator. More detailed description of these methods can be found, e.g., in [4] and [3].

### 2.1.1 Variance-time plot

The variance-time plot is constructed based on the following asymptotic property of LRD processes [4],

$$\text{Var}\left[X^{(m)}\right] = m^{2H-2}\text{Var}\left[X\right] \qquad \text{as } m \to \infty, \tag{2.1}$$

where $X^{(m)}$ denotes the $m$-aggregated process of $X$, $X_k^{(m)} = \frac{1}{m}\sum_{i=(k-1)m}^{km} X_i$, $m$ is the aggregation level, $m = 1, 2, \ldots$

In practice, for a given time series $X$ of size $n$, one chooses the maximum value of $m$ such that $\lfloor n/m \rfloor$[1] is still large enough and then logarithmically increases $m$ from 1 to that value. For those successive values of $m$, the logarithm of the sample variance of $X^{(m)}$ is plotted versus the logarithm of $m$. If $X$ is LRD this variance-time plot should be a straight line with a slope of $2H - 2$. An estimation of the Hurst parameter can be calculated by fitting a least-squares line to points of the plot over the large values of $m$.

Since $0.5 < H < 1$ the asymptotic slope of the variance-time has value between $-1$ and $0$. The variance-time plot with slope $-1$ suggests that the series has no LRD and it has finite variance.

---

[1]The operation $\lfloor a \rfloor$ means the greatest natural number that is smaller or equal $a, a \in \mathbb{R}$.

### 2.1.2 R/S analysis

Consider a time series $X$ of size $n$ with sample mean $\bar{X}_n$ and sample variance $S^2(n) = (1/n)\sum_{i=1}^{n}(X_i - \bar{X}_n)^2$. The *rescaled adjusted range* [4] R/S statistics of $X$ is given by the ratio:

$$\frac{R(n)}{S(n)} = \frac{\max\{W_i : i = 1, 2, \ldots, n\} - \min\{W_i : i = 1, 2, \ldots, n\}}{S(n)}, \qquad (2.2)$$

where $W_i = \sum_{k=1}^{i}(X_k - \bar{X}_n)$. It can be proven for any stationary process with LRD of parameter $H$ that the R/S ratio has the following characteristics for large $n$:

$$\mathrm{E}\left[\frac{R(n)}{S(n)}\right] \sim \left(\frac{n}{2}\right)^H, \qquad (2.3)$$

which is known as *Hurst effect* [4].

Given an empirical time series of length $n$ $(X_j : j = 1, 2, \ldots, n)$, subdivide the series into $K$ blocks of size $\lfloor n/K \rfloor$. Then for each lag $d := \lfloor n/K \rfloor$, compute the $R(t_i, d)/S(t_i, d)$ ratios, where $t_i$ denotes the starting point of the data block $d$, i.e., $t_i = \lfloor n/K \rfloor (i - 1) + 1$, $i = 1, 2, \ldots, d$. Thus one has $K$ estimates of $R/S(d)$ for each value of $d$. Choosing logarithmically spaced values of $d$ $(d < n)$ and plotting $\log[R/S(t_i, d)]$ versus $\log d$ results in the R/S plot.

Next, a least squares regression line should be fitted to points of the R/S plot. The slope of the regression line gives an estimate of the Hurst parameter of LRD. The smallest values of $d$ should be disregarded because these points are dominated by short-range dependence in the series. We also do not use the high end of the plot because only a few points in this region may make the estimate unreliable. In practice, values of $d$ in the middle region of the R/S plot are used to estimate $H$.

### 2.1.3 Periodogram

The method is used to identify the manifestation of LRD exhibited in the frequency domain (see Eq. (1.4) in Section 1.1). For a discrete time series $X = \{X_1, X_2, \ldots, X_n\}$ the periodogram, i.e., the sample power spectral density as estimated using a Fourier transform, is defined as

$$I(\lambda) = \frac{1}{2\pi n}\left|\sum_{k=1}^{n}(X_k - \bar{X})e^{ik\lambda}\right|^2, \qquad (2.4)$$

where $\lambda$ denotes the frequency, $\lambda \in [0, \pi)$.

The main idea of periodogram analysis is simply to plot the periodogram in a log-log grid and to estimate $H$ from the slope of the regression line fitted to the plot at low frequencies. Practically, the periodogram plot is the graph of $\{\log \lambda_j, \log I(\lambda_j)\}$, $j = 1, 2, \ldots, M$ where $\lambda_j = 2\pi j/n$ and $M$ is always chosen to be $n/4, n/8, n/16$ or $n/32$ and so on depending on how large $n$ is. According to Eq. (1.4), the plot should be a straight line with slope $-\gamma = 1 - 2H$ in case of LRD processes.

### 2.1.4  Wavelet-based estimator

Wavelet analysis of LRD traffic is introduced by P. Abry and D. Veitch in [3]. The estimator is found to be very unbiased and highly robust against the presence of deterministic trends. The description of the wavelet estimator is briefly reviewed here.

The discrete wavelet transform (DWT) represents a discrete series $\{X_1, X_2, \ldots, X_n\}$ by a combination of the scaled and delayed versions of the mother wavelet function $\psi(.)$. At scale level $j$ the wavelet coefficients $d_x(j, k)$ are defined as follows:

$$d_x(j,k) = 2^{j/2} \sum_{i=1}^{n} X_i \psi(2^{-j}n - k) \qquad j = 1, 2, \ldots; \quad k = 1, 2, \ldots, 2^{-j}n \qquad (2.5)$$

Let $X$ be a second-order stationary process. Then its wavelet coefficients $d_x(j, k)$ satisfy:

$$\mathrm{E}\left[d_x(j,k)^2\right] = \int f(\lambda) 2^j |\Psi(2^j \lambda)|^2 d\nu \qquad (2.6)$$

where $f(\lambda)$ and $\Psi(\lambda)$ are the power spectrum of $X$ and the Fourier transform of the wavelet function $\psi(.)$, respectively. Based on Eq. (1.4) we have

$$\mathrm{E}\left[d_x(j,k)^2\right] \sim 2^{j(2H-1)} c_f C(H, \psi), \qquad (2.7)$$

where $C(H, \psi) = \int |\lambda|^{-(2H-1)} |\Psi(\lambda)|^2 d\lambda$ is a constant which depends on $H$ and $\psi$.

If the length of $X$ is $n$ then the available number of wavelet coefficients at octave $j$ is $n_j$, $n_j = 2^{-j}n$. Then,

$$\mu_j = \mathrm{E}\left[d_x(j,k)^2\right] \approx \frac{1}{n_j} \sum_{k=1}^{n_j} |d_x(j,k)|^2. \qquad (2.8)$$

Eq. (2.7) provides a possible way to estimate the Hurst parameter of the LRD processes:

$$\log_2 \mu_j \approx \log_2 \left( \frac{1}{n_j} \sum_{k=1}^{n_j} |d_x(j,k)|^2 \right) \sim (2H - 1)j + c, \qquad (2.9)$$

where $c = \log_2\left(c_f C(H, \psi)\right)$ is a constant. This means that if $X$ is LRD with Hurst parameter $H$, then the graph of $\log_2(\mu_j)$ versus $j$, called the Logscale Diagram (LD), should be linear with slope $2H - 1$.

As discussed in detail in [3], the effects of polynomial trends with the degree $P$ on this estimator can be avoided by increasing the vanishing moment $N$ of the wavelet function such that $N \geq P + 1$. This observation is justified by simulations presented later. Moreover, the effect of level shift is also investigated.

## 2.2  Types of non-stationarities

The analysis of measured packet traffic can reveal various deterministic changes in the data on different time scales. These traffic variations are not stochastic by nature but

rather caused by deterministic mechanisms like protocols [27]. These mechanisms can, for example, introduce quasi-periodic patterns in the traffic data which can be, if not detected and removed, the reason for several statistical pitfalls, e.g. the conclusion of slowly decaying correlations.

On longer time scales we can observe also a regular character of the traffic due to daily or weekly variations. These traffic trends should also be identified and removed prior to any statistical analysis. These are not easy but important parts of a comprehensive statistical analysis [9, 7].

Different trend models are candidates for investigations, e.g. linear trend, parabolic trend, exponential trend, logistical trend or Gompertz trend, etc. We have chosen the non-stationary effects and trends which are frequently observed in practice. These are the *level shift*, which can be observed when during our traffic measurements suddenly a new source starts to emit traffic to the aggregation and the *linear and parabolic trends*, which can be observed in daily traffic variations. For example, when people start to work in their office between 8 and 10 am a monotonic increase of the total load of the aggregated traffic can be observed.

## 2.3 Analytical investigations

In this section an analytical study is presented which shows how some non-stationarities can change the results of some widely used LRD tests. Three cases were concerned: variance-time plot of LRD data with level shift, with linear trend, and R/S analysis of LRD data with level shift.

Consider a data series $X = \{X_1, X_2, ...X_n\}$ which is LRD with Hurst parameter $H$. To make the later calculations simple two assumptions were applied: (1) $n$ is large enough so that aggregated series of $\{X\}$ used in computation of the variance-time plot still contains a large amount of data; (2) the mean of $\{X\}$ is zero, i.e., $\bar{X}_n = 0$. The second assumption can be taken into account because the non-zero mean of LRD data does not change the result of LRD tests (see definitions in Section 2.1).

### 2.3.1 Variance-time plot of LRD data series with level shift

The variance-time plot is the log-log plot of the variance of the data series versus the aggregation level. The corrected sample variance of $\{X\}$ series:

$$\text{Var}\left[X\right] = \frac{1}{n-1} \sum_{i=1}^{n} X_i^2, \tag{2.10}$$

since the mean of $\{X\}$ is zero. Similarly, the corrected sample variance of the $m$-aggregated series of $\{X\}$ is:

$$\text{Var}\left[X^{(m)}\right] = \frac{1}{\lfloor n/m \rfloor - 1} \sum_{j=1}^{\lfloor n/m \rfloor} \left(X_j^{(m)}\right)^2, \tag{2.11}$$

where $\lfloor z \rfloor$ denotes the greatest integer smaller than or equal to $z$. Eq. (2.11) holds because the assumption that $\lfloor n/m \rfloor$ is still large enough so $\bar{X}^{(m)}_{\lfloor n/m \rfloor} \approx \bar{X}_n = 0$[2]. The following relation holds for LRD series:

$$\mathrm{Var}\left[X^{(m)}\right] = \frac{\mathrm{Var}\left[X\right]}{m^{2-2H}}. \tag{2.12}$$

After adding a level shift to the series $X$, the $i$-th element of the new series, denoted by $X_i^{LS}$ has the value:

$$X_i^{LS} = \begin{cases} X_i & \text{if } i \le \lfloor n/2 \rfloor \\ X_i + K_{LS} & \text{if } i > \lfloor n/2 \rfloor \end{cases} \;,$$

where $K_{LS}$ denotes the value of the level shift occurred in the middle of the investigated time period[3]. It is easy to observe that the mean of the $X^{LS}$ series is $K_{LS}/2$. Thus its variance is of the form:

$$\begin{aligned}
\mathrm{Var}\left[X^{LS}\right] &= \frac{1}{n-1} \sum_{i=1}^{n} \left(X_i^{LS} - K_{LS}/2\right)^2 \\
&= \frac{1}{n-1} \left[ \sum_{i=1}^{\lfloor n/2 \rfloor} \left(X_i - K_{LS}/2\right)^2 + \sum_{i=\lfloor n/2 \rfloor+1}^{n} \left(X_i + K_{LS} - K_{LS}/2\right)^2 \right] \\
&= \frac{1}{n-1} \sum_{i=1}^{n} X_i^2 + \frac{n}{n-1}\frac{K_{LS}^2}{4} + \frac{K_{LS}}{n-1}\left[ \sum_{i=\lfloor n/2 \rfloor+1}^{n} X_i - \sum_{i=1}^{\lfloor n/2 \rfloor} X_i \right] \\
&\approx \mathrm{Var}\left[X\right] + \frac{K_{LS}^2}{4}\;, \qquad \text{if } n \text{ is large enough.} \tag{2.13}
\end{aligned}$$

The $j$-th element of the $m$-aggregated series $X^{(m)}$ is given by $X_j^{(m)} = \sum_{k=(j-1)m+1}^{jm} X_k$, therefore

$$X_j^{LS\ (m)} = \begin{cases} X_j^{(m)} & \text{if } j \le \lfloor n/2m \rfloor \\ X_j^{(m)} + K_{LS} & \text{if } j > \lfloor n/2m \rfloor \end{cases} \;,$$

with only one exception when the element contains the location of the level shift. Since $\lfloor n/m \rfloor$ is large enough this exception does not change the result. Thus doing the same calculations as in Eq. (2.13) we have

$$\mathrm{Var}\left[X^{LS\ (m)}\right] \approx \mathrm{Var}\left[X^{(m)}\right] + \frac{K_{LS}^2}{4}. \tag{2.14}$$

By inserting Eq. (2.13) and Eq. (2.14) into Eq. (2.12) we get the final result:

$$\mathrm{Var}\left[X^{LS\ (m)}\right] = \frac{\mathrm{Var}\left[X^{LS}\right] - K_{LS}^2/4}{m^{2-2H}} + \frac{K_{LS}^2}{4}. \tag{2.15}$$

---

[2]This equality only holds when dealing with stationary data series.
[3]The location of the level shift jump has no effect on analytical and simulation results.

18

By plotting $\log\left(\text{Var}\left[X^{LS\ (m)}\right]\right)$ against $\log m$ we get a convex curve bounded by two lines: the line with slope $2H-2$ and ordinate $\log\left(\text{Var}\left[X^{LS}\right]-K_{LS}^2/4\right)$ as $m \to 0$ and a horizontal line with ordinate $K_{LS}^2/4$ as $m \to \infty$. The estimation of $H$ for LRD processes should be performed at large $m$ (in theory as $m \to \infty$). Therefore it can be concluded that the estimation is highly destroyed in the presence of level shifts. More details about this distortion are demonstrated by examples given in Section 2.4.

### 2.3.2   Variance-time plot of LRD data series with linear trend

In this case the maximum value of the linear trend is denoted by $K_L$. The LRD series with linear trend $X^L$ can be given as:

$$X_i^L = X_i + \frac{(i-1)\ K_L}{n-1}\ . \tag{2.16}$$

Because the mean of $X$ is zero, i.e., $\bar{X}_n = 0$, the mean of the new series is $\bar{X}^L = K_L/2 \approx \bar{X}_{\lfloor n/m \rfloor}^{L\ (m)}$, where $\bar{X}_{\lfloor n/m \rfloor}^{L\ (m)}$ denotes the mean of $m$-aggregated series of $X^L$. The variance of $X^L$ can be calculated as follows:

$$
\begin{aligned}
\text{Var}\left[X^L\right] &= \frac{1}{n-1}\sum_{i=1}^{n}\left(X_i^L - \frac{K_L}{2}\right)^2 = \frac{1}{n-1}\sum_{i=1}^{n}\left[X_i + \frac{(i-1)\ K_L}{n-1} - \frac{K_L}{2}\right]^2 \\
&= \text{Var}\left[X\right] + \frac{2K_L}{(n-1)^2}\sum_{i=1}^{n} i\ X_i + \frac{K_L^2}{4(n-1)^3}\sum_{i=1}^{n}(2i-n-1)^2 \\
&\approx \text{Var}\left[X\right] + \frac{2K_L}{(n-1)^2}\sum_{i=1}^{n} i\ X_i + \frac{K_L^2}{12} = \text{Var}\left[X\right] + C_1\ , \tag{2.17}
\end{aligned}
$$

where $C_1$ is a constant independent of $m$ for a given data.

Similarly, for $m$-aggregated series we have:

$$X_j^{L\ (m)} = X_j^{(m)} + \frac{K_L}{2(n-1)}(2jm-m-1) \qquad j = 1, 2, \ldots, \lfloor n/m \rfloor. \tag{2.18}$$

and

$$
\begin{aligned}
\text{Var}\left[X^{L\ (m)}\right] &= \frac{1}{\lfloor n/m \rfloor - 1}\sum_{j=1}^{\lfloor n/m \rfloor}\left[X_j^{L\ (m)} - \frac{K_L}{2}\right]^2 \\
&= \frac{1}{\lfloor n/m \rfloor - 1}\sum_{j=1}^{\lfloor n/m \rfloor}\left[X_j^{(m)} + \frac{K_L}{2(n-1)}(2jm-m-1) - \frac{K_L}{2}\right]^2 \\
&\approx \text{Var}\left[X^{(m)}\right] + \frac{2K_L\ m}{(n-1)\left(\lfloor n/m \rfloor - 1\right)}\sum_{j=1}^{\lfloor n/m \rfloor} j\ X_j^{(m)} + \\
&\quad + \frac{K_L^2}{4(n-1)^2\left(\lfloor n/m \rfloor - 1\right)}\sum_{j=1}^{\lfloor n/m \rfloor}(2jm-m-n)^2. \tag{2.19}
\end{aligned}
$$

Using the condition that $\lfloor n/m \rfloor$ is large enough, i.e., $m \ll n$ or $n/m \to 0$ and the approximation $\lfloor n/m \rfloor \approx n/m$, Eq. (2.19) can be simplified:

$$\text{Var}\left[X^{L\ (m)}\right] \approx \text{Var}\left[X^{(m)}\right] + \frac{2K_L\ m^2}{(n-1)(n-m)} \sum_{j=1}^{\lfloor n/m \rfloor} j\ X_j^{(m)} + \frac{K_L^2}{12}\frac{(7m-6)}{m}. \quad (2.20)$$

Finally, by inserting Eq. (2.17) and Eq. (2.20) into Eq. (2.12) we get the following:

$$\begin{aligned}
\text{Var}\left[X^{L\ (m)}\right] &\approx \frac{\text{Var}\left[X^L\right]-C_1}{m^{2-2H}} + \frac{2K_L\ m^2}{(n-1)(n-m)} \sum_{j=1}^{\lfloor n/m \rfloor} j\ X_j^{(m)} + \frac{K_L^2}{12}\frac{(7m-6)}{m} \\
&= \frac{\text{Var}\left[X^L\right]-C_1}{m^{f_L(m)}}, \quad\quad\quad\quad\quad\quad\quad\quad\quad\quad (2.21)
\end{aligned}$$

where

$$f_L(m) = \frac{\log\left(\dfrac{\text{Var}\left[X_L\right]-C_1}{\dfrac{\text{Var}\left[X_L\right]-C_1}{m^{2-2H}} + \dfrac{2K_L\ m^2}{(n-1)(n-m)} \sum_{j=1}^{\lfloor n/m \rfloor} j\ X_j^{(m)} + \dfrac{K_L^2}{12}\dfrac{(7m-6)}{m}}\right)}{\log m}. \quad (2.22)$$

Eq. (2.21) shows that the presence of a linear trend in LRD data turns the result of variance-time plot to be quite different from its original form. Plotting $\log\left(\text{Var}\left[X^{L\ (m)}\right]\right)$ versus $\log m$ instead of a straight line with slope $(2H-2)$ we should observe a curve described by $f_L(m)$, which is a complicated function of $m$. The estimation of the Hurst parameter of LRD from the variance-time plot should be done by fitting a regression line to the plot at large values of $m$, so from Eq. (2.21) and using the fact that $X_j^{(m)}$ is close to the sample mean $\bar{X}$ we get:

$$\begin{aligned}
\frac{2K_L\ m^2}{(n-1)(n-m)} \sum_{j=1}^{\lfloor n/m \rfloor} j\ X_j^{(m)} + \frac{K_L^2}{12}\frac{(7m-6)}{m} &\approx \frac{2K_L\ m^2}{(n-1)(n-m)} C_2 \frac{n/m(n/m+1)}{2} + \\
&\quad + \frac{K_L^2}{12}\frac{(7m-6)}{m} \\
&\approx C_2\ K_L + \frac{7\ K_L^2}{12}, \quad \text{as } m \to \infty, \quad (2.23)
\end{aligned}$$

where $C_2$ denotes a constant close to 0. Thus Eq. (2.21) can be rewritten as

$$\text{Var}\left[X^{L\ (m)}\right] \approx \frac{\text{Var}\left[X^L\right]-C_1}{m^{2-2H}} + C_2\ K_L + \frac{7\ K_L^2}{12}, \quad \text{as } m \to \infty. \quad (2.24)$$

Eq. (2.24) concludes that the variance-time plot of a LRD process with linear trend asymptotically approaches a horizontal line with ordinate $C_2 K_L + 7\, K_L^2/12$, where the constant $C_2$ is independent of $m$. The variance-time plots of the LRD process and a process with no LRD are no longer distinguishable in the presence of a linear trend. For more details see examples in Section 2.4.

### 2.3.3   R/S plot of LRD data series with level shift

The R/S analysis of an $\{X_1, X_2, \ldots, X_n\}$ data series is defined by the log-log plot of the rescaled adjusted range R/S ratio versus the actual data window size $d$:

$$\frac{R}{S} = \frac{\max\{W_i;\ i = 1, 2, \ldots, d\} - \min\{W_i;\ i = 1, 2, \ldots, d\}}{\sqrt{\operatorname{Var}\left[X_{off,d}\right]}}, \tag{2.25}$$

where $X_{off,d}$ denotes the considered sub-series $\{X_{off+1}, X_{off+2}, \ldots, X_{off+d}\}$ and $W_i = \sum_{k=1}^{i}(X_{off+k} - \bar{X}_{off,d})$. With a given value of $d$ several R/S ratios are calculated by sliding the window size $d$ throughout the $X$ series.

By adding a level shift to the series $X$, we get the new series denotes by $X^{LS}$, $X^{LS} = \{X_1, X_2, \ldots, X_{\lfloor n/2 \rfloor - 1}, X_{\lfloor n/2 \rfloor}, X_{\lfloor n/2 \rfloor + 1} + K_{LS}, \ldots, X_n + K_{LS}\}$, where $K_{LS}$ denotes the value of the level shift. According to the definition of the R/S ratio we can observe that this ratio does not change if the data window $d$ does not cover the level shift point. It is simply due to the fact that the $k$-th element of $X_{off,d}$ is $X_{off+k} + C_3$ where $C_3$ is a constant. More precisely, $C_3 = 0$ if the data window is placed entirely at the first level and $C_3 = K_{LS}$ if it stays entirely at the region of the second level. Thus it is seen that $R = \max\{W_i\} - \min\{W_i\} = \max\{W_i + C_3\} - \min\{W_i + C_3\}$, where $i = 1, 2, \ldots, d$, and $S = \sqrt{\operatorname{Var}\left[X_{off,d}\right]} = \sqrt{\operatorname{Var}\left[X_{off,d} + C_3\right]}$. Therefore the R/S ratio holds its original value.

The situation is different when the data window $d$ contains the jump of the level shift. Concern the simple case when the location of the shift is placed at the center of the window:

$$X^{*\, LS}_{off+k} = \begin{cases} X_{off+k} & \text{if } k \le \lfloor n/2 \rfloor \\ X_{off+k} + K_{LS} & \text{if } k > \lfloor n/2 \rfloor \end{cases},$$

where $k = 1, 2, \ldots, d$ and the symbol (*) means that it only relates to those $d$-windows mentioned above. As proven in subsection 2.3.1,

$$\operatorname{Var}\left[X^{*\, LS}_{off,d}\right] \approx \operatorname{Var}\left[X_{off,d}\right] + \frac{K_{LS}^2}{4}. \tag{2.26}$$

Moreover, for the new series

$$W^{*\, LS}_i = \sum_{k=1}^{i}\left[X^{*\, LS}_{off+k} - \left(\bar{X}_{off,d} + \frac{K_{LS}}{2}\right)\right] = \begin{cases} W_i - i\, K_{LS}/2 & \text{if } i = 1, 2, \ldots, \lfloor d/2 \rfloor \\ W_i - (d-i)\, K_{LS}/2 & \text{if } i = \lfloor d/2 \rfloor + 1, \ldots, d \end{cases}.$$

Different R/S values are computed by increasing the window size $d$ and moving this window along the data. There is one window $d$ that contains the shift location at most when $d$ has a small value. However, the change of only one value of the R/S ratio at a fixed $d$ can be counted as a noise and it does not change the look of the plot. In contrast when $d$ assumes a large enough value the following can be justified:

$$
\begin{aligned}
R^{*\ LS} &= \max\{W_i^{*\ LS}\} - \min\{W_i^{*\ LS}\} = W_d^{*\ LS} - W_{\lfloor d/2 \rfloor}^{*\ LS} \\
&= W_d - W_{\lfloor d/2 \rfloor} + \lfloor d/2 \rfloor \frac{K_{LS}}{2} \approx d\frac{K_{LS}}{4}.
\end{aligned}
\tag{2.27}
$$

Moreover, as $d$ is large,

$$
S^{*\ LS} = \sqrt{\mathrm{Var}\left[X_{off,d}^{*\ LS}\right]} \approx \sqrt{\mathrm{Var}\left[X_{off,d}\right] + \frac{K_{LS}^2}{4}} \approx \sqrt{\mathrm{Var}\left[X_n\right] + \frac{K_{LS}^2}{4}}
\tag{2.28}
$$

Therefore,

$$
\left(\frac{R}{S}\right)^{*\ LS} \approx \frac{d\dfrac{K_{LS}}{4}}{\sqrt{\mathrm{Var}\left[X_n\right] + \dfrac{K_{LS}^2}{4}}} = d\ C_4,
\tag{2.29}
$$

where $C_4$ is a constant independent of $d$. These points create a separate part on the log-log plot which should be placed closely around a straight line with slope 1. The other large cluster of points remains at the same place as before adding the level shift and this part of the R/S plot of LRD data with level shift looks similar to the R/S plot of the original LRD data.

This result shows that the R/S plot can also be used for detection of level shifts in the data. Moreover, the linear part with slope 1 in the plot should be disregarded in the estimation of Hurst parameter of LRD processes. In this way in the cases when this separation is feasible a reliable estimate of $H$ can be made even in the presence of level shifts.

## 2.4 Simulations

Beyond the analytical study the approach is added and completed by simulation examples which are presented in this Section. A comprehensive LRD test has been carried out with both synthetic and measured traffic data.

### 2.4.1 Setup

**Reference data sets**  A sample series of fractional Gaussian noise (fGn) was used as a reference for data exhibiting LRD. In this generated set the Hurst parameter was set to be 0.7. The other reference set is generated by Poisson process. In order to make a good

comparison, these data sets were set to have the same mean and variance of the value 10. Both data sets have the same size of 32 768 data.
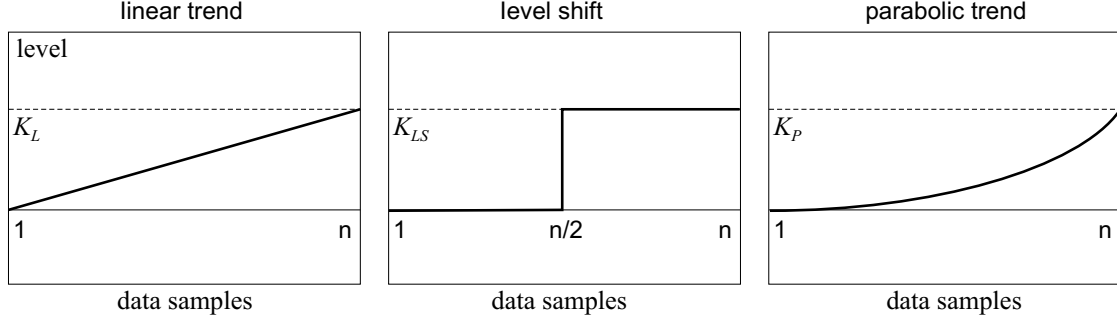


Figure 2.1: Types of non-stationarities: linear trend (left), level shift (middle), and parabolic trend (right). The value of $K_L$ (or $K_{LS}$, $K_P$) is set to be 5 in each case.

**Measured SUNET ATM cell-traffic**  Some series of ATM cell arrivals obtained from a real-time traffic measurement on the Swedish University NETwork (SUNET) [39] were also analyzed. Data traces were collected in 1996 based on a custom-built measurement tool which is able to record more than 8 million consecutive cell arrivals. The traces of the number of cell arrivals in a 1 ms time window were considered in LRD tests. The analysis of these data traces can illustrate the non-stationary effects in LRD estimation of real traffic.

**Types of non-stationarities**  There are two typical classes of non-stationarities observed in real traffic data: the level shift and the polynomial trends. Three simple cases were concerned in simulations: level shift with two states, linear trend, and parabolic trend. These effects were added to both data sets (see Figure 2.1 for the detailed information of these non-stationarities). Denote by 0.7-FGN the original fGn data, by 0.7-FGN_L the fGn set with linear trend, by 0.7-FGN_P the one with parabolic trend, and by 0.7-FGN_LS the one with level shift. The Poisson sets are marked with the same notations: POISS, POISS_L, POISS_P, POISS_LS. The following table gives more information about these data sets.

| Data sets | $K\_$ | $\hat{\mu}$ | $\hat{\sigma}^2$ | Data sets | $K\_$ | $\hat{\mu}$ | $\hat{\sigma}^2$ |
|---|---|---|---|---|---|---|---|
| 0.7-FGN | - | 10 | 10 | POISS | - | 10 | 10 |
| 0.7-FGN_L | 5 | 12.5 | 11.81 | POISS_L | 5 | 12.5 | 12.19 |
| 0.7-FGN_LS | 5 | 12.5 | 16.02 | POISS_LS | 5 | 12.5 | 16.35 |
| 0.7-FGN_P | 5 | 11.66 | 11.89 | POISS_P | 5 | 11.71 | 12.33 |

Table 2.1: The detailed information of investigated data sets ($\hat{\mu}$ and $\hat{\sigma}^2$ denote the sample mean and the sample variance, respectively).

The datagram of these data sets can be seen in Figure 2.2.
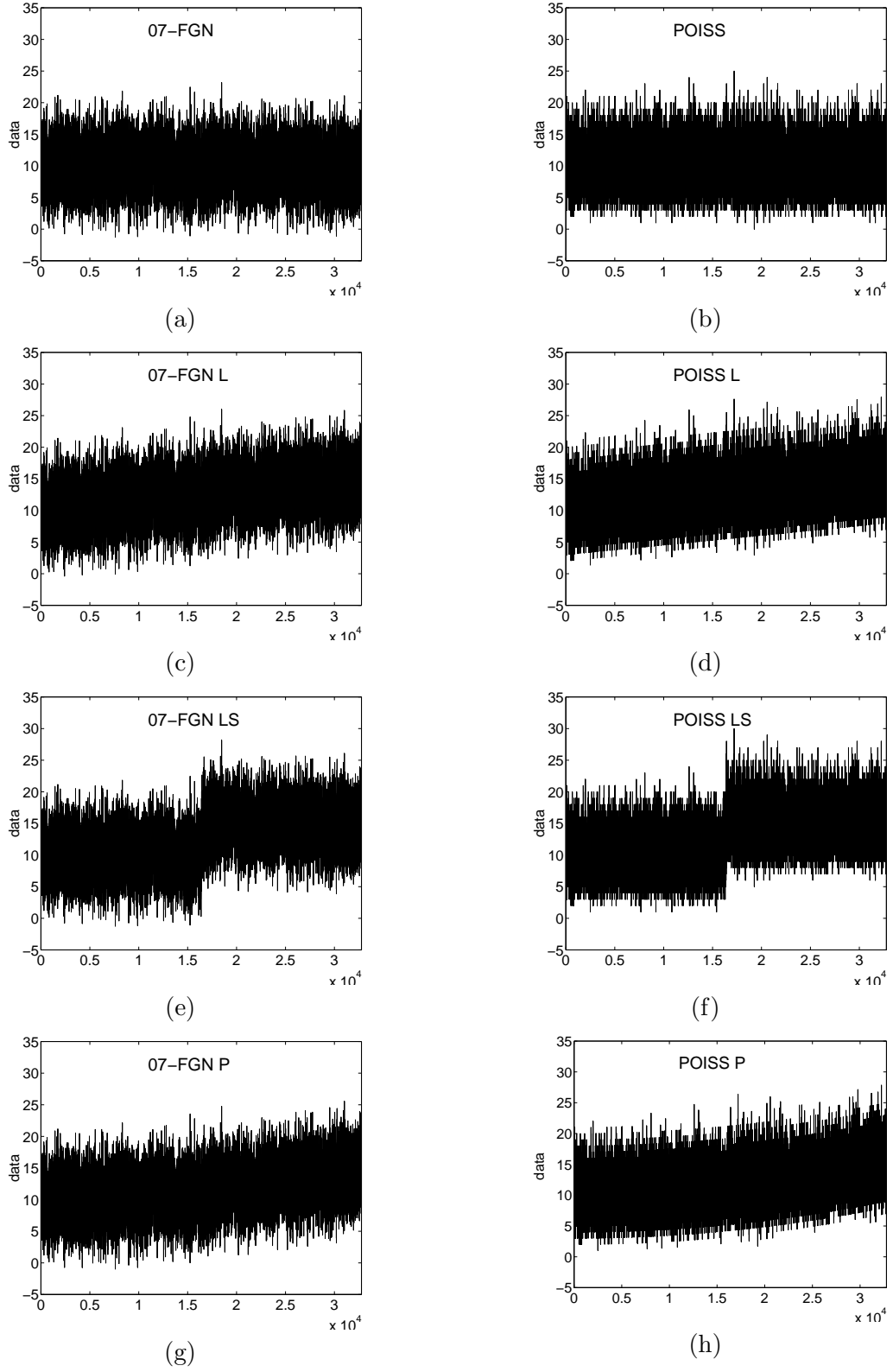
Figure 2.2: The datagrams of the investigated data sets. The 0.7-FGN means $m + \text{fGn}(\sigma^2, H)$, where $m = 10$, $\sigma^2 = 10$, $H = 0.7$; the POISS means Poissonian samples with $\lambda = 10$ ($\sigma^2 = 10$).
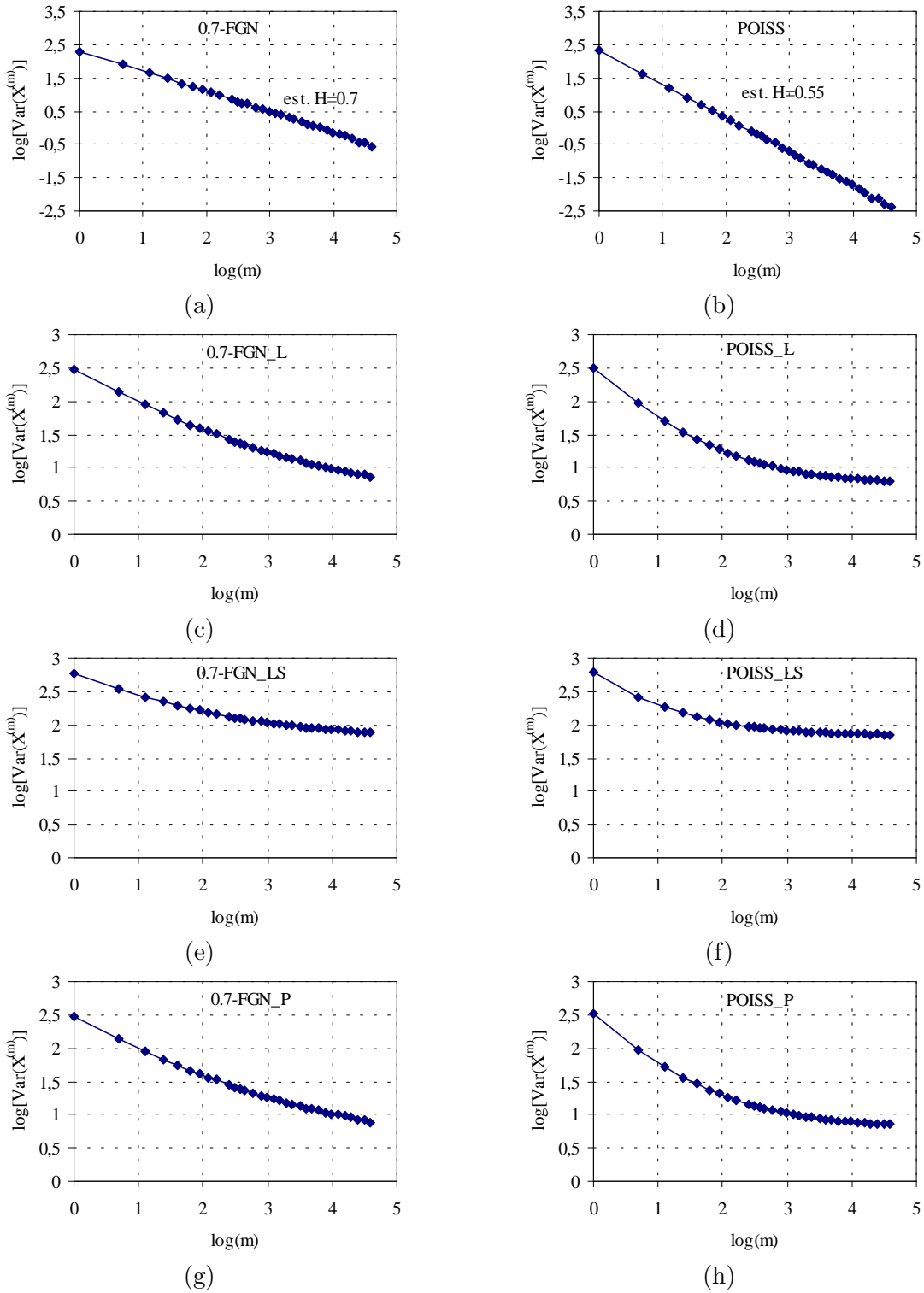
Figure 2.3: The variance-time plots. Left: variance-time plots of 0.7-FGN, 0.7-FGN_L, 0.7-FGN_LS, and 0.7-FGN_P. Right: variance-time plots of POISS, POISS_L, POISS_LS, and POISS_P.
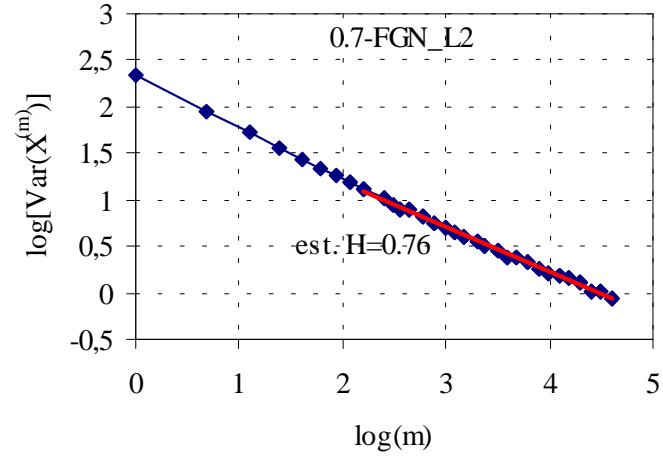
Figure 2.4: The variance-time plot of the 0.7-FGN_L2 set ($K_L = 2.5, \hat{\mu} = 11.25, \hat{\sigma}^2 = 10.38$)
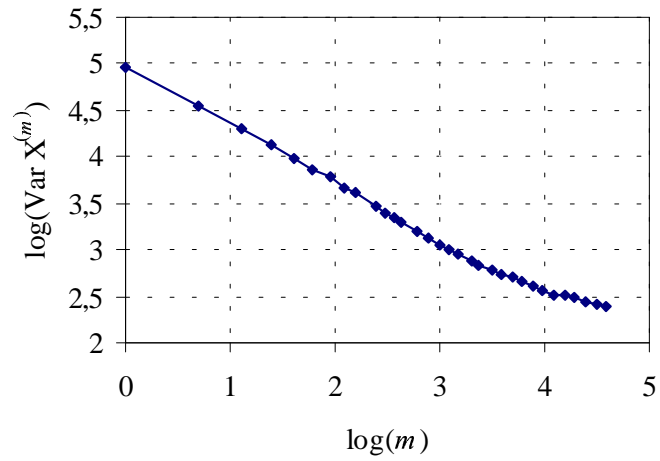


Figure 2.5: The variance-time plot the SUNET ATM data

### 2.4.2   Empirical results

**Variance-time plot**   Results of variance-time analysis can be seen in Figure 2.3. The variance-time plot estimated on the original data sets, 0.7-FGN and POISS, gives the exact values of Hurst parameter that were expected: $H = 0.7$ for 0.7-FGN data set and $H = 0.5$ for POISS one (see Figures 2.3.a and 2.3.b). However, variance-time plot is very sensitive to the investigated non-stationarities. As seen in Figures 2.3.c, 2.3.d, 2.3.e, 2.3.f, 2.3.g, and 2.3.h, the variance-time plots are all convex curves and a careful observation reveals that no linear parts are found in these plots. Moreover, comparing 2.3.c with 2.3.d, 2.3.e with 2.3.f, and 2.3.g with 2.3.h, there are no significant differences between the variance-time plots of the data sets of the fGn with trends and level shift and the Poisson with trends and level shift, respectively.

The variance-time plots were also analyzed for the 0.7-FGN data set with a smaller linear trend (the value of $K_L$ of this linear trend is 2.5), see Figure 2.4. In this case the plot of the new series 0.7-FGN_L2 seems to be linear which is tempting to make an estimate but the estimated value of $H$ is 0.76, which is far from the real value. It means that getting an estimate from the linear part (at large time-scales) of the variance-time plot (as usually done in practical analysis) can produce misleading results.

A result of variance-time analysis of the SUNET ATM data, presented in Figure 2.5, is shown for example. The measured ATM traffic is bursty in nature and although several pre-processing procedures were done in this trace it is difficult to detect a certain trend. However, the curve is very similar to those obtained with level shift or trends in Figure 2.3.e and 2.3.f. As discussed above to avoid misleading results estimation of $H$ cannot be applied in this case.

These simulation result confirms the analytical results presented in Section 2.3.1 and 2.3.2 and also shows that short-range dependent (SRD) processes with non-stationarities can produce the same variance-time plot as LRD processes. Moreover, in the case of LRD processes trends can significantly destroy the accuracy of the estimation of the $H$ parameter.

**R/S plot**   Figure 2.6 shows the results of the R/S tests. The effects of the linear and the parabolic trend are revealed in the rise of the upper tail of the R/S plots (see Figure 2.6.c, 2.6.d, 2.6.e, and 2.6.f). However, if we extract this part from the plot, the linear rest of the plot shows the exact slope which is seen in the R/S plot of the original data sets, Figure 2.6.a and 2.6.b.

The interesting results are found in the plots of data sets with level shift, see Figure 2.6.e and 2.6.f. On one hand, these plots seem to be constructed from two parts which are independent of each other. The lower parts look almost like the R/S plot of the original sets as comparing 2.6.e with 2.6.a and 2.6.f with 2.6.b. On the other hand, the upper parts are nearly the same in both plots. Thus it is reasonable to assume that the lower parts belong to the original data sets and the upper parts are due to the level shift. The R/S analysis is then applied for the level shift only and this assumption seems to be justified. Figure 2.9, which is the R/S plot of the level shift contains only the upper part. These results are in good agreement with the analytical investigation presented in Section 2.3.3.
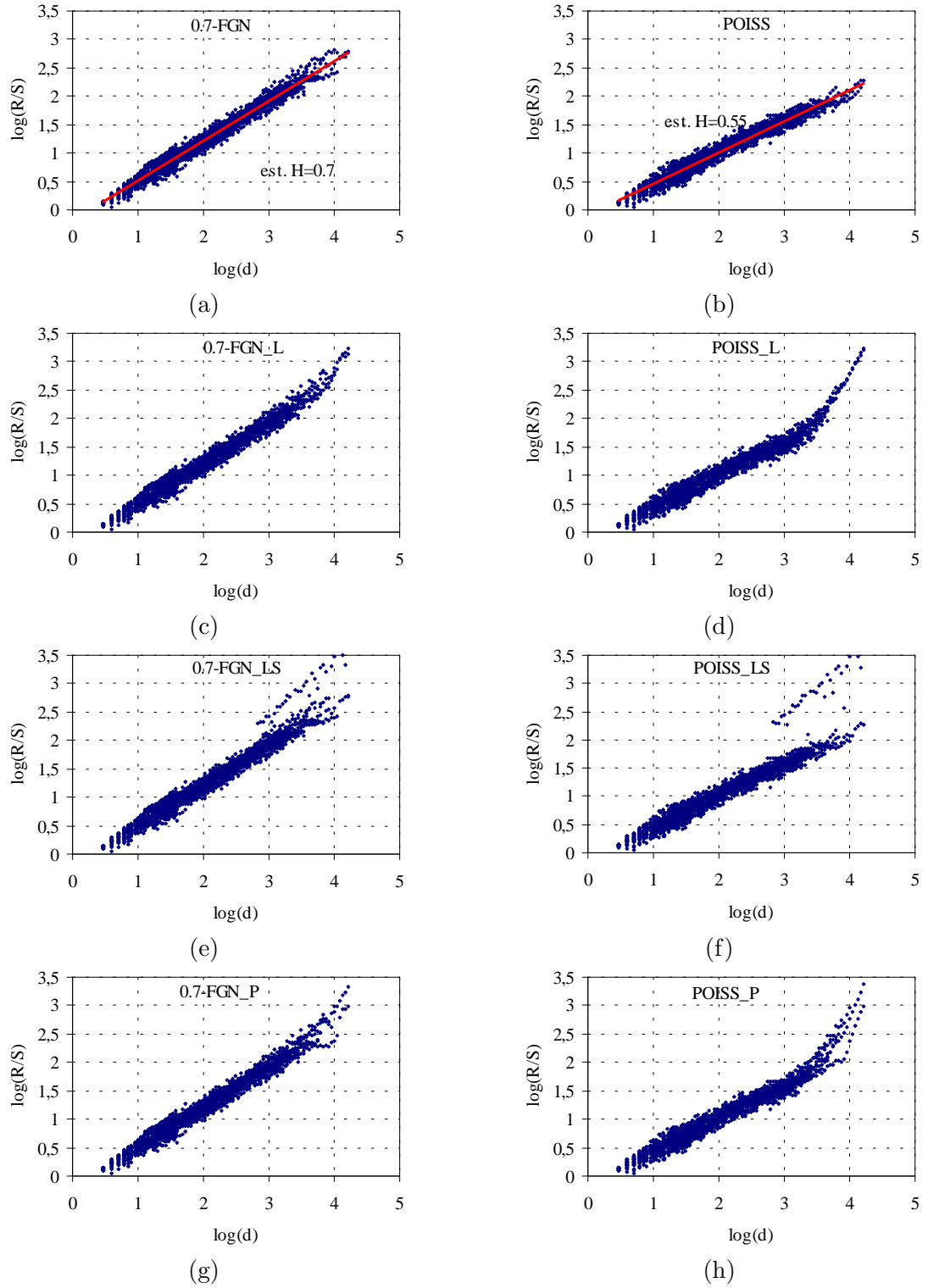
Figure 2.6: The R/S plots. Left: R/S plots of 0.7-FGN, 0.7-FGN_L, 0.7-FGN_LS, and 0.7-FGN_P. Right: R/S plots of POISS, POISS_L, POISS_LS, and POISS_P.
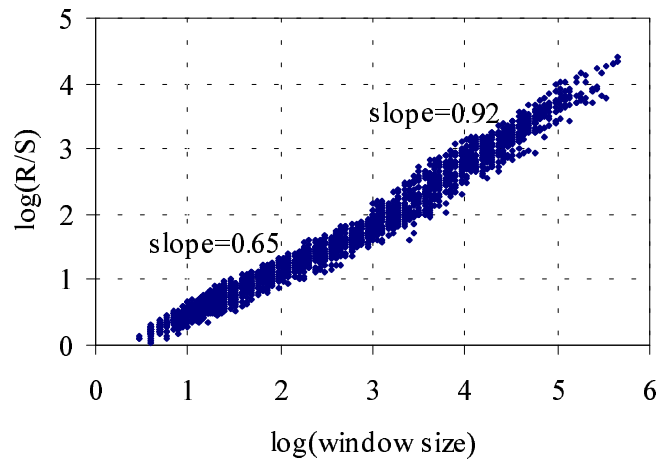
Figure 2.7: The R/S plot of the SUNET ATM data series
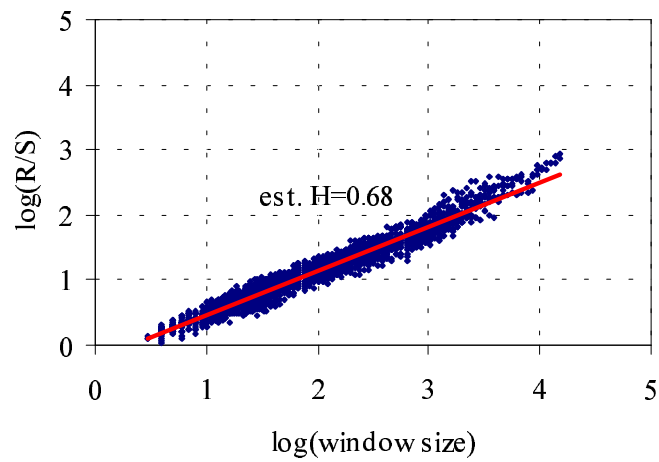


Figure 2.8: The R/S plot of the "stationary" subset of the the SUNET ATM data set

It can be seen that the presence of level shifts can be revealed by R/S plot and the reliable estimation of $H$ parameter for LRD processes with level shifts are possible if the cluster produced by the level shift is separable.
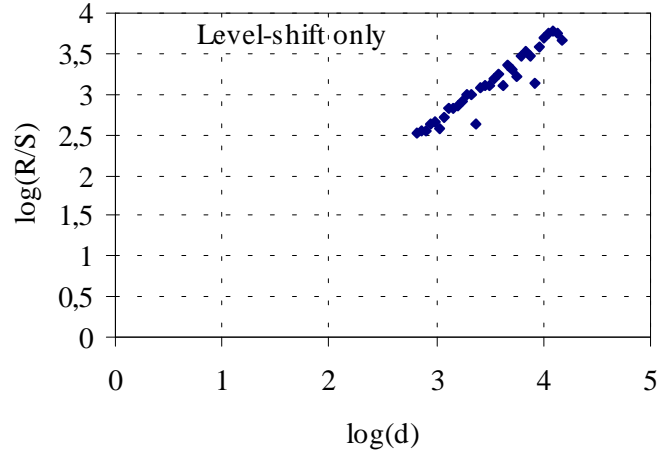


Figure 2.9: The R/S plot of a pure level shift.

An illustrative example from practice of such an effect can be seen in the R/S plot of the SUNET ATM series (Figure 2.7). The plot contains a breakpoint where the slope of the curve changes approximately in the middle of the figure. If one tries to estimate $H$ from the upper part of the plot it will result in a wrong value as we demonstrate it in the following. Figure 2.8 shows the R/S plot of a subset of the SUNET ATM set. The subset is gained from the original set after erasing some suspected non-stationary parts of the data selected by some stationarity analysis [16]. In Figure 2.8 the part of the curve with the higher slope disappeared and the lower part continues growing nearly as a straight line. An explanation of this phenomenon is the possible presence of several local level shifts in the original SUNET ATM data. The result also demonstrates that the important part for LRD parameter estimation is distorted by level shifts.

**Periodogram plot**   In the frequency domain, adding trend to data produces the increasing of low frequency components. Thus it is not surprising that the rise of the lower tail of the periodograms under the influence of different trends is observed (see Figure 2.10.c, 2.10.d, 2.10.e, 2.10.f, 2.10.g, and 2.10.h). This affects adversely the periodogram in both cases (the 0.7-FGN sets and the POISS sets) and the estimation of the Hurst parameter. Besides, the periodogram plot of the fGn with trend can be easily confused with the Poisson case.

Since the periodogram at low frequencies should be counted for estimation of the Hurst parameter, the presence of trends in LRD data destroys the testing and estimating capability of the periodogram plot.
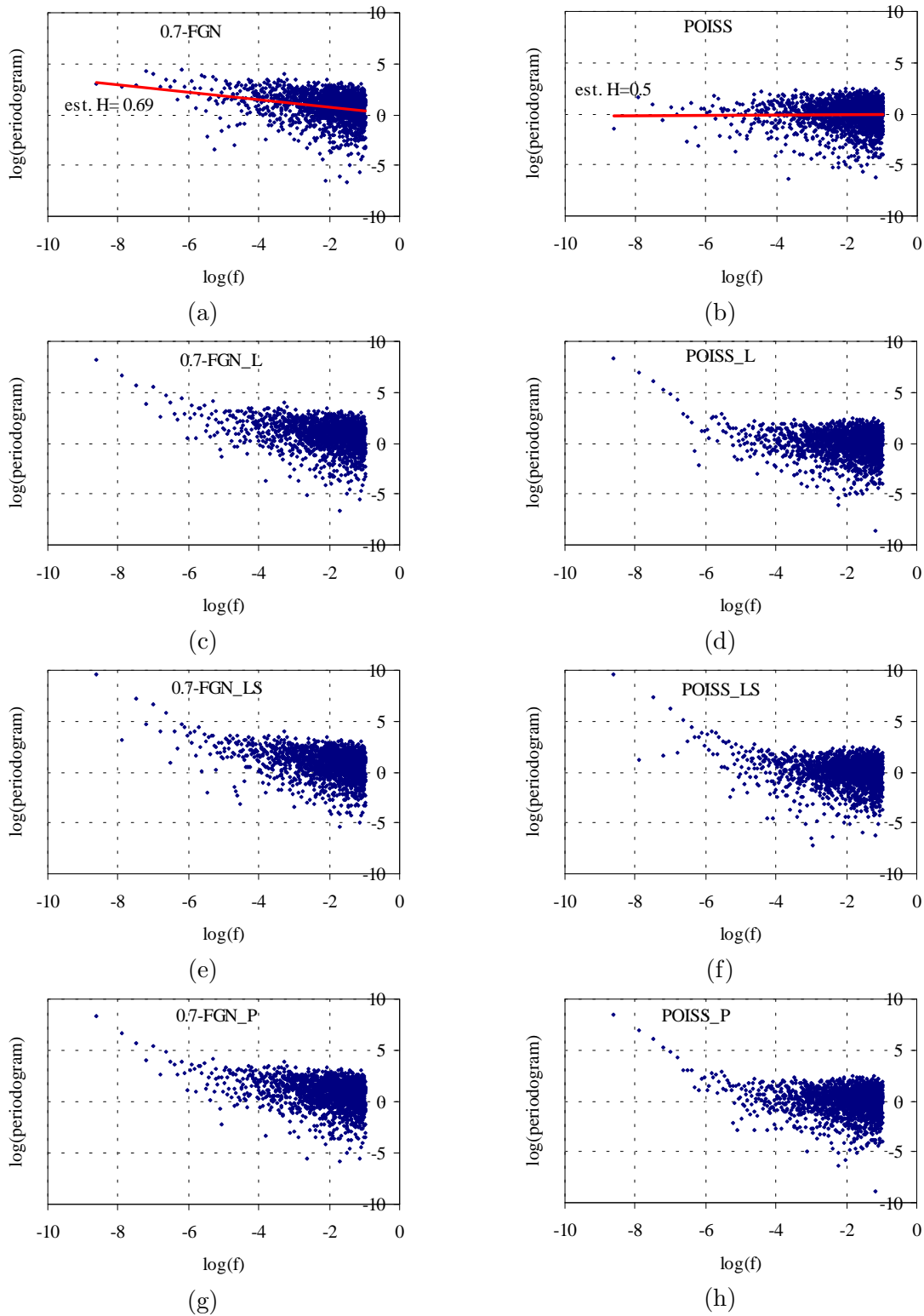
Figure 2.10: The periodogram plots. Left: periodogram plots of 0.7-FGN, 0.7-FGN_L, 0.7-FGN_LS, and 0.7-FGN_P. Right: periodogram plots of POISS, POISS_L, POISS_LS, and POISS_P.
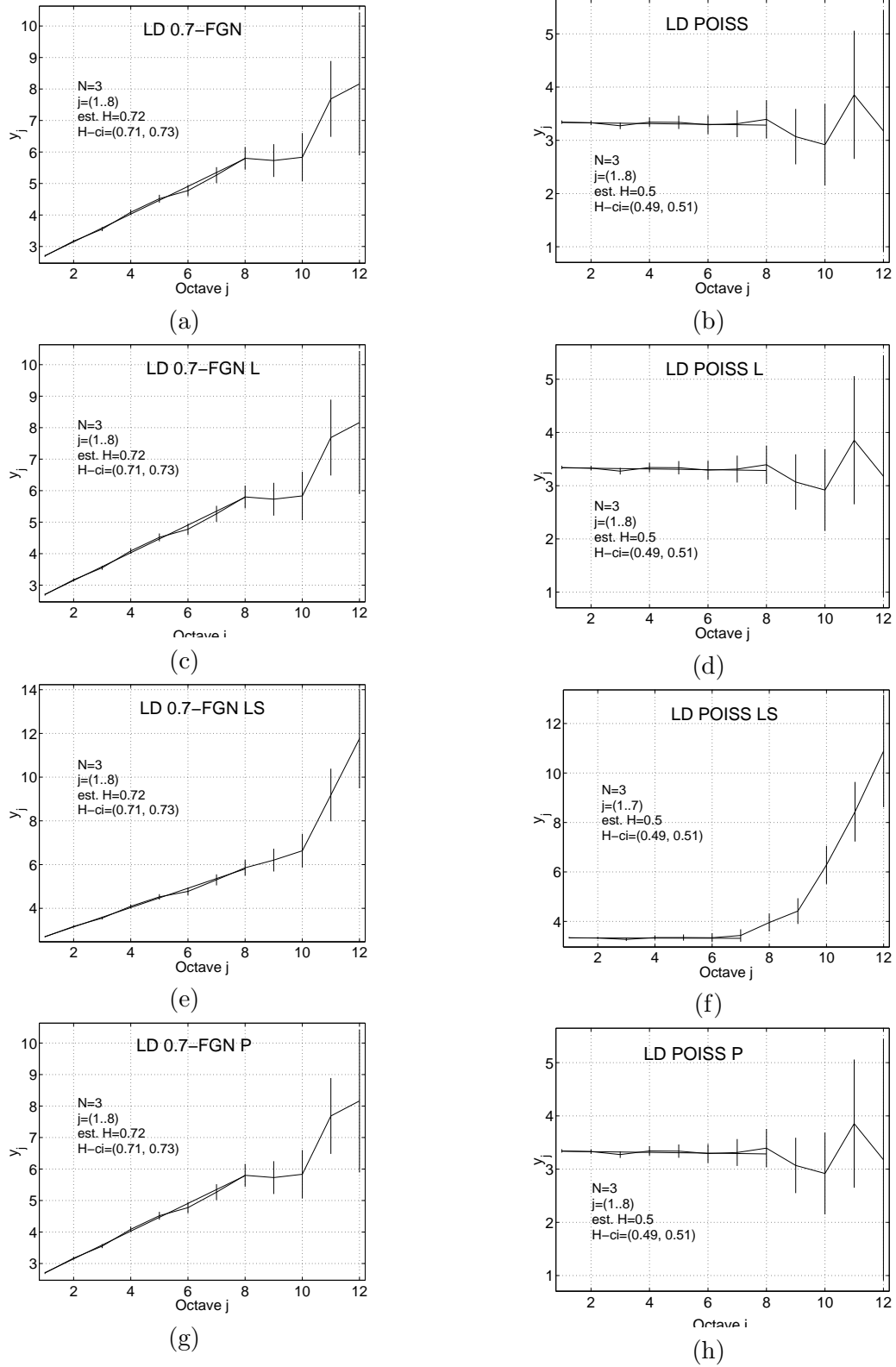
Figure 2.11: The Logscale diagrams. Left: Logscale diagrams of 0.7-FGN, 0.7-FGN_L, 0.7-FGN_LS, and 0.7-FGN_P. Right: Logscale diagrams of POISS, POISS_L, POISS_LS, and POISS_P.

**Wavelet based estimator** The LRD test based on the wavelet transformation (the Logscale diagram (LD)) is also investigated. As mentioned before, the influence of polynomial trends on this kind of LRD test can be avoided by an adequate choice of the vanishing moment $N$ of the wavelet function. This empirical work has justified this observation. In Figure 2.11 we see that the Logscale Diagrams give the robust estimate of the Hurst parameter around 0.72 for the 0.7-FGN sets and 0.5 for POISS sets independently of the presence and of the type of trends. Moreover, the simulation also shows that the LD is still robust in the presence of level shifts. As seen in Figure 2.11.e and 2.11.f the level shift added to the 0.7-FGN and the POISS sets slightly changes the result: the estimation of H is 0.72 with confidence interval (0.71, 0.73) for the 0.7-FGN_LS set and 0.5 with confidence interval (0.49, 0.51) for POISS_LS set.

## 2.5 Conclusion

Based on both analytical and simulation studies and examples from measured traffic it has been shown that the presence of different non-stationarities (level shifts, linear and polynomial trends) in the data can deceive several detecting and estimating methods of LRD.

These effects result in poor estimates of the Hurst parameter in the case of the variance-time plot and periodogram. Moreover, the estimated results can be confused with processes having short-range dependence with non-stationary effects. The suggestion is that the variance-time plot and the periodogram methods should not be used without a stationarity analysis.

The wavelet based method (the Logscale diagram) was found to provide a very robust estimation of $H$. Its estimation results are almost independent of the presence of the investigated trends and level shifts. The R/S analysis was also verified to be a robust estimator of the Hurst parameter of LRD processes. In addition, it was also demonstrated that the level shift can be detected by the R/S analysis, therefore this method can be well utilized in stationarity analysis.

The use of the R/S plot and the Logscale diagram for the estimation of Hurst parameter of LRD processes in the possible presence of the investigated non-stationarities is recommended.

# Chapter 3

# Scaling Analysis of IP Traffic Components

A number of studies, e.g. [46, 19, 47], have reported that aggregated LAN/WAN traffic is consistent with monoscaling (or self-similarity) at large time scales and multifractal scaling at small time scales. The physical explanations and engineering implications are also addressed in several papers [18, 47]. However, most of the studies have investigated the aggregated traffic and only a few papers have examined the nature of traffic components [5]. We think that the understanding of the characteristics of the individual components in the aggregation, i.e., a comprehensive analysis of different protocol layers with distinct traffic components is vital for establishing a correct physical understanding and modeling methodology.

In this chapter a comprehensive scaling analysis of IP traffic and its components is presented. The study focuses on the correlation and scaling behavior of IP traffic components on both transport and application layers. It is shown that the correlation structure of the aggregation is mainly determined by the component with the highest variance and correlations at the investigated time scale. It is also demonstrated that WAN traffic can exhibit complex multifractal structure even at large time scales. The aim of the study is to understand the characteristics of the aggregated IP traffic by analyzing its individual components.

## 3.1 Structure of the IP traffic

### 3.1.1 IP traffic measurements

Figure 3.1 presents the traffic measurements setup. A number of LANs located at the Informatics Building of the Budapest University of Technology and Economics are connected to the outside world by a 100MB FDDI and a 155MB ATM link. These networks are composed of several Ethernet based LANs which are referred to as Department Groups (DG) and each

DG consists of about 100 workstations. Connections between DGs and between a DG and the outer world are guaranteed by an ATM backbone. Ethernet frames are transmitted over the ATM backbone using LAN emulation. Workstations belong to staff members, Ph.D. students, and student laboratories using a variety of operating systems and network interfaces ranging from 10Base2 (BNC) through 100BaseT (UTP) to 100VGAnyLAN. A traffic monitoring tool, called Captie [49], captured the IP traffic on the ATM link between DG1 and the switch. The analyzer can monitor the data traffic transmitted over the link and record different statistics of data flows according to user requests. In the measurements both the incoming and outgoing traffic of the DG1 have been collected but only the aggregated incoming IP traffic, which is mainly generated by the WAN environment, is concerned.
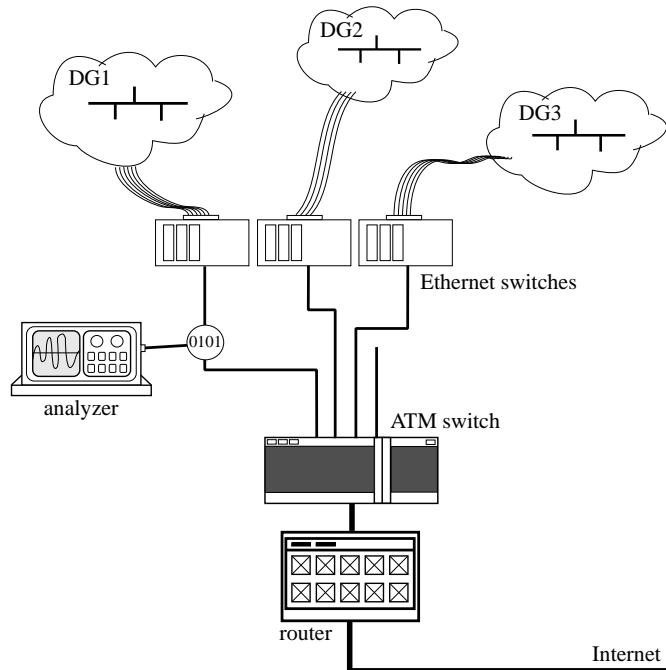


Figure 3.1: The configuration of the IP traffic measurements

During weekdays of April 1999 statistics of IP and non-IP traffic were continuously collected in log files every day from 8am to 6pm. The traffic measurements concentrated on the data volume transferred under IP packets, transport layer protocols such as TCP, UDP, ICMP, and OSPF, as well as application layer protocols such as HTTP, FTP, SSH, and SMTP. Data series representing the traffic measured in bytes per second used in most of analyzes are gained from these measurements.
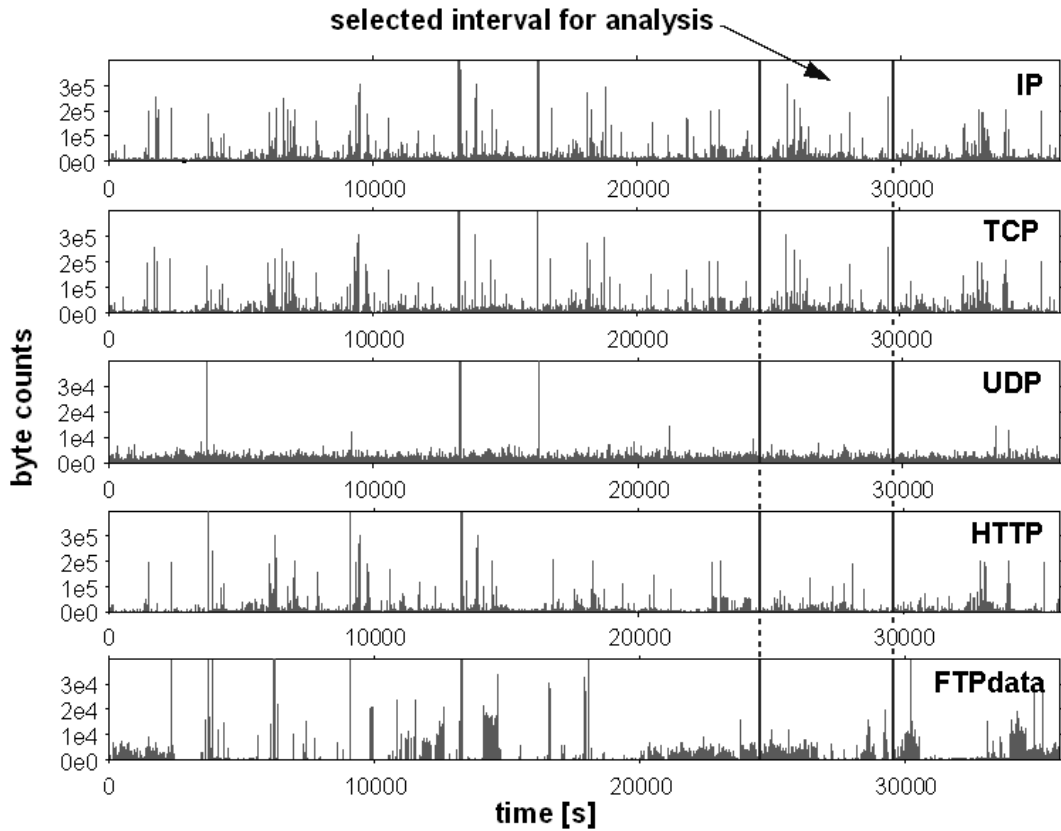
Figure 3.2: Traffic intensity of the IP and some higher layer protocols

### 3.1.2 Overview of the traffic

Figure 3.2 shows the traffic intensity in bytes per second for a typical IP traffic flow and its main components from the measured traces. Traffic bursts can be observed over the whole period of the measurement. It can be concluded from Figure 3.2 and from some more detailed investigations that huge peaks over a short period can occur at any time of the day so the well-known busy period concept from telephone traffic engineering cannot be applied. Visual investigation suggests that at the transport layer the TCP data is dominant and its behavior determines the characteristics of the IP traffic.

Besides the TCP traffic there is a considerable amount of UDP traffic as well but this sort of traffic is much smoother than the TCP and it does not seem to have any influence on the nature of the IP traffic. At application layer the HTTP and the FTPdata traffic take the main roles (the FTPdata traffic is differentiated from the FTPcontrol traffic because FTP control messages are transported over the IP network by separate packets) . However, the behavior of the FTPdata traffic is rather complex since the most of the FTPdata connections are transferred at low speed but traffic intensity also contains some extremely high jumps during short periods. The size of these jumps is often $10^3 - 10^5$ times greater than the typical

FTPdata connection speed. Therefore the empirical autocorrelation function computed from a finite series with such a peak may give misleading results. In addition, the analysis of a short time period of the FTPdata traffic (in order to validate the assumption about stationarity) may not give the complete characteristics of this traffic type.

### 3.1.3  Bandwidth share

Figure 3.4 and Figure 3.3 present the ratio of different protocols contributing to the overall load at the transport layer and the application layer, respectively. These results are the average values of several measurement days.
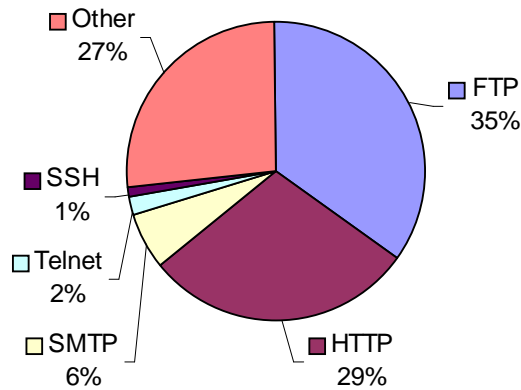


Figure 3.3: Bandwidth share of application layer protocols

On the one hand, at the transport layer the majority of data is carried by the TCP protocol which takes about 90% bandwidth of the whole volume of transferred data. The rest of the load mainly corresponds to the UDP protocol. The ICMP and OSPF control messages share only 1-2% of the transport layer traffic volume. On the other hand, based on the results in Figure 3.3 it can be concluded that among the applications the HTTP and the FTP traffic are dominant in volume.

### 3.1.4  Stationarity analysis

An important assumption in traffic modeling is stationarity. However, it is rather difficult to justify completely this assumption on the investigated data series. The real traffic data over a longer time period often appear to have local trends, load jumps, cycles, etc., which are the characteristics of non-stationary processes. As presented in the previous chapter analysis of traffic data without regard to stationary effects may end in misleading results. Thus a straightforward approach to overcome this problem is to select time periods where
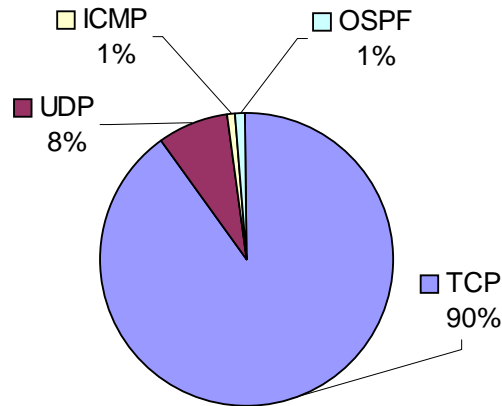
Figure 3.4: Bandwidth share of transmission layer protocols

the assumption of stationarity can be accepted, more precisely, where the appearance of non-stationarity is not detected.

A simple test to detect stationary periods in the data is to slide a window along the measured data and investigate the variations of the data averages in the windows. The datagram of this series may give some information about level shift, trends, etc. However, for bursty data like the measured traffic presented above this method does not provide appreciable results. To achieve this goal another tool is also applied which is based on the *change point detection method*. The main idea of this method is to slide a window along the data series and then compare the distribution of data samples in two equal halves of the window. If the two distributions are significantly different then the assumption of the stationarity covered by the window is rejected. The comparison task of distributions of the two series with equal size is performed by applying the Kolmogorov-Smirnov test, see more details in [16].

Based on the stationarity tests several subsets from the whole measured data have been selected for analysis. The subsets are obtained from time intervals where the IP traffic and also each component of both transport layer protocol traffic and application layer protocol traffic can be justified to be stationary.

The next Section presents the analysis of about an hour trace chosen from a collection of selected series by the stationary test (see the selected part in Figure 3.2).

## 3.2 Correlation and scaling analysis

In this Section the characteristics of the investigated IP traffic and its components is presented. First, the study of the correlation structure is shown in details and the question

how the correlation of the different components produces its effect on the aggregation is discussed. Second, the long-term scaling is investigated and the LRD test results are presented and discussed. Third, the detailed scaling of each component of the IP traffic is analyzed.

### 3.2.1   Correlation structure

There are a number different components with different contribution effects on the correlation structure of the aggregated IP traffic. The identification of the characteristics of the components which mainly determine the characteristics of the aggregated IP correlation structure is vital for the understanding of IP traffic structure.

Consider the superposition of a number of independent traffic streams, i.e. $A = \sum_{i=1}^{N} A_i$. Denote the autocorrelation function and the covariance function of $A_i$ by $\rho_{A_i}(k)$ and $\gamma_{A_i}(k)$, respectively. A straightforward calculation shows that $\gamma_A(k) = \sum_{i=1}^{N} \gamma_{A_i}(k)$. Therefore the autocorrelation function of the aggregated traffic stream is given by

$$\rho_A(k) = \frac{1}{\sum_{i=1}^{N} \sigma_{A_i}^2} \sum_{i=1}^{N} \sigma_{A_i}^2 \rho_{A_i}(k), \tag{3.1}$$

where $\sigma_{A_i}^2$ is the variance of the component traffic volume in the chosen time unit for the stream $i$, $\sigma_A^2 = \sum_{i=1}^{N} \sigma_{A_i}^2$.

As $k \to \infty$ the autocorrelations of short-range dependent (SRD) streams vanish rapidly and the autocorrelations of LRD streams decay asymptotically as $k^{-\beta}, \beta = 2 - 2H$ (see details in Section 1.1). The autocorrelation of $A$ is determined by the LRD stream which decays at the lowest rate, i.e. $\rho_A(k) \sim k^{-\min \beta_i}$. Therefore the LRD stream with the highest $H$ parameter will dominate and the aggregation will be LRD with this parameter. However, in practice the correlation lag $k$ can be only investigated for large values instead of infinity. In this case the variance of the streams should also be considered because the variance is the weight in the sum in Eq. (3.1). Consequently, it may happen that there is a stream with a faster decaying autocorrelation function but with a high variance and this stream will dominate in the autocorrelation function of the aggregated traffic stream on the investigated time scale. Moreover, it also follows from Eq. (3.1) that the volume of traffic has no influence, so a small fraction of traffic with high variance and slowly decaying autocorrelation can determine the autocorrelation of the whole aggregation.

The properties discussed above can be observed in the analysis of the measured IP traffic. The sample autocorrelation functions of different measured traffic flows are presented in Figure 3.5. In the evaluation of these functions (and especially investigating correlation coefficients at large lags) it is observed that the correlation coefficients often have small values. In these cases one has to take care of the confidence interval which can be roughly estimated by the $\pm 2/\sqrt{n}$ rule corresponding to significance 0.05. In this analysis case 3600 samples were used which give about 0.03 for this confidence interval. A slow decay can be observed in correlation of the IP traffic which indicates a possible presence of LRD. The transport layer protocols, TCP, UDP, ICMP, and OSPF, work above the IP layer so the IP traffic is the aggregation of these flows. Among these components the TCP
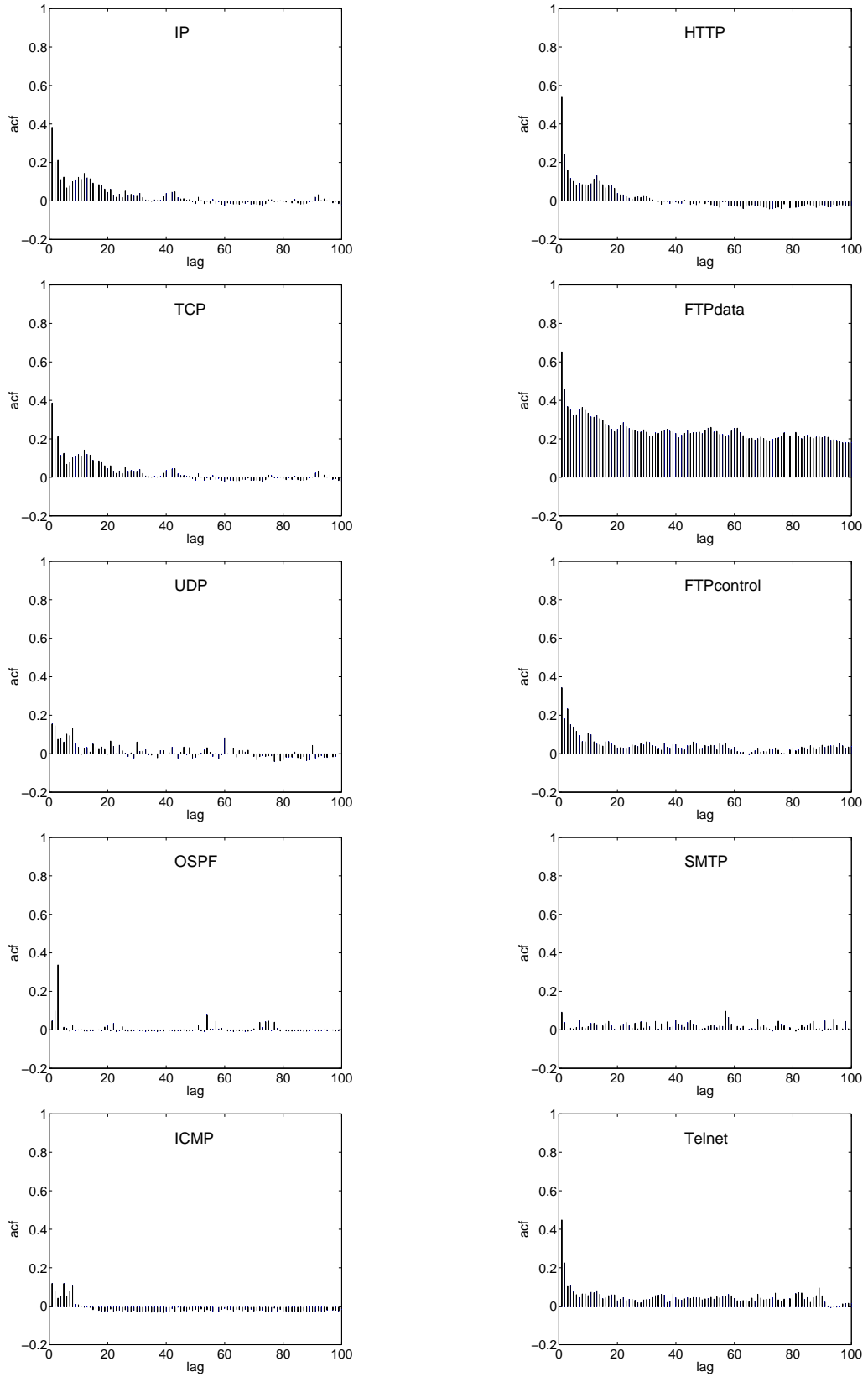
Figure 3.5: Correlation structure of IP traffic and its components

traffic takes the dominant role since the form of its correlation absolutely determines the correlation structure of the IP. This is so because the TCP series has sample variance which is much greater than that of the other transport traffic series (see in Table 3.1). This observation is in accordance with Eq. (3.1) and the discussions above. *Note that TCP has a significant impact on the correlation structure of the IP aggregation because it has the highest variability on the investigated time scale and not because it has the highest bandwidth share in the IP aggregation.* Besides the TCP a possible long-term decay of the UDP was also observed. The ICMP and the OSPF seem to be SRD. However, the final conclusions about correlation structure are stated just after detailed investigations of LRD presented in the next subsection.

At the application layer traffic carried by the HTTP, FTP, SMTP, and the Telnet protocols is considered. All of these traffic flows are components of the TCP traffic aggregation. Figure 3.5 shows that the autocorrelation functions of HTTP, FTPdata, FTPcontrol, and Telnet all seem to have a long-term decay. Moreover, it is also seen that the correlation structure of the TCP inherits the form of the correlation structure of HTTP traffic in spite of the fact that the FTPdata appears to have stronger correlation and slower decay. By investigating the sample variance of these components in Table 3.1 it is found that the HTTP traffic has the greatest variance value, which is at least 60 times greater than the variances of the other traffic flows and this is the reason for its dominance to form the autocorrelation of the TCP aggregation. *Note again that HTTP is the dominant protocol to influence the correlation structure of the TCP aggregation because its high variability on the investigated time scale.* Of course, the correlation structures of these protocols are the results of the interactions between these protocols. For example, the correlation structure of TCP is the joint result of the contributing protocols (mainly HTTP) and the TCP mechanism rather than simply the "HTTP forms the correlation structure of TCP".

### 3.2.2 Long-range dependence analysis

In this study the variance-time plot, the R/S analysis, and the periodogram plot were used for LRD testing and estimation. The results are verified by the Logscale Diagram based on the wavelet transform (see more details in Section 2.1).

Results of the LRD analysis are summarized in Table 3.1. It should be noted that traffic volumes of the transport layer protocols and of the application layer protocols are compared to the IP and the TCP volume, respectively. The LRD behavior of the IP traffic is determined by the TCP traffic because it has both the largest Hurst parameter and variance among the transport protocols. This finding is in accordance with the discussions in the previous subsection. In the case of general protocols used for network control (ICMP and OSPF) the LRD tests failed. Considering also their correlation structure shown in Figure 3.5 it can be concluded that they are in the class of SRD traffic. UDP was found to be LRD but with smaller variance and Hurst parameter compared to TCP.

In the application layer traffic the HTTP is dominant to form the LRD characteristics of the TCP traffic in spite of the fact that the FTPdata has larger Hurst parameter (see

| Traffic type | volume | variance ($.10^5$) | VT plot | R/S | Per. | corr. struct. |
|---|---|---|---|---|---|---|
| IP | 100% | 1951.4 | 0.72 | 0.73 | 0.75 | LRD H=0.73 |
| TCP | 88.5% | 1946.6 | 0.72 | 0.73 | 0.75 | LRD H=0.73 |
| UDP | 8.87% | 4.3 | 0.67 | 0.68 | 0.7 | LRD H=0.68 |
| OSPF | 0.88% | 2.1 | - | - | - | SRD |
| ICMP | 1.68% | 2.9 | 0.63 | - | - | SRD |
| TCP | 100% | 1946.6 | 0.72 | 0.73 | 0.75 | LRD H=0.73 |
| HTTP | 47.64% | 800.4 | 0.72 | 0.74 | 0.72 | LRD H=0.73 |
| FTPdata | 12.29% | 14.6 | 0.85 | 0.78 | 0.86 | LRD H=0.85 |
| FTPcontrol | 0.26% | 0.004 | 0.72 | - | 0.74 | LRD H=0.72 (!) |
| SMTP | 1.69% | 5.8 | - | - | - | SRD |
| Telnet | 1.99% | 1.5 | 0.7 | - | - | SRD |
| Others | 36.13% | | | | | |

Table 3.1: Summary of the LRD analysis of the IP based protocols

Table 3.1). As discussed above this is due to the fact that HTTP has a significantly larger variance compared to FTP. Note that some other analyzed FTPdata subsets do not exhibit LRD properties so a general conclusion about the correlation structure of this traffic type is carefully avoided. It has been found that the SMTP is SRD. Concerning the Telnet data series the comprehensive analysis has shown that this traffic is SRD in opposition to the LRD suggestion of the variance-time plot test. In the case of the FTPcontrol the LRD analysis indicates the presence of LRD with $H = 0.72$. By analyzing the datagram of this series it was found that the occurred long-term dependence is caused by the periodicity in control messages sending. Beyond that, the FTP control messages take only a negligible amount of the whole traffic with small variance. Therefore from a traffic engineering point of view the presence of this flow can be disregarded.

### 3.2.3 Scaling analysis

**Tests of scaling properties**

There are two simple methods for estimation of the scaling function $\tau(q)$ which can be found in fractal modeling literature[1]. The first one is based on the absolute moments of the process and it calculates $\tau(q)$ directly from the raw data. For a time series $X = \{X_i, i = 1, 2, \ldots, n\}$ the so-called *partition function* $S^m(q)$ can be given by

$$S^m(q) = \sum_{k=1}^{\lfloor n/m \rfloor} |Z_k^{(m)}|^q, \tag{3.2}$$

---

[1]It is more correct to call these methods as scaling tests because they are concentrated in estimation of only the scaling function. However, as presented in Def. 1.3.1 the full description of multifractality also consists of the moment factor $c(q)$.

| Traffic type | volume | scaling structure |
|---|---|---|
| IP | 100% | multifractal |
| TCP | 88.5% | multifractal |
| UDP | 8.87% | none |
| OSPF | 0.88% | none |
| ICMP | 1.68% | none |
| TCP | 100% | |
| HTTP | 47.64% | multifractal |
| FTPdata | 12.29% | monofractal $h = 0.74$ |
| SMTP | 1.69% | none |
| Telnet | 1.99% | none |
| Others | 36.13% | |

Table 3.2: Summary of the scaling analysis of the IP based protocols

where $Z_k^{(m)} = \sum_{i=1}^m X_{km-m+i}$. It is easy to derive from the definition of multifractality (Def. 1.3.1) that the logarithm of $S^m(q)$ scales linearly with the logarithm of $m$, i.e. $\log S^m(q) = \tau(q) \log m + c_1(q)$. Thus a process is tested to have scaling properties if the plot of $\log S^m(q)$ against $\log m$ is a linear line for different values of $q$. The scaling function $\tau(q)$ is then calculated from the slopes of these lines [44].

The second method also shares the same principle as the first one but it differs considering that the calculation is done in the wavelet domain of the process. Denote the discrete wavelet transform representations (wavelet coefficients) of the series $X$ of size $n$ at scaling level $j$ by $d_X(j,k)$, $k = 1, 2, \ldots, n_j$, where $n_j = 2^{-j} n$. The $q^{th}$-order Logscale Diagram (q-LD) is the defined by the log-linear graph of the moment $\mu_j(q) = 1/n_j \sum_{k=1}^{n_j} |d_X(j,k)|^q$ against the octave $j$. Linearity of the q-LDs at different moment order $q$ suggests the scaling property of the series, i.e. $\log_2 \mu_j(q) = j\alpha(q) + c_2(q)$ where $\alpha(q)$ is called the *scaling exponent* and $c_2(q)$ is a constant [2]. Note that the scaling function $\tau(q)$ can be given by the re-transformation of $\alpha(q)$.

**Analysis results**

In this analysis study both the partial function method and the wavelet-based method were used. It was found that in some cases multifractal scaling is more convincing without subtracting the mean from the time series because the centered data has several disadvantages, see [46]. The scaling analysis was performed both with and without subtracting the mean but no significant differences were found in the results. The results presented here are related to the centered data because it is the case when there are hopes to find possible self-similar scaling [51]. A summary of the scaling analysis results are shown in Table 3.2.

The results for the IP data series are presented in Figure 3.6. Concerning the LD of moment order $q = 2$ in Figure 3.6(a) a nearly linear interval of the LD plot at octaves

$1 \leq j \leq 5$ can be observed[2]. The larger values of $j$ were not considered because of the limited size of the data set and also because the set of the wavelet coefficients at large scaling levels contains only a few values, which cannot give a reliable approximation. (These considerations are also taken into account in scaling analysis of other flows.) A linear regression to the interval gives an estimation of LRD parameter $H = 0.76$ with confidence interval $(0.73, 0.8)$. The result deviates slightly from estimates of $H$ provided by other LRD tests in Table 3.1 but the confidence interval still includes those values.
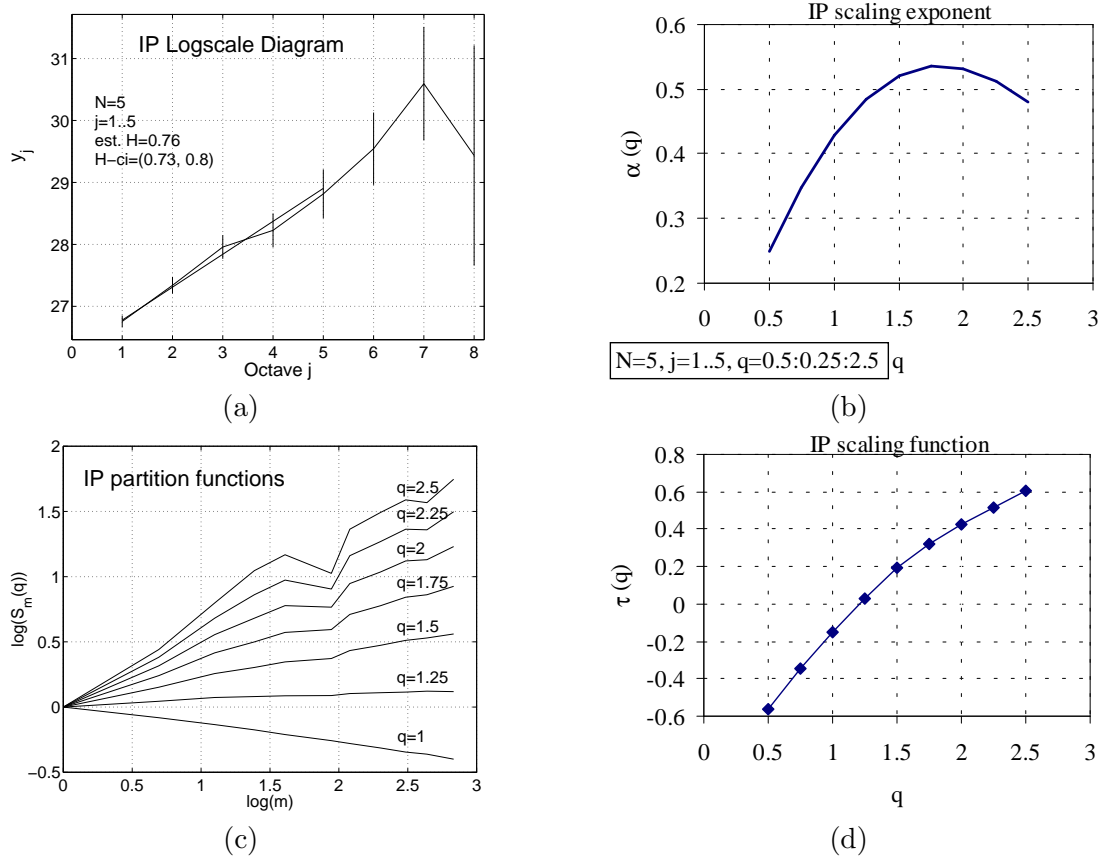


Figure 3.6: Scaling analysis results of the IP traffic

LDs of the IP traffic computed at different $q$ provide the estimation of the scaling exponent $\alpha(q)$ presented in Figure 3.6(b). The non-linear curve of the scaling function suggests that IP traffic has a multifractal structure on these time scales. The re-normalized partition functions of the IP traffic are depicted in Figure 3.6(c). (Re-normalization was performed in order to have the same intercepts of the curves for all $q$.) The estimation of the scaling function $\tau(q)$ in Figure 3.6(d) based on the partition functions shown in Figure 3.6(c) also confirms these findings concerning multifractal scaling.

---

[2]In this LD plot an improved estimation was used ($y_j = \log \mu_j + g_j$) with a correcting factor $g_j$ described in [2]

In investigation of data series at the transport layer protocols the scaling analysis showed that although the UDP traffic may have LRD property as discussed but the scaling tests of UDP failed. It has been found that the OSPF and the ICMP traffic flows also do not have scaling structure. In the case of the TCP traffic it can be observed that its scaling structure is similar to the scaling structure of the IP traffic. The estimated $\alpha(q)$ and $\tau(q)$ shown in Figure 3.7 rather resemble these functions of the IP traffic. It can be concluded that the TCP traffic also exhibits multifractal scaling.
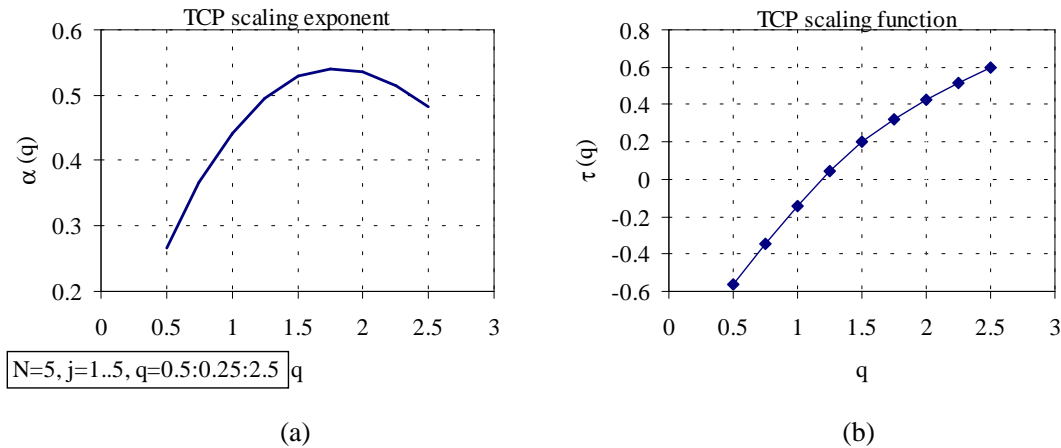


Figure 3.7: Scaling analysis results of the TCP traffic

The scaling structure of application layer protocols was also analyzed. The analysis results of the HTTP can be seen in Figure 3.8. Both the scaling exponent $\alpha(q)$ and the scaling function $\tau(q)$ have convex curves which suggest the presence of multifractality. Moreover, the estimated $\tau(q)$ is nearly the same as in the case of the IP and the TCP traffic. Analysis results of the FTPdata are shown in Figure 3.9. It can be seen that both the scaling exponent $\alpha(q)$ and the scaling function $\tau(q)$ are linear functions of $q$. Therefore, the selected FTPdata set reveals clear evidence of monofractality. However, according to the earlier discussions, the identified monofractal structure is not the general conclusion about the characteristics of the traffic carried by the FTP protocol. Finally, it was also found the SMTP and the Telnet traffic do not exhibit a scaling structure.

These results confirm the results presented in [19, 18, 22] showing that WAN traffic is LRD. However, these findings are also complemented by demonstrating that *WAN traffic can exhibit a complex multifractal structure not only at small but also at large time scales.* This result questions some explanations arguing that self-similarity at large time scales is due to the additive property of aggregated traffic streams and multifractal phenomena at small time scales are mainly caused by the hierarchical structure of TCP/IP protocols [46, 47]. A possible answer for this problem is that the traffic aggregation of not so many sources still inherits the scaling structure observed at small time scales. However, more accurate explanation should be found for the large scale multiscaling behavior of the traffic.

In addition, the analysis revealed that *the aggregation is composed of components with*
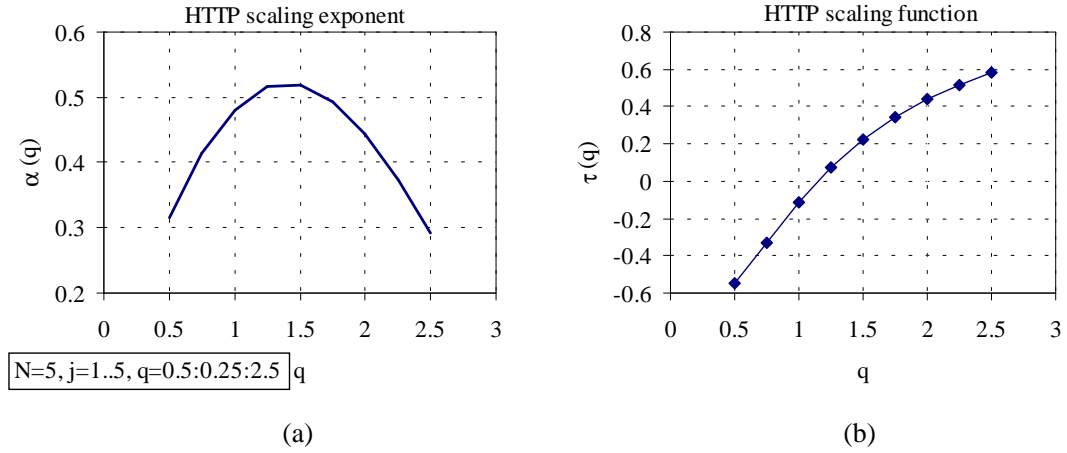
Figure 3.8: Scaling analysis results of the HTTP traffic
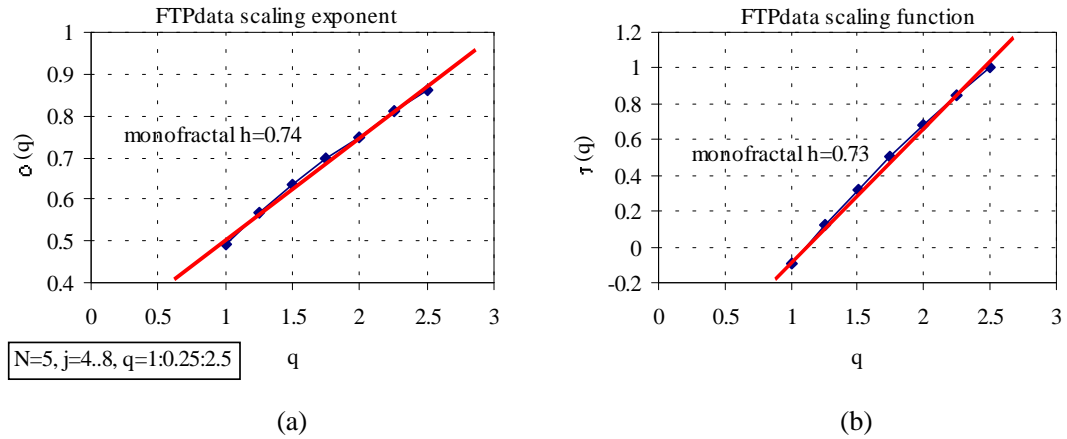


Figure 3.9: Scaling analysis results of the FTPdata traffic

*very different scaling behavior* (no scaling, multifractal scaling, monofractal scaling). The typical data traffic do not have permanent scaling characteristics like self-similarity or multifractal. The actual fractal property depends on where and when the traffic is observed. Therefore modifications and developments to guaranties the quality of data transmission in the networks should be elaborated to avoid doing blind applications with useless results.

## 3.3 Conclusion

In this chapter a complete scaling study of a wide range of IP traffic measurements has been presented. It has been found that the IP traffic is bursty during the whole day and sometimes it also contains extremely high traffic peaks over a short time period. These

observations are questioning the concept of busy period in case of this kind of IP traffic.

A stationarity analysis has been carried out prior to the correlation and scaling studies. A time period of the IP traffic, in which the aggregated IP traffic and all of its analyzed components at both transport and application layers can be considered to be stationary, is then selected.

The impacts of different characteristics of the correlation structures of the components on the correlation structure of the aggregation has been investigated. It was found that the ruling impact is due to the component which has the highest variance and also significant correlations on the investigated time scale. Among the transport layer and the application layer protocols the TCP and the HTTP were found to have these properties, respectively, which is the main reason (and not the high bandwidth share!) of the dominance of these protocols.

At the transport layer both TCP and UDP exhibit LRD but only the TCP has detectable multifractal structure. Other protocols at this layer were found to be SRD with no scaling properties.

At the application layer both HTTP and FTP have LRD properties. Multifractal and monofractal scaling have been identified for HTTP and FTP, respectively. However, it was observed that the scaling of FTP traffic is not a general characteristics.

It can be concluded that the investigated IP traffic is a LRD aggregate of components with different scaling properties resulting in a complex multifractal structure for the aggregated WAN traffic even at large time scales.

# Chapter 4

# Queuing Performance Estimation for General Multifractal Traffic

Queuing performance evaluation is an essential issue of network dimensioning and resources management. With the finding of the fractal nature in network traffic queuing analysis of fractal traffic input becomes a challenge in queuing theory. Several important results have been published so far [57, 6, 53, 23, 35], but most of the results are restricted to self-similar traffic types. A group of studies has proven that the fBm based models have a tail queue distribution that decays asymptotically like a Weibullian law [42, 14]. This important result shows that queues with fBm input have a much slower decay than that of the exponential. However, these approaches are based on Gaussian property of the input process and cannot be extended to other processes with scaling properties. In addition, there are only few queuing results available in the cases when traffic has more complex scaling behavior [45].

The objective of this study is to contribute to the queuing theory of multifractal queues and also to the traffic engineering implications. In this chapter an approximation for the tail asymptotics in an infinite capacity single server queue serviced at a constant rate driven by general multifractal input process is presented. It is shown that in the special and important case of the monofractal fractional Brownian motion (fBm) input traffic the result gives the well-known Weibullian tail. It is also proved that the class of Gaussian processes with scaling properties is in the class of monofractal processes and the related characterization functions are derived. The queuing formula in the case of Gaussian input processes gives a queuing result which is in good agreement with the theory of Gaussian processes. A new practical method for queuing performance estimation of general multifractal traffic is provided applying the approximation. The validation of the method based on both analysis of simulations and measured network traffic have also been presented.

## 4.1 Queuing model

Consider a simple queuing model: a single server queue in continuous time, the serving principle for offered work is defined to be FIFO (First In, First Out), the queue has infinite buffer and constant service rate $s$. Denote by $X(t)$ the total size of work arriving to the queue from time instant $-t$ in the past up to this moment, time instant 0. The so called *workload process* $W(t)$ is the total amount of work stored in the buffer in time interval $(-t, 0)$, i.e.,

$$W(t) = X(t) - st \tag{4.1}$$

However, the current buffer length of the queue, denoted by $Q$, is of interest. This is the queue length in the equilibrium state of the queue when the system has been running for a long time and the initial queue length has no influence. If this state of the system does exist, i.e., stationarity and ergodicity of the workload process hold, and the stability condition for the system is also satisfied, i.e., $\limsup_t \mathbb{E}[X(t)]/t < s$, then:

$$Q = \sup_{t \geq 0} W(t), \tag{4.2}$$

where $W(0)$ is assumed to be 0. This equation is also referred to as *Lindley's equation*.

The input arrival process $X(t)$ is considered as a generally defined multifractal process presented in chapter 1 Def. 1.3.1, i.e., $\mathrm{E}[|X(t)|^q] = c(q)t^{\tau(q)+1}$. For the sake of simplicity the notion $\tau_0(q) = \tau(q) + 1$ is used later and it is also called the scaling function. The definition presents multifractal processes in terms of moments which leads to a more intuitive understanding of multifractality. In addition, it is the definition which describes multifractal in a complete way for possible analytical study of queuing systems.

## 4.2 Approximation for queue tail probabilities

The main proposition is now stated:

**Proposition 4.2.1.** *The probabilities for the queue tail asymptotic of a single queuing model with general multifractal input is accurately approximated by:*

$$\log(\mathrm{P}[Q > b]) \approx \min_{q>0} \log \left\{ c(q) \frac{\left[ \frac{b\,\tau_0(q)}{s(q-\tau_0(q))} \right]^{\tau_0(q)}}{\left[ \frac{b\,q}{q-\tau_0(q)} \right]^q} \right\}, \quad b \text{ large} \tag{4.3}$$

*where $\tau_0(q) := \tau(q) + 1$. The scaling function $\tau(q)$ and $c(q)$ are the functions which define the multifractal input process.*

**Proof**

Using Lindley's equation the tail probabilities of queue length can be rewritten of the form:
$P[Q > b] = P[\sup_{t \geq 0} W(t) > b]$. First consider the quantity $P[W(t) > b]$:

Replacing $W(t)$ by Eq. (4.1) we have

$$
\begin{aligned}
P[W(t) > b] &= P[X(t) - st > b] \\
&\leq P[|X(t)| > b + st] & (4.4) \\
&= P[|X(t)|^q > (b + st)^q], \qquad \text{for arbitrary } q > 0 \\
&\leq \frac{E[X(t)^q]}{(b + st)^q}, \qquad \text{using Markov's inequality.} & (4.5)
\end{aligned}
$$

Since the input process is multifractal defined by Def. 1.3.1 then:

$$
P[W(t) > b] \leq \frac{c(q) t^{\tau_0(q)}}{(b + st)^q}
$$

$$
\Rightarrow \sup_{t \geq 0} P[W(t) > b] \leq \sup_{t \geq 0} \frac{c(q) t^{\tau_0(q)}}{(b + st)^q} =: \sup_{t \geq 0} f(t). \qquad (4.6)
$$

By straightforward calculation it is easy to see that that derivative of $f(t)$ equals zero when

$$
t_0 = \frac{b \tau_0(q)}{s[q - \tau_0(q)]} > 0.
$$

The second derivative of $f(t)$ at this point is

$$
f''(t_0) = c(q) t_0^{\tau_0(q) - 1} (b + s t_0)^{-q-1} s[\tau_0(q) - q] < 0,
$$

thus $f(t)$ has its maximal value at $t = t_0$. Note that $q > \tau_0(q)$ was assumed, this is justified by the fact that in the monofractal case $\tau_0(q) = qH < q$ and by the concavity of $\tau(q)$.

Therefore

$$
\sup_{t \geq 0} P[W(t) > b] \leq \sup_{t \geq 0} f(t) = c(q) \frac{\left[\frac{b \tau_0(q)}{s(q - \tau_0(q))}\right]^{\tau_0(q)}}{\left[\frac{bq}{q - \tau_0(q)}\right]^q}
$$

$$
\Rightarrow \log\left(\sup_{t \geq 0} P[W(t) > b]\right) \leq \log\left(c(q) \frac{\left[\frac{b \tau_0(q)}{s(q - \tau_0(q))}\right]^{\tau_0(q)}}{\left[\frac{bq}{q - \tau_0(q)}\right]^q}\right), \qquad \text{for arbitrary } q > 0
$$

$$
\Rightarrow \log\left(\sup_{t \geq 0} P[W(t) > b]\right) \leq \min_{q > 0} \log\left(c(q) \frac{\left[\frac{b \tau_0(q)}{s(q - \tau_0(q))}\right]^{\tau_0(q)}}{\left[\frac{bq}{q - \tau_0(q)}\right]^q}\right). \qquad (4.7)
$$

For a large class of stochastic processes (including fBm) the following limit holds [26]:

$$
\lim_{b \to \infty} \frac{\log(P[Q > b])}{\log(\sup_{t \geq 0} P[W(t) > b])} = 1. \qquad (4.8)
$$

In addition,

$$\log(\mathrm{P}[Q > b]) \geq \log(\sup_{t \geq 0} \mathrm{P}[W(t) > b]), \tag{4.9}$$

then the right-hand side of Eq. (4.7) is a upper bound of a lower bound on $\log(\mathrm{P}[Q > b])$. The used inequalities in Eq. (4.9) and Eq. (4.5) become tight for finite large $b$. Thus the approximation for the queue tail asymptotics is the following:

$$\log(\mathrm{P}[Q > b]) \approx \min_{q>0} \log \left( c(q) \frac{\left[ \frac{b\,\tau_0(q)}{s(q-\tau_0(q))} \right]^{\tau_0(q)}}{\left[ \frac{b\,q}{q-\tau_0(q)} \right]^q} \right), \qquad b \text{ large.}$$

$\square$

For positive multifractal processes, i.e. $X(t) > 0$, Eq. (4.4) is an equality. In addition, the approximation in Eq. (4.9) and the inequality in Eq. (4.5) turn to be more accurate approximations as $b$ tends to infinity. Thus the presented approximation is supposed to be asymptotically tight. The tightness and accuracy of the approximation is also experimentally investigated later in Section 4.3.4 and Section 4.4.

Considering the formula in Eq. (4.3) it can be seen that it has an implicit form and only the given form of the functions $c(q)$ and $\tau_0(q)$ can provide the final result. The reason behind this is that the definition for the class of multifractal processes gives no restrictions for the functions $c(q)$ and $\tau_0(q)$ (beyond that $\tau_0(q)$ is concave). *The conjecture is that the analysis of queuing systems with general multifractal input may produce some similar general results.* It means that there is no general queuing behavior for these systems as the Weibullian decay in the case of Gaussian self-similar processes [42]. An actual multifractal model will determine, for example, the queue length probabilities of the system.

## 4.3   Applications

### 4.3.1   Fractional Brownian motion

As a simple application, first consider a monofractal Gaussian process, called fractional Brownian motion (fBm) . The fBm is self-similar which is a simple case of monofractality and it is also Gaussian. The increment process of fBm is called fractional Gaussian noise (fGn). Queuing analysis of a single queue with fBm input is first presented by Norros [42] which showed the Weibullian decay for the asymptotic tail behavior, i.e., $\mathrm{P}[X > x] \sim \exp(-\gamma x^{\beta})$ with $\beta \leq 1$. This result is also justified by Large Deviation techniques in [14]. Applying this input process model to the queuing formula should show its use and robustness when comparing to these available results.

First it can be proven that any Gaussian process with scaling property is in the class of monofractal processes. Furthermore the following lemma also gives the explicit forms for $\tau(q)$ and $c(q)$.

**Lemma 4.3.1.** *A Gaussian process with scaling property is monofractal with parameters*

$$\begin{cases} \tau(q) & = & \frac{q}{2}\left[\tau(2)+1\right]-1 \\ c(q) & = & \frac{[2c(2)]^{q/2}}{\sqrt{\pi}}\Gamma\left(\frac{q+1}{2}\right), \end{cases}$$

*where $\Gamma(\cdot)$ denotes the Gamma function, $\Gamma(z) = \int_0^{+\infty} x^{z-1}\exp^{-x}\,\mathrm{d}x,\ z > 0$.*

The proof of this Lemma is provided in Appendix A.1.

Turning back to the fBm case with $c(2) = 1$ and $\tau(2) = 2H - 1$ where $H$ is referred to as the Hurst parameter, we have

$$\begin{cases} \tau(q) & = & qH - 1 \\ c(q) & = & \frac{2^{q/2}}{\sqrt{\pi}}\Gamma\left(\frac{q+1}{2}\right). \end{cases}$$

Insert these two functions into our formula in Eq. (4.3) we get

$$\log(\mathrm{P}[Q > b]) \approx \log\left(\min_{q>0}\left\{\frac{2^{q/2}}{\sqrt{\pi}}\Gamma\left(\frac{q+1}{2}\right)\frac{\left(\frac{bH}{s(1-H)}\right)^{qH}}{\left(\frac{b}{1-H}\right)^q}\right\}\right) =: \log(\min_{q>o} g(q)).$$

The minimum value of the $g(q)$ for $q > 0$ function can be easily determined by taking its derivatives. The result is the following:

$$\log(\mathrm{P}[Q > b]) \approx \log(\min_{q>o} g(q)) = \log\left(\frac{1}{\sqrt{\pi}}\frac{\Gamma\left(\Psi^{-1}\left(\log K\right)\right)}{K^{\Psi^{-1}(\log K)-1/2}}\right) =: \log(T_{fBm}(H, s, b)), \quad (4.10)$$

where $K = K(H, s, b) = \frac{1}{2}b^{2(1-H)}s^{2H}(1-H)^{-2(1-H)}H^{-2H}$, $\Psi(\cdot)$ is the *digamma* function, $\Psi(x) = \frac{\mathrm{d}}{\mathrm{d}x}\log\Gamma(x) = \frac{\Gamma'(x)}{\Gamma(x)}$, and $\Psi^{-1}(\cdot)$ denotes the inverse function of $\Psi(\cdot)$.

The $T_{fBm}(H, s, b)$ function is quite complex with the presence of Gamma, digamma, and its inverse function. However, there is an accurate approximation of $T_{fBm}(H, s, b)$:

**Proposition 4.3.2.** *The approximation*

$$\frac{1}{\sqrt{\pi}}\frac{\Gamma\left(\Psi^{-1}\left(\log x\right)\right)}{x^{\Psi^{-1}(\log x)-1/2}} \approx \exp(-x) \qquad (4.11)$$

*holds for large $x$, $x > 0$.*

The proof and the precise sense of this approximation can be found in Appendix A.2. Applying this approximation it is found that the queue tail for the fBm case satisfies:

$$\log\left(T_{fBm}(H, s, b)\right) \approx -\frac{1}{2}b^{2(1-H)}s^{2H}(1-H)^{-2(1-H)}H^{-2H}, \qquad b \text{ large.} \qquad (4.12)$$
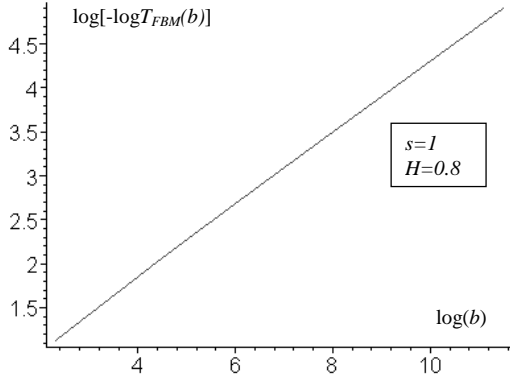
Figure 4.1: By setting fixed values for $H$ and $s$, the line in the log-log plot of $-\log T_{fBm}(b)$ versus $b$ clearly shows the Weibullian decay for $T_{fBm}(H, s, b)$.
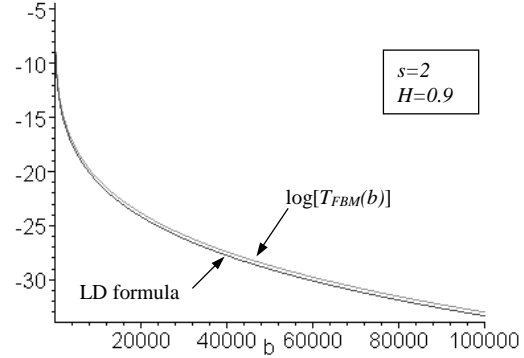
Figure 4.2: Our approximation compared to the Large Deviation technique result: the two plots almost coincide for all values of queue size.

Eq. (4.12) shows the Weibullian decay of this queue which was first recognized and proven by Norros [42]. Numerical evaluations of the result are presented in Fig. 4.1 and Fig. 4.2. In Fig. 4.1 the values of $H$ and $s$ were fixed, then the queue tail approximation $T_{fBm}(H, s, b)$ versus the queue size $b$ was calculated and plotted in the log-log scale. The linearity of the plot also demonstrates the Weibullian decay.

Now compare this result to the result obtained by Duffield and O'Connell. The asymptotic formula for queue tail probabilities provided by Large Deviation technique presented in [14] is

$$\lim_{b \to \infty} b^{-2(1-H)} \log P[Q > b] = -\inf_{c > 0} c^{-2(1-H)} \frac{(c + s)^2}{2}$$

$$\Leftrightarrow \quad \log P[Q > b] \to -\frac{1}{2} b^{2(1-H)} s^{2H} (1 - H)^{-2(1-H)} H^{-2H}, \quad \text{as } b \to \infty, \quad (4.13)$$

where $s$ also denotes the service rate. Therefore it can be concluded that the approximation yields the Large Deviation result, see Eq. (4.12) and Eq. (4.13). The two results are depicted in Fig. 4.2 and it can be observed that the plots almost coincide for all calculated values of the queue size.

The conclusions can be summarized in two main points: (i) the asymptotic tail approximation for the case of fBm has Weibullian decay; (ii) this result is also consistent with the formula presented by Norros [42] and by Duffield *et al.* with Large Deviation technique [14].

## 4.3.2 Gaussian input process with independent, stationary increments

In the case of a Gaussian input model $\{Z(t), t > 0\}$ with independent, stationary increments (Brownian motion) the following equation holds for its variance: $\sigma_t^2 = \text{E}\left[|Z(t)|^2\right] = \sigma^2 t$.

Then the similar calculation as in the proof of Lemma 4.3.1 shows that:

$$\mathrm{E}\left[|Z(t)|^q\right] = \frac{\left(2\sigma^2\right)^{q/2}\Gamma(\frac{q+1}{2})}{\sqrt{\pi}}t^{q/2}, \tag{4.14}$$

which means that the concerned Gaussian input model also satisfies the general definition of multifractality with

$$\begin{cases} \tau(q) &= q/2 - 1 \\ c(q) &= \frac{\left(2\sigma^2\right)^{q/2}}{\sqrt{\pi}}\Gamma\left(\frac{q+1}{2}\right). \end{cases}$$

Thus the approximation formula can also be applied for this case. The same minimization procedure for this process shows that

$$\begin{aligned} \log(\mathrm{P}[Q > b]) &\approx \log\left(\min_{q>0}\left\{\frac{\left(\frac{2sb}{\sigma^2}\right)^{-q/2}}{\sqrt{\pi}}\Gamma\left(\frac{q+1}{2}\right)\right\}\right) = \log\left(\frac{1}{\sqrt{\pi}}\frac{\Gamma\left(\Psi^{-1}\left(\log(\frac{2sb}{\sigma^2})\right)\right)}{\left(\frac{2sb}{\sigma^2}\right)^{\Psi^{-1}(\log(\frac{2sb}{\sigma^2}))-1/2}}\right) \\ &= \ :\log(T_{Gaussian}(\sigma^2,s,b)) \approx -\frac{2sb}{\sigma^2} \end{aligned} \tag{4.15}$$

The result is also in agreement with the queuing formula provided in the theory of Gaussian processes [38].

### 4.3.3 Practical solutions

The practical use of the formula is now presented. Assume that we are interested in the behavior of the tail of the steady-state buffer occupancy (queue length) distribution at a specific multiplexer in a traffic network. The first step should be the fine resolution measurements of the input process. Assume that the input process exhibits multifractal scaling properties. Then the scaling function $\tau(q)$ and the function $c(q)$ can be estimated from the collected data for some available parameters $q > 0$. *The importance of the function $c(q)$ should be emphasized as the quantity factor of multifractal processes which is sometimes neglected in a number of studies dealing with multiscaling properties of the high-speed network traffic. The scaling function $\tau(q)$ defines only the quality of multiscaling and it is not enough for the description of a multifractal model and therefore for the analysis of queuing models with multifractal input processes.*

Now two practical methods for the approximation of the queue tail distribution are suggested:

1. Given the service rate $s$ and the two sets $\{c(q)\}$ and $\{\tau(q)\}$, using Eq. (4.3) the approximation of $\log(\mathrm{P}[Q > b])$ can be computed for each value of $b$. This method is very simple but it is the more useful from network planning and capacity dimensioning point of view since we are only interested in some values of the tail probabilities. The practical use of this method is mainly focused in this study.

2. The input process is fitted to a multifractal model. The two measured sets of $c(q)$ and $\tau(q)$ are fitted by $\tilde{c}(q)$ and $\tilde{\tau}(q)$. Then the analysis of the Eq. (4.3) with these functions can result in simple closed form of the queue tail probabilities. This method is used in the study of the queue tail behavior of a multifractal model. It seems to be obvious to apply this method. However, characteristic functions of multiscaling processes are often complex, thus it is difficult to give a closed queuing form for these cases. The more details on this topic is in focus of future work.

### 4.3.4   Simulation evaluation of the approximation

For simulation validation of the presented approximation for queuing performance estimation a queuing model with the simplest multifractal input was considered: the multiplicative cascades. The detailed construction of this multifractal model is presented in the next chapter, Section 5.1.
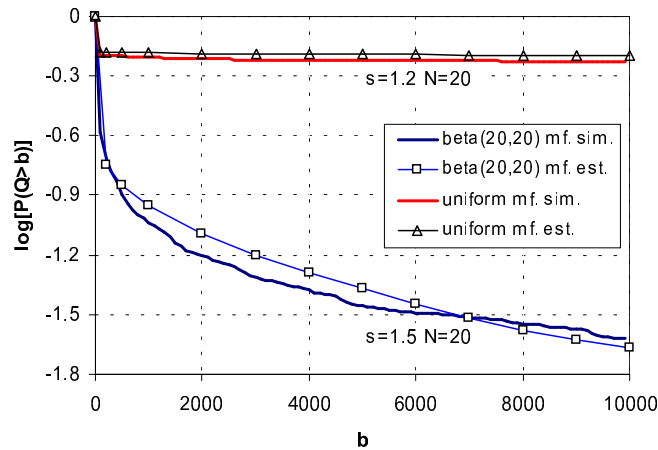


Figure 4.3: Comparison of simulated queue tail probabilities and their theoretical values.

Synthetic data series of length $2^N$ of this multiplicative multifractal were used in queuing evaluation of the method. After rescaling the multifractal model of unit mean and time has the following characteristic functions:

$$\begin{cases} \tau_0(q) & = & -\log_2 \mathrm{E}\left[r^q\right] \\ c(q) & = & 2^{N(q-\tau_0(q))} \end{cases}$$

Two multifractals were simulated which are differentiated by the chosen distribution of the multiplier $r$: uniform and symmetric $\beta(\alpha, \alpha)$ distribution. In the case of $\beta$-multiplier a multifractal example with $\alpha = 20$ is chosen for simulation. The queuing simulations are compared to the numerical calculation of the formula in a simple queuing system with a single server, constant service rate, infinite buffer, and FIFO serving principle. The

numerical calculation method is discussed in the previous subsection (see more details of this estimation method in the next section). The results are presented in Figure 4.3.

Note that the scaling function $\tau_0(q)$ is $\log_2(q+1)$ and $\log_2\left(\frac{\Gamma(\alpha)\Gamma(2\alpha+q)}{\Gamma(\alpha+q)\Gamma(2\alpha)}\right)$ for uniform multiplier and $\beta$-multiplier, respectively. With given values of these functions the tail probabilities of the system can be numerical counted using the queuing formula. As seen in the figure the theoretical queue tail probabilities are really close to the simulation results. This shows that the suggested queuing estimation method can be effectively used in practice.

### 4.3.5 The impacts of multifractality

As discussed, the tail behavior of a queuing system depends on both the scaling function and the moment factor of the multifractal traffic input. Applying the estimation method presented above this section shows a deeper study on these effects through some typical numerical examples.

**Multifractal versus monofractal**

Consider a multiplicative multifractal process with symmetric Beta$(\alpha, \alpha)$ distributed multiplier (see details in the next chapter, Section 5.1). For this multifractal the characteristic functions can be exactly calculated at a certain cascade level. The scaling function of a multiplicative cascade example with $\alpha = 15$, level $N = 20$ is presented in Figure 4.4. Assume that there exists a (mono)fractal process with exactly the same moment factor $c(q)$ as of the mentioned multifractal but it has the uniscaling fractal structure $\tau_0(q) = qH$ (also see in Figure 4.4 with $H = 0.8$ and $H = 0.9$).

With the knowledge of the characteristic functions of these scaling processes the estimation for the tail probabilities of the queue system can be calculated for large queue sizes (the service rate is set to be $s = 2.0$) by using the numerical method. The results are presented in Figure 4.5. It can be observed that the approximated queue tail probabilities of the multifractal case are noticeably greater than the monofractal cases. This result clearly indicates that in the same queuing environment, with the same moment function for the input process increments, and with the scaling functions are not far from each others in "value" (see Figure 4.4), the queuing behavior of the multifractal case is considerably worse than of the monofractal case.

**The impact of the moment factor**

The impacts of the moment factor of the multifractal input process were also examined with the similar consideration. Given a known scaling process fBm with $\tau_0(q) = qH, H = 0.8$ and $c(q) = \frac{2^{q/2}}{\sqrt{\pi}}\Gamma\left(\frac{q+1}{2}\right)$ Some modifications on the moment factor were made, thus create a new theoretical scaling process with only differences in the absolute moments of the increments.
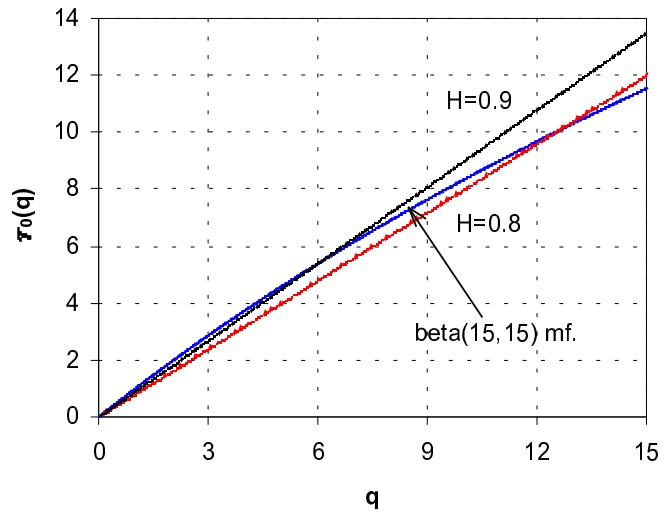
Figure 4.4: The scaling functions of the examined fractal processes.
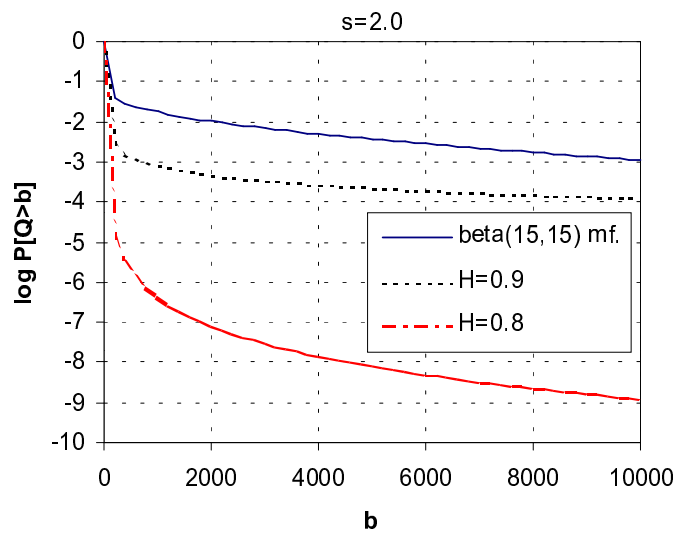


Figure 4.5: Queue tail approximation of the examined fractal processes.
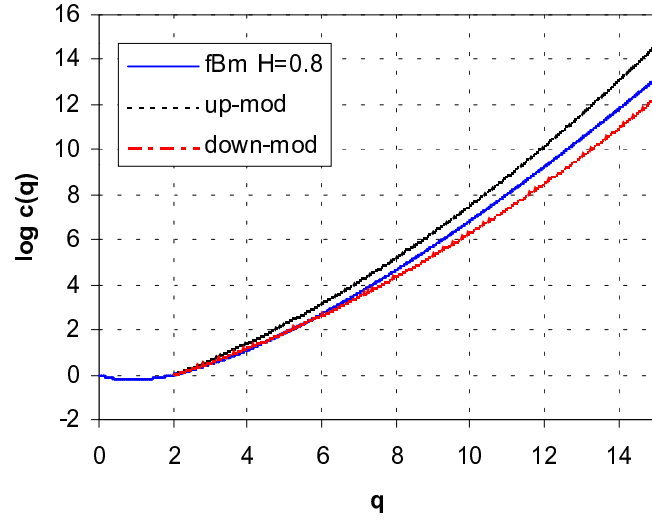
Figure 4.6: The moment functions of the examined fractal processes.
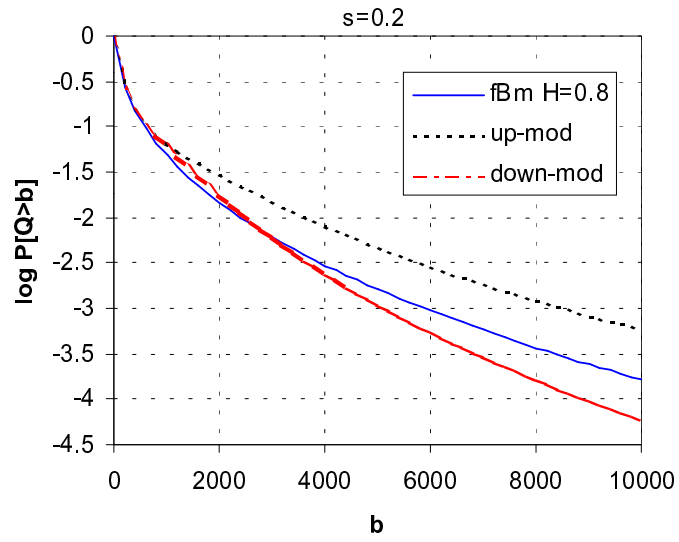


Figure 4.7: Queue tail approximation of the examined fractal processes.

Assume the following fractal process with the characteristic functions:

$$\begin{cases} \tau_0(q) & = & qH, \quad\quad H = 0.8 \\ c(q) & = & \begin{cases} \frac{2^{q/2}}{\sqrt{\pi}}\Gamma\left(\frac{q+1}{2}\right) & \text{if} \quad 0 \le q \le 2 \\ a(q-2)(q+b) & \text{if} \quad q > 2 \end{cases} \end{cases}$$

Denote the process with the setting $\{a = 0.037, b = 15.51\}$ and $\{a = 0.031, b = 15.51\}$ *up-mod* and *down-mod*, respectively. With these modifications the concerned process increments have the same moments up to the moment order $q = 2$, thus they have the same mean and variance. The difference between the moment factors is seen in Figure 4.6.

In the performance study of these processes presented in Figure 4.7 the effects of these slight modifications of the moment factor can be clearly noticed. The change of higher order moments has a strong impact on the queuing behavior of the process. The *up-mod* scaling process gives rise to the worse queuing performance and the *down-mod* process courses the better behavior in the same system setting as compared to of the original fBm process.

In summary, although one should deal carefully with the presented results because they are based on queuing performance approximation it can be concluded that in general the monofractal processes have a better queue behavior as compared to of the multifractals and the moment factor also exerts influence on the queuing performance. These important observations should be considered in traffic modeling and queuing study of the scaling processes.

## 4.4 Practical case study

In this section the validation for the mentioned practical solution presented above is shown by the queuing analysis of some real traffic traces. A simple modification of the absolute moment based method is also presented for estimation of multiscaling functions $c(q)$ and $\tau(q)$.

### 4.4.1 Data traces

Three data traces were considered in the analysis which are freely available at the Internet Traffic Archive [1]. These traces contain an hour's worth of all wide-area traffic each between Digital Equipment Corporation and the rest of the world. The traces, denoted by DEC-PKT-1, DEC-PKT-2, and DEC-PKT-3, were gathered at Digital's primary Internet access point, which is an Ethernet DMZ network operated by Digital's Palo Alto research groups. The raw traces were made using `tcpdump` on a DEC Alpha running Digital's OSF/1 operating system, which includes a kernel filter with capabilities comparable to those of BPF. `Tcpdump` captured all IP packet header information with millisecond precision timestamps. Each trace contains more than 3 million packet headers.

| Data set | Number of arrivals | Mean | Variance |
|----------|-------------------|--------|----------|
| DEC-PKT-1 | 3 027 907 | 2.5232 | 4.4153 |
| DEC-PKT-2 | 3 987 942 | 3.3234 | 5.2416 |
| DEC-PKT-3 | 4 518 090 | 3.7652 | 5.9968 |

Table 4.1: Summary of the investigated data sets.

The packet arrival counts traces of time sample of 3 milliseconds were constructed from the raw data. Preliminary analysis of these traces exhibits scaling properties, therefore they were used as the inputs for the queuing system under investigation.

### 4.4.2 Modified method for estimation of multifractal functions

The full description of a multifractal model consists of both the scaling function $\tau(q)$ and the moment factor $c(q)$. The estimation method based on the absolute moments (details are shown in chapter 3, Section 3.2.3) provides a simple way for testing of scaling properties and also for the estimation of the scaling function. However, the moment factor is also needed for analysis, thus the following modification is introduced for this goal.
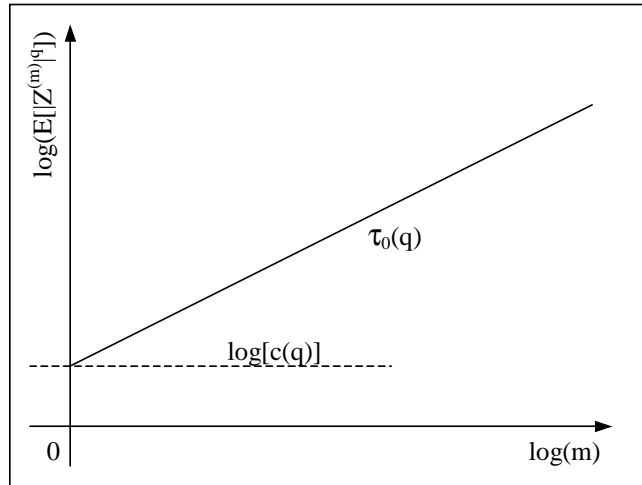


Figure 4.8: A simple method for scaling test and the estimation of $c(q)$ and the scaling function $\tau(q)$.

The definition of multifractal processes (Def. 1.3.1) claims the stationarity condition for the increments. Therefore it is easy to verify the following relation for the moments of the increments:

$$\mathrm{E}\left[|Z^{(\triangle t)}|^q\right] = c(q)(\triangle t)^{\tau(q)+1} = c(q)(\triangle t)^{\tau_0(q)}, \qquad q > 0, \tag{4.16}$$

where $Z^{(\triangle t)}$ denotes the increment process of time sample $\triangle t$. Thus this equality also holds

for $m = 1, 2, \ldots$

$$\mathrm{E}\left[|Z^{(m\triangle t)}|^q\right] = c(q)(m\triangle t)^{\tau_0(q)}, \qquad q > 0. \tag{4.17}$$

Choose $\triangle t$ as the time unit, then

$$\log \mathrm{E}\left[|Z^{(m)}|^q\right] = \tau_0(q)\log m + \log c(q), \qquad q > 0. \tag{4.18}$$



(a)

(b)

(c)

(d)
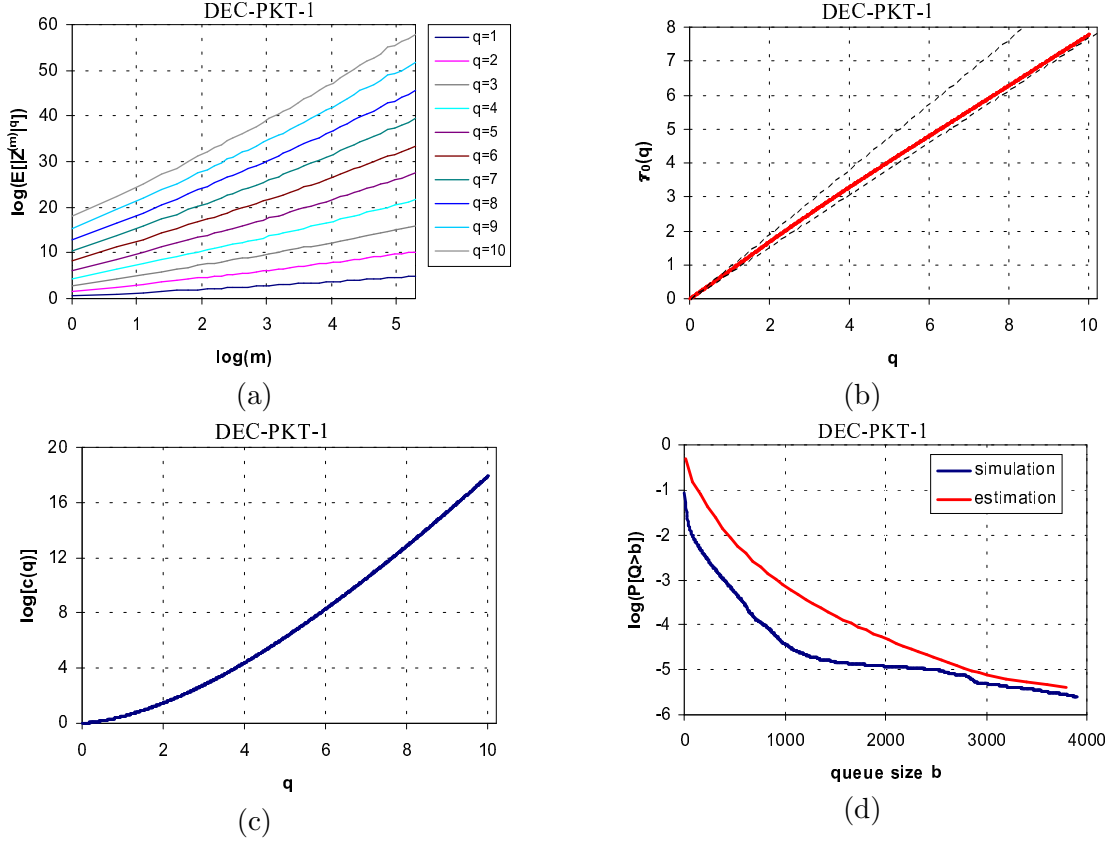
Figure 4.9: Analysis results of the DEC-PKT-1 data set: (a) the plots of the absolute moments, (b) and (c) estimated form of $\tau_0(q)$ and $c(q)$, respectively, (d) queuing simulation compared with the theoretical approximation.

Based on this property, the method is the following: Given a data series of a process increments $Z_1, Z_2, \ldots, Z_n$ and define its corresponding *real* aggregated sequence $\{Z^{(m)}\}$ of the aggregation level $m$ by

$$Z_k^{(m)} = Z_{(k-1)m+1} + Z_{(k-1)m+2} + \ldots + Z_{km}, \qquad k, m = 1, 2, \ldots \tag{4.19}$$

If the sequence $\{Z_k\}$ has scaling property then the plot of absolute moments $\mathbb{E}[|Z^{(m)}|^q]$ versus $m$ on a log-log plot should be a straight line due to Eq. (4.18). The slope of the

straight line provides the estimate of $\tau_0(q)$ and the intercept is the value for $\log c(q)$. The illustration of the method can be seen in Fig. 4.8.

Note that there is no need to estimate $c(q)$ and $\tau_0(q)$ for all positive value of $q$, which is an impossible task. In fact, the largest value of $q$ one should consider depends on the interested finite queue length of the involved queue length probability, see below.

### 4.4.3 Analysis results

The analysis results of the mentioned data sets are presented below. These results together with the simulation results of some exact multifractals shown in Section 4.3.4 validate the use of the approximation for a single queue with constant service rate and general multifractal input.
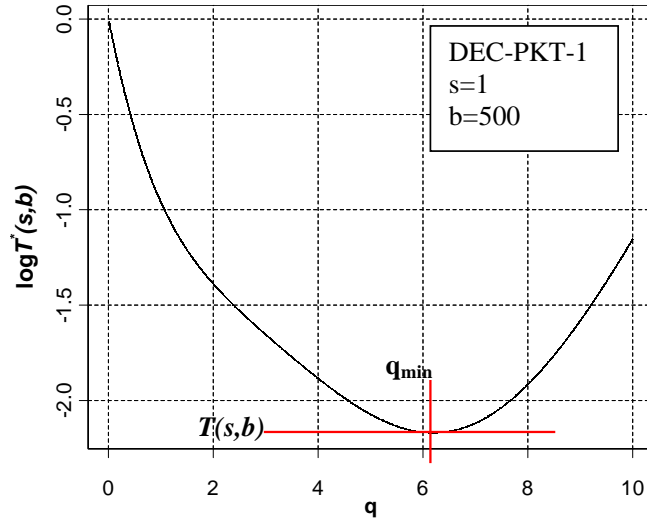


Figure 4.10: Theoretical queue tail probability at each value of queue size $b$ is the minimum of $\log T^*(s, b)$, for example DEC-PKT-1, $s = 1, b = 500$.

Figure 4.9(a) shows the plot of absolute moments of the aggregated sets of the set DEC-PKT-1 versus the aggregation level in a log-log plot for some values of the moment order $q$. The linearity of the plots observed in the figure clearly indicates the scaling property of this data set. After applying the estimation method presented in the previous subsection the two sets of $\tau_0(q)$ and $c(q)$ were estimated which are drawn in Fig. 4.9(b) and Fig. 4.9(c) ($\log c(q)$ was estimated instead of $c(q)$). The plot of the function $\tau_0(q) = \tau(q) + 1$ is a concave curve which suggests the multifractal property of DEC-PKT-1.

Next a comparison between the approximation and the queuing simulation of real data traces was made to validate the use of the formula in practice. The approximation for

probabilities of queue tail presented in Proposition 4.2.1 can be rewritten in the form

$$
\begin{aligned}
\log \mathrm{P}[Q > b] &\approx \min_{q>0}\left\{\log c(q) + \tau_0(q)\log\frac{b\tau_0(q)}{s(q-\tau_0(q))} - q\log\frac{bq}{q-\tau_0(q)}\right\} \\
&=: \min_{q>0}\left\{\log T^*(s,b)\right\} = T(s,b). \tag{4.20}
\end{aligned}
$$

For the sake of calculation simplicity the service rate was chosen such that $s = 1$. The lower curve in Fig. 4.9(d) shows the simulation result of the DEC-PFT-1 data set. Using Eq. (4.20) the value of the logarithmic tail probability at each concerned value of queue size $b$ is taken by the numerical minimization of $\log T^*(s,b)$ with the estimated sets $\{c(q)\}$ and $\{\tau_0(q)\}$. An example is shown in Fig. 4.10.



(a)

(b)

(c)

(d)
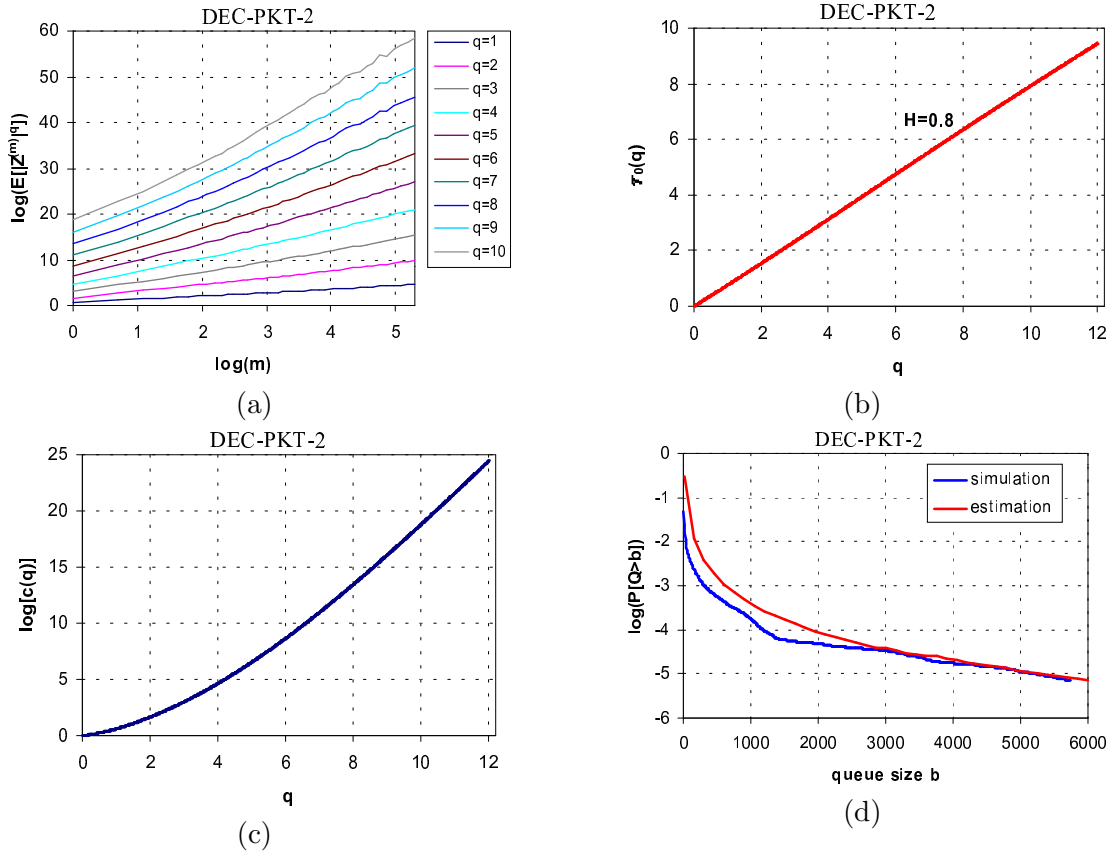
Figure 4.11: Analysis results of the DEC-PKT-2 data set: (a) the plots of the absolute moments, (b) estimated form of $\tau_0(q)$ which shows the data set can be modeled by statistical self-similarity with $H = 0.8$, (c) estimation of $\log[c(q)]$, (d) queuing simulation compared with the theoretical tail probabilities.

In addition, there is no need to plot $\log T^*(s,b)$ at each value of $q$ to find its minimum. A simple program routine can do it for all concerned value of $b$ at once. The theoretical tail

probabilities are on the upper curve in Fig. 4.9. As comparing with the simulation result which is seen in the same figure it is found that these curves have the similar shape and become tight as $b$ increases. This validates the approximation.
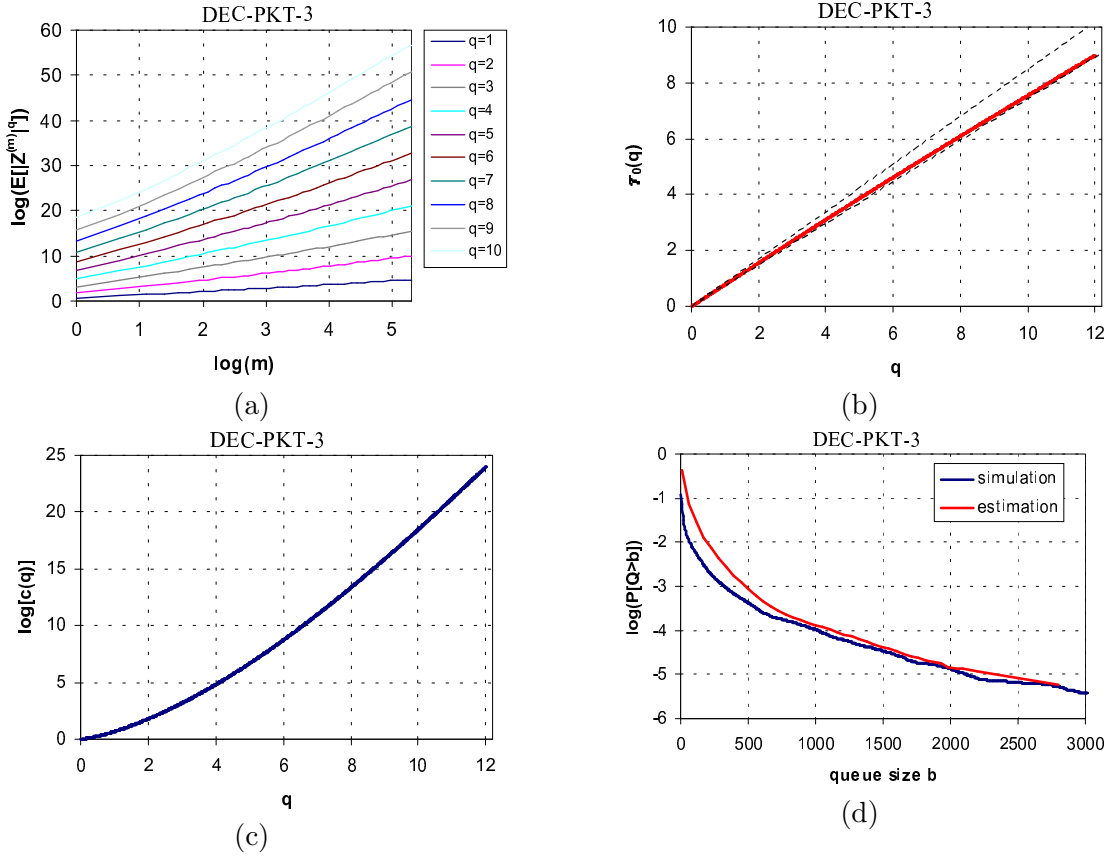


Figure 4.12: Analysis results of the DEC-PKT-3 data set: (a) the plots of the absolute moments, (b) and (c) estimated form of $\tau_0(q)$ and $\log[c(q)]$, respectively; the concavity of $\tau_0(q)$ shows the multiscaling nature of the data set, (d) queuing simulation compared with the theoretical tail probabilities.

The same analysis were performed with two other data sets DEC-PFK-2 and DEC-PKT-3. The results are summarized in Fig. 4.11 and Fig. 4.12. The DEC-PKT-3 set also exhibits multifractal structure as the DEC-PKT-1 and its queuing analysis gives some similar results. The DEC-PKT-2 data set, however, has the exact monofractal structure and can be well modeled by statistical self-similarity with Hurst parameter $H = 0.8$. The queuing model deals with general multifractal processes so it also involves the case of monofractal cases. Thus it is not surprising that the analysis also provides the correct queuing results in this case.

## 4.5   Conclusion

In this chapter a study of the queuing performance of a single server infinite capacity queue with a constant service rate fed by general multifractal input process was presented. The results can be summarized by the followings:

(i) An asymptotic approximation of the steady-state queue length probabilities was derived.

(ii) It is shown that the approximation results in the well-known Weibullian queue tail in case of the monofractal fractional Brownian motion input process.

(iii) It was proved that the class of Gaussian processes with scaling properties is limited to monofractal processes and their characteristic functions were derived.

(iv) The formula was applied for the case of Gaussian input processes and it justified the results from the theory of Gaussian processes.

(v) The practical applicability of the approximation was demonstrated and validated by simulation of two multiplicative multifractal processes.

(vi) Some impacts of multifractality were investigated and presented.

(vii) It have been shown that the formula gives the correct result in analysis of both multifractal and monofractal network traffic cases.

# Chapter 5

# A Complete Model of Multifractal Traffic

In the self-similar traffic characterization framework a large number of traffic models has been developed (fractional Brownian motion (fBm) models, FARIMA models, Cox's M/G/$\infty$ models, on/off models, etc.) [57]. There are also different processes which are candidates for multifractal modeling. *Multiplicative cascades* were first used as a multifractal model for data traffic [22, 44]. This class is the most well-known member of the class of multifractal processes. The simplest case of this process is the *binomial cascade* which can be defined by a binary tree structure [20, 44]. Combining this process with the aforementioned fBm we can define a new class called the *fractional Brownian motions in multifractal time* [20]. This process has several nice properties, e.g. it is able to capture LRD and multifractal scaling independently. The *self-similar $\alpha$-stable process* [50] is a different multifractal process. Its statistics of order $q \geq \alpha$ are not finite resulting in an irregular multifractal structure. One of the simplest process from this class is the *linear fractional stable motion.*

This chapter proposes a new multifractal traffic model for network traffic. The model is a combination of a multiplicative cascade with an independent lognormal process. It is shown that the model has all the important properties observed in data traffic including LRD, multifractality and lognormality. It is also demonstrated that the model is flexible enough to capture the complete multifractal characteristics of data traffic including both the scaling function and the moment factor. On the other hand, the model is simple enough from practical point of view having only three parameters. Practical applications for measured data traffic and validation of the model with queuing performance evaluation are also presented.

## 5.1 Multiplicative cascades

The simplest multifractals are typically constructed by an iterative procedure called multiplicative cascade. Consider a unit interval associated with a unit mass. At stage $k = 1$

divide the unit interval into two equal subintervals and associate with them the mass $r$ and $1 - r$, respectively. The fraction $r$ is called the multiplier. The same rule is applied to each subinterval and its associated mass. The iterative procedure of cascade construction is shown in Fig. 5.1. The multipliers $r$ are chosen to be independent random variables $R$ concentrated on $[0, 1]$ with the probability distribution function $F_R(x)$, $\mathrm{E}[R] = 1/2$. The multiplier $r$ is also chosen to have a symmetric density function so that $r$ and $1 - r$ have the same marginal distribution. Thus at the stage $k$ a dyadic interval of length $\triangle t_k = 2^{-k}$ starting at $t = 0.\eta_1...\eta_k = \sum \eta_i 2^{-i}$ has the mass (measure)

$$\mu(\triangle t_k) = R(\eta_1)R(\eta_1, \eta_2) \ldots R(\eta_1, \ldots, \eta_k),$$

where $R(\eta_1, \ldots, \eta_i)$ indicates the multiplier at stage number $i$. Since multipliers are i.i.d. it is easy to show that the measure $\mu$ satisfies the scaling relationship:

$$\mathrm{E}[\mu(\triangle t_k)^q] = (\mathrm{E}[R^q])^k = \triangle t_k^{-\log_2 \mathrm{E}[R^q]},$$

which defines a multifractal process with scaling function $\tau_0(q) = -\log_2 \mathrm{E}[R^q]$.

Note that the multifractal process constructed above is also referred to as *conservative cascade*. An important property of this random cascade is its dependence structure due to the construction. If the multipliers used in the construction have the same fixed value $r_0$ ($0 < r_0 < 1$) then the obtained multiplicative measure is called *binomial*. Binomial measure is a deterministic cascade, its scaling function being $\tau_0(q) = -\log_2(r_0^q + (1 - r_0)^q) + 1$. In addition, if the iteration only conserves mass on the average, i.e., multipliers at each mass division are also i.i.d. but have mean of $1/2$, the corresponding measure is called *canonical* [20]. An example of the multiplicative cascades can be seen in Fig. 5.2
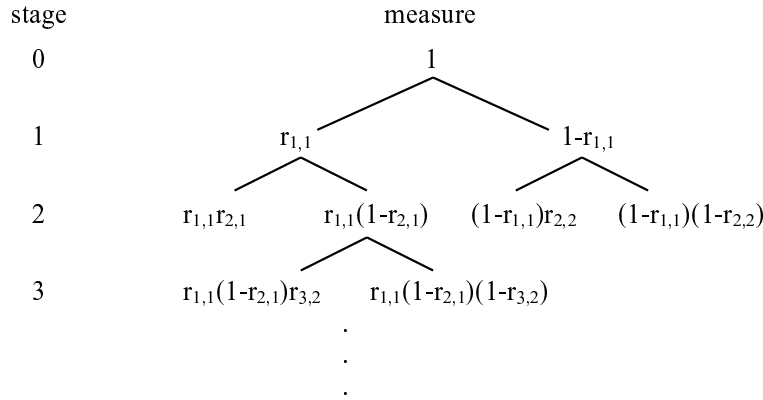


Figure 5.1: The iterative procedure of cascade construction.

Note that the multifractal process constructed above is also referred to *conservative cascade*. An important property of this random cascade is its dependence structure due to the construction. If the multipliers used in the construction have the same fixed value $r_0$ ($0 < r_0 < 1$) then the obtained multiplicative measure is called *binomial*. Binomial measure
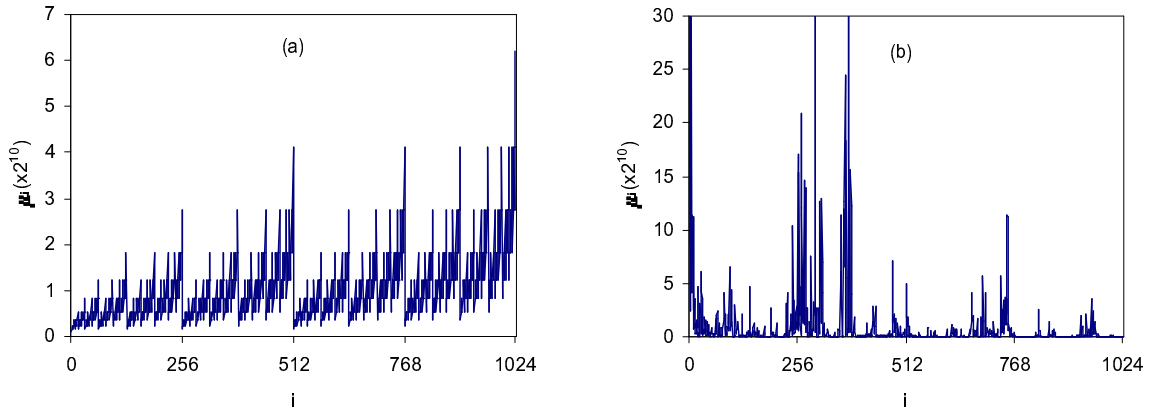
Figure 5.2: Multiplicative measures at stage $k = 10$: (a) binomial cascade ($r_0 = 0.4$), (b) conservative cascade ($R \sim \text{Uniform}(0, 1)$).

is a deterministic cascade, its scaling function being $\tau_0(q) = -\log_2(r_0^q + (1 - r_0)^q) + 1$. In addition, if the iteration only conserves mass on the average, i.e., multipliers at each mass division are also i.i.d. but have mean of $1/2$, the corresponding measure is called *canonical* [20]. An example of the multiplicative cascades can be seen in Fig. 5.2 .

From the network modeling point of view only conservative cascades are of interest. The binomial cascade is naturally excluded because it is a deterministic process. The canonical cascade cannot be used since it is an independent random process, while network traffic flows are long-range dependent. In this study the conservative cascade is used as a building block of the traffic model.

## 5.2　A multifractal traffic model

The multifractal model based on multiplicative cascades is presented in details in this section. Statistical properties of the model are also derived. In addition, a comparison to the different multifractal models, which can be found in teletraffic literature, is given.

### 5.2.1　Construction of the model

Suppose that the multifractal analysis of a real data series obtained form measured network traffic shows its multifractal properties characterized by the scaling function $\tau_0(q)$ and the moment factor $c(q)$. The obvious task of cascade modeling is to find a convenient probability distribution for multipliers $R$ such that $-\log_2(\text{E}[R^q]) = \tau_0(q)$. However, this cascade model captures only the multifractal properties given by the scaling function and fails to furnish any information on the moment factor $c(q)$. The idea for a more comprehensive traffic model is the following: $2^N$ synthetic data $\mu(\triangle t_N)$ is first generated by multiplicative cascade with multipliers governed by the distribution of $R$. Then $2^N$ data series of our model is the

pairwise product of the cascade data series and an i.i.d. random samples of a positive random variable $Y$ with the same length. The variable $Y$ is chosen to be independent of the cascade measure $\mu(\triangle t_N)$, thus the obtained series, denoted by $X(\triangle t_N)$, satisfies

$$\mathrm{E}\left[X(\triangle t_N)^q\right] = \mathrm{E}\left[Y^q\right]\mathrm{E}\left[\mu(\triangle t_N)^q\right] = \mathrm{E}\left[Y^q\right]\triangle t_N^{\tau_0(q)}. \tag{5.1}$$

The model fitting task is to find the suitable random variable $R$ and $Y$ such that

$$\begin{cases} -\log_2(\mathrm{E}\left[R^q\right]) &= \tau_0(q) \\ \mathrm{E}\left[Y^q\right] &= c(q). \end{cases}$$

The presented model is relevant to multifractal network traffic for the following reasons. First, it is based on the multiplicative construction of a cascade which, in deep, seems to closely match the TCP/IP protocol operating mechanics as suggested in a number of traffic research studies [18, 22, 47] as the main cause of multifractality in traffic data at small time scales. Second, the model traffic can be interpreted as the product of the random peak rate of the flow $Y$ and the measure of burstiness $\mu(\triangle t_N)$ at the modeled time scale $\triangle t_N$.

For practical use, some modifications to the model are introduced. The measure $\mu(\triangle t_N)$ has a very small value since it is the product of $N$ multipliers $0 < r < 1$, so to avoid loss of information the cascade measures are multiplied by $2^N$. Since $\mathrm{E}\left[\mu(\triangle t_N)\right] = 2^{-N}$, this normalizes the cascade increment so that it has unit mean. Another modification is to rescale the cascade process to have unit time interval at stage $N$ instead of $\triangle t_N = 2^{-N}$. For a multifractal increment process $X_\triangle$

$$\begin{aligned} \mathrm{E}\left[X_\triangle^q\right] &= c_1(q)\triangle t_1^{\tau_0(q)} \\ &= c_1(q)\left(\frac{\triangle t_2}{\triangle t_1}\right)^{-\tau_0(q)}\triangle t_2^{\tau_0(q)} = c_2(q)\triangle t_2^{\tau_0(q)}, \end{aligned} \tag{5.2}$$

which means that the choice of time unit influences the value of the moment factor $c(q)$. After applying these changes to the model it can be obtained that

$$\mathrm{E}\left[X(\triangle t_0)^q\right] = \mathrm{E}\left[Y^q\right]2^{N[q+\log_2 \mathrm{E}[R^q]]}\triangle t_0^{-\log_2 \mathrm{E}[R^q]}, \tag{5.3}$$

where $\triangle t_0$ denotes the unit time interval of the data traffic to be modeled.

## 5.2.2 Model parameters

For multifractal traffic data, the scaling function $\tau_0(q)$ and the logarithm the moment factor $c(q)$ can be estimated by a simple absolute moment method, see in Chapter 3 Section 3.2.3 for details. Denote these estimated functions by $\tilde{\tau}_0(q)$ and $\log \tilde{c}(q)$, respectively. Owing the modifications mentioned above, the random variable $R$ and $Y$ should be chosen such that

$$\begin{aligned} -\log_2(\mathrm{E}\left[R^q\right]) &= \tilde{\tau}_0(q) & (5.4) \\ \log \mathrm{E}\left[Y^q\right] &= \log \tilde{c}(q) - [q + \log_2 \mathrm{E}\left[R^q\right]]N\log 2 \\ &= \log \tilde{c}(q) - [q - \tilde{\tau}_0(q)]N\log 2. & (5.5) \end{aligned}$$

Analysis of various measured traffic traces with multifractal properties shows that the choice of $R$ as a *symmetric beta random variable* on [0,1] Beta$(\alpha, \alpha)$ with only one parameter $\alpha > 0$ is accurate enough to model the estimated scaling function. In this case

$$\tau_0(q) = \log_2 \frac{\Gamma(\alpha)\Gamma(2\alpha + q)}{\Gamma(\alpha + q)\Gamma(2\alpha)}, \tag{5.6}$$

where $\Gamma(.)$ denotes the Gamma function, see definition in chapter 1 Eq. (1.5).

The random variable $Y$ is also chosen to have *lognormal distribution*. It has two parameters $m$ and $\sigma$ and the moment is of the form $\mathrm{E}\left[Y^q\right] = e^{mq + \sigma^2 q^2/2}$. Thus from Eq. (5.5) $m$ and $\sigma$ should be chosen such that

$$mq + \frac{\sigma^2 q^2}{2} = \log \tilde{c}(q) - \left\{ q - \log_2 \frac{\Gamma(\alpha)\Gamma(2\alpha + q)}{\Gamma(\alpha + q)\Gamma(2\alpha)} \right\} N \log 2. \tag{5.7}$$

Note that the distribution for the random variable $Y$ can be freely chosen, it does not change the property of the model. However, the lognormal distribution is selected because it has the simplest log-moment function.

In summary, the presented multifractal model has three parameters $(\alpha, m, \sigma)$ and the following characterization functions:

$$\begin{cases} \tau_0(q) & = & \log_2 \frac{\Gamma(\alpha)\Gamma(2\alpha + q)}{\Gamma(\alpha + q)\Gamma(2\alpha)} \\ c(q) & = & e^{mq + \sigma^2 q^2/2} 2^{N\left(q - \log_2 \frac{\Gamma(\alpha)\Gamma(2\alpha + q)}{\Gamma(\alpha + q)\Gamma(2\alpha)}\right)}. \end{cases}$$

Note that if the right-hand side of Eq. (5.5) is a concave function of $q$ then the examined traffic data cannot be captured by the presented model since the absolute moment of any stochastic process is a *log-convex* function of the moment order $q$. (This property is easily derived from the Hölder inequality.) These kind of multifractal traffic cannot be fully characterized by a cascade based model.

### 5.2.3   Statistical properties

Statistical properties of multiplicative cascades are studied in a number of papers, see [56, 21] for examples. The following properties are extended for $2^N$ synthetic samples of the multifractal model.

(i) As an extension of the conservative cascade the traffic model is an exact *positive multifractal process*. In the model construction presented in the previous section, the multifractality is characterized by scaling function $\tau_0(q) = \log_2 \frac{\Gamma(\alpha)\Gamma(2\alpha + q)}{\Gamma(\alpha + q)\Gamma(2\alpha)}$ and the logarithm of the moment factor $\log c(q) = (mq + \sigma^2 q^2/2) + \left( q - \log_2 \frac{\Gamma(\alpha)\Gamma(2\alpha + q)}{\Gamma(\alpha + q)\Gamma(2\alpha)} \right) N \log 2$ where $(\alpha, m, \sigma)$ are model parameters.

(ii) The mean and the variance of the model process are:
$\mathrm{E}\left[X(\triangle t_0)\right] = \mathrm{E}\left[Y\right] = e^{m + \sigma^2/2}$;
$\mathrm{Var}\left[X(\triangle t_0)\right] = \mathrm{E}\left[Y^2\right] 2^{2N} \mathrm{E}\left[R^2\right]^N - \mathrm{E}\left[X(\triangle t_0)\right]^2 = e^{2m + 2\sigma^2} (\frac{\alpha + 1}{\alpha + 1/2})^N - e^{2m + \sigma^2}$.

(iii) For $N \gg 1$, $X(\triangle t_0)$ has lognormal distribution. This property is deduced directly from the fact that $X(\triangle t_0) = 2^N.Y.R(\eta_1)\ldots R(\eta_1,\ldots,\eta_N)$ and the central limit theorem.

(iv) $X(\triangle t_0)$ has long-range dependent correlation structure.

Consider the covariance $\text{Cov}\,[X(\triangle t_0)_n, X(\triangle t_0)_{n+k}]$, where $k = 2^p, p = 1, 2, \ldots$, which can be derived as follows:

$$\text{Cov}\,[X(\triangle t_0)_n, X(\triangle t_0)_{n+k}] = \text{E}\,[Y]^2 \left\{ 2^{2N}\text{E}\,[\mu(\triangle t_N)_n.\mu(\triangle t_N)_{n+k}] - 1 \right\}. \qquad (5.8)$$

The two measures $\mu(\triangle t_N)_n$ and $\mu(\triangle t_N)_{n+k}$ are created by the same mass at stage $N - p - 1$, denoted by $\mu(\triangle t_{N-p-1})$, thus $\mu(\triangle t_N)_n = \mu(\triangle t_N)_{N-p-1}.r_{N-p} \prod_{i=N-p+1}^{N} r_{i,j_1}$ and $\mu(\triangle t_N)_{n+k} = \mu(\triangle t_N)_{N-p-1}.(1 - r_{N-p}) \prod_{i=N-p+1}^{N} r_{i,j_2}$ where $r_{i,j}$ denotes the actual multiplier values at stage $i$. Then $\text{E}\,[\mu(\triangle t_N)_n.\mu(\triangle t_N)_{n+k}] = \text{E}\,[\mu(\triangle t_{N-p-1})^2]$ $\text{E}\,[r_{N-p}(1 - r_{N-p})]\,\text{E}\left[\prod_{i=N-p+1}^{N} r_{i,j_1} r_{i,j_2}\right] = \text{E}\,[R^2]^{N-p-1}[\frac{1}{2} - \text{E}\,[R^2]](1/2)^{2p}$. Insert this into Eq. (5.8) we get

$$\text{Cov}\,[X(\triangle t_0)_n, X(\triangle t_0)_{n+k}] = e^{2m+\sigma^2} \left\{ \frac{\alpha(\alpha + 1)^{N-1}}{(\alpha + 1/2)^N} \left[ \frac{\alpha + 1}{\alpha + 1/2} \right]^{-p} - 1 \right\}$$

$$= e^{2m+\sigma^2} \frac{\alpha(\alpha + 1)^{N-1}}{(\alpha + 1/2)^N} k^{-\log_2\left(\frac{\alpha+1}{\alpha+1/2}\right)} - e^{2m+\sigma^2}. \qquad (5.9)$$

Thus when $N, k$ are large the covariance is ruled by $k^{-\log_2\left(\frac{\alpha+1}{\alpha+1/2}\right)}$, i.e., the model has LRD structure with Hurst parameter $H = 1 - \frac{\log_2 \frac{\alpha+1}{\alpha+1/2}}{2}$. It is easy to check that for $\alpha > 0$ $H \in (0.5, 1)$.

### 5.2.4   Comparison with other multifractal models

The reasons which explain the suitability of the described multifractal model for network traffic modeling are first summarized: (1) it is a positive process, hence reasonable for the simulation of the traffic counting processes; (2) it captures the full multifractal characteristics defined by the scaling function $\tau_0(q)$ and the moment factor $c(q)$; (3) it has approximately lognormal marginal distribution, which seems to match the real traffic; (4) it also has LRD correlation structure, which is an important property of high-speed LAN/WAN network traffic.

Since the observation of the flexible scaling structure in some WAN traffic environments [46, 37, 18] network researchers have suggested several multifractal models for characterization of these traffic flows among which two distinct approaches can be identified. The first one uses multifractal time for subordinating a monofractal process (FBM) to model multifractals, e.g. in [33]. The disadvantages of this approach lie in the presence of some negative values and Gaussian marginal of the model synthetic processes, which is not always suitable for network traffic simulation. The other approach is based on the multiplicative

cascades [45, 22, 10, 21, 34]. In general, multiplicative cascades are very attractive for traffic modeling. They are positive processes, easy to generate, and also possessing a plausible explanation for the origin of multiscaling properties in the traffic, see [22, 47] for more details. However, authors in [10] and [21] only fit the model to the LRD structure of the measured traffic, thus these models do not capture the multifractal characteristics of the traffic which is also ruled by the higher order moments. Cascade models in [45, 22] provide a better fit to the traffic multifractality but require $N$ parameters for $2^N$ synthetic data. Then it is difficult to use these models in analytic approaches, e.g., in queuing performance estimations for multifractal traffic input.

In contrast, the presented traffic model suggests an alternative method of cascade modeling with only three parameters. The model provides the close analytic form of the characteristic functions of multifractality with properties close to the real data traffic.

## 5.3 Analysis

In this section the effectiveness of the model is examined by simulation of some real data traces. After fitting the parameters, synthetic data is generated and compared with the real traces in a queuing performance analysis.
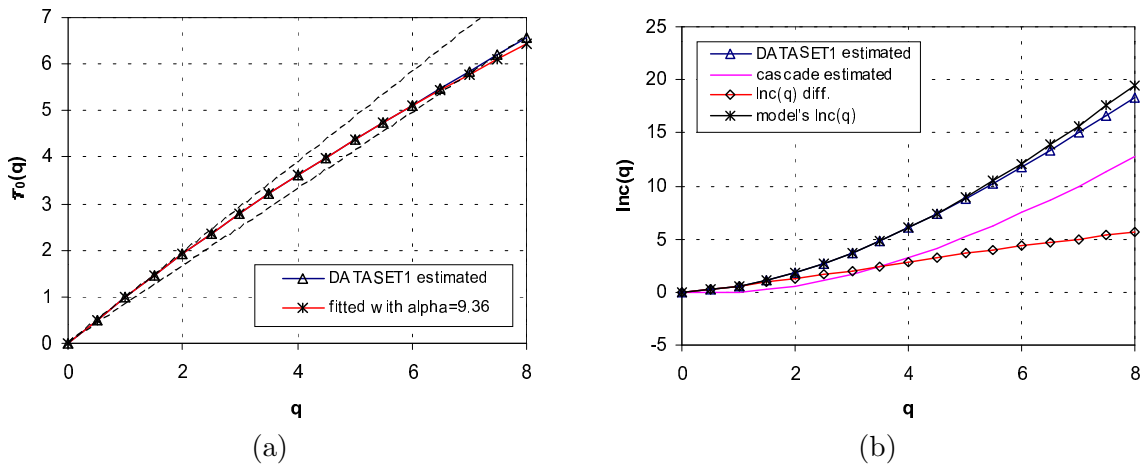


Figure 5.3: Model fitting results for the DASTASET1: (a) the estimated scaling function and the fitted curve; (b) moment factor fitting.

### 5.3.1 Model fitting

Data traces were collected from the traffic measurements carried out at an outgoing Internet connection of the Informatics Building, Budapest University of Technology and Economics in 2000. The traffic traces, captured by `tcp-dump`, were the aggregated traffic of about 100

workstations used by staff member, Ph.D. students, and student laboratories. We use two data sets, denoted by DATASET1 and DATASET2, for analysis. The both sets contain $2^{17}$ data samples of IP traffic bytes, counted in 100 bytes for simple calculation, arriving in consecutive time intervals of 60ms. The modified absolute moment based method presented in chapter 4 Section 4.4.2 was used to test the multifractal characteristics of the traces.

Figure 5.3 presents the multifractal analysis and model fitting results for the DATASET1. As observed in Fig. 5.3(a) the concavity of the estimated scaling function shows evidence for multiscaling structure of the DATASET1. It can also be seen in this figure the theoretical multiscaling function of the multiplicative cascade with parameter $\alpha_1 = 9.36$ of the Beta$(\alpha, \alpha)$-distributed multipliers. As it is seen, the multiscale function of the cascade process (also of the model) provide a very tight fit to the estimated curve. The next step is to determine the value of the parameters $m$ and $\sigma$ of the lognormal distribution to account for the difference between the logarithm of the estimated moment factor and the moment factor of the multiplicative cascade. The two moment factors and their difference are plotted in Fig. 5.3(b). It was found that the lognormal distribution with $m_1 = 0.57$ and $\sigma_1 = 0.23$ is adequate for this goal.
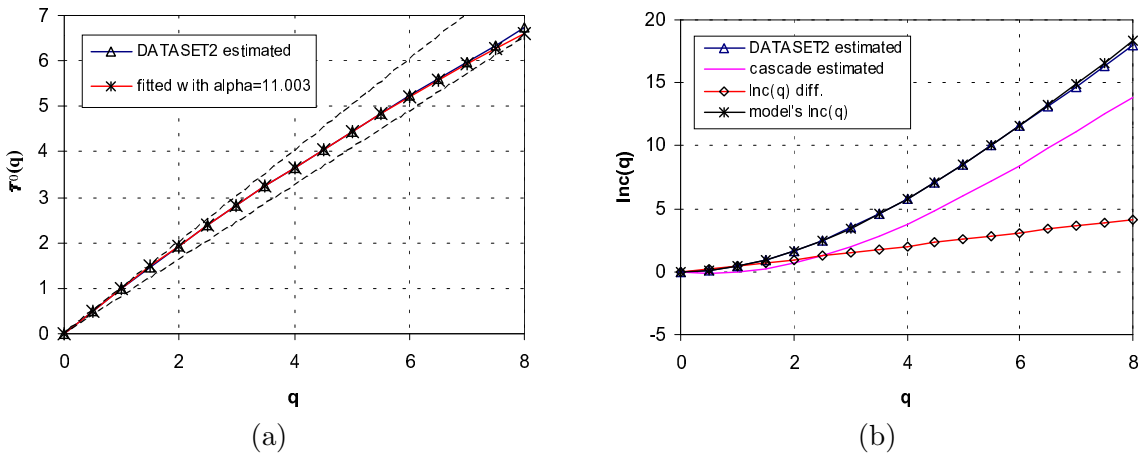


Figure 5.4: Model fitting results for the DASTASET2: (a) the estimated scaling function and the fitted curve; (b) moment factor fitting.

A similar procedure is carried out for the DATASET2 and the results are presented in Fig. 5.4. The analysis also indicates the multiscaling properties for this data set. The model can be fitted to the estimated multifractal characteristic functions with $\alpha_2 = 11.003$, $m_2 = 0.46$, and $\sigma_2 = 0.15$.

## 5.3.2   Queuing analysis

Next the queuing performance of the real data traces is compared to that of their simulated data sets generated using the new model. Consider the simulation in an infinite-buffer single-server queue with constant service rate and FIFO serving discipline. The synthetic
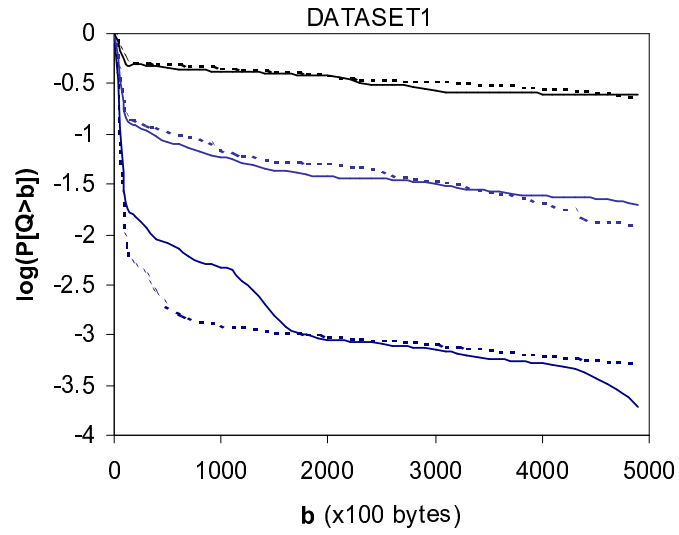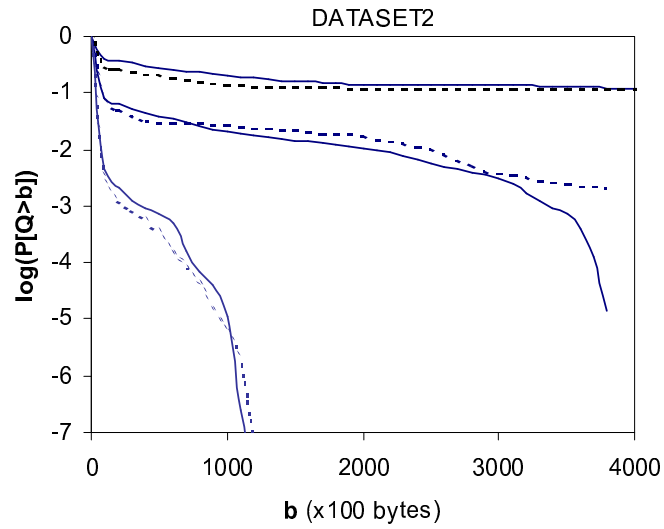
Figure 5.5: Experimental queue tail distributions of the DATASET1 and DATASET2 (solid lines) and their corresponding synthetics (dashed lines) at different server utilization of 0.9, 0.7, and 0.5 (from top to bottom).

data sets for each real trace are generated using the estimated model parameters. The analysis results are shown in Fig. 5.5.

Figure 5.5(a) presents the observed queue tail probabilities for the DATASET1 and their synthetic sets. The analysis is considered at different server utilization $\rho$. In the plot the solid lines present the tail probabilities of the real trace and the dashed lines the results of the trace simulation. The curves, from top to bottom, correspond to $\rho = 0.9, 0.7,$ and 0.5, respectively. The results show that the queuing behavior of the real trace and their synthetic sets are approximately similar.

Queuing performance comparison on the DATASET2 and its synthetics, as seen in Fig. 5.5(b), also exhibits a very good match. The results show that the multifractal traffic model provides queuing behavior close to that of the measured traffic.

## 5.4   Conclusion

A new multifractal traffic model has been introduced in this paper. The modeling process is the pairwise product of a multiplicative cascade and an independent, identically distributed lognormal process. The obtained traffic model thus can capture the full characteristics of multifractality defined by its scaling function and the moment factor. The detailed statistical properties of the model are also discussed and it was found that they match the most important properties of the real WAN traffic like long-range dependence and lognormal marginal.

The traffic model is then applied to two real traffic traces which are found to have multiscaling structure. The real traces and their corresponding synthetic sets generated by the model are compared in a queuing performance test of an infinite-buffer single-server queuing system with constant service rate. The results show that the queue tail behaviors, simulated at different server utilization, are very close to each other. It can be concluded that the model provides a good alternative method for multifractal traffic modeling.

The model construction possesses the opportunities for further developments. One can choose other distributions for the multipliers and/or the random variable $Y$ which provide an even better fit for multifractal characteristic functions.

# Chapter 6

# Summary of the Dissertation

The mathematical background of the fractal traffic theory was first briefly overviewed in Chapter 1. The findings and results of the dissertation were presented in the next four chapters. In Chapter 2 the implications of non-stationary effects in long-range dependence tests were investigated by both analytical and simulation studies. In Chapter 3 the aim is to find how the correlation and scaling structure of the IP components influence the aggregated IP traffic. Chapter 4 contains the performance estimation for a simple queuing system with the general multifractal traffic input. In Chapter 5 a new model was introduced for multifractal network traffic.

## 6.1 Implications of non-stationarity in long-range dependence testing and estimation

In Chapter 2 both analytical and simulation investigations of the implications of non-stationarity on some most used long-range dependence tests were presented. Analytical studies were first shown for three cases:

- I have proven the relation between the variance of the aggregated data series and the original variance in the presence of the level shift, thus predicted the behavior of the variance-time plot in the cases of both long-range dependent and short-range dependent series with level shift presented.

- I have proven the connection between the variance of the aggregated data series and the original variance in the presence of linear trend. This results in the distortion of the variance-time plot in long-range dependence test and may provide misleading conclusion.

- I have also proven the behavior of the R/S analysis in testing data series containing level shift. It was shown that the test is still valid in the case of simple level shift.

Moreover the R/S plot may detect the level shift present in the data. More complicated level shifts could make the estimation of the Hurst parameter unreliable.

The analysis study was verified and completed by simulation examples. A fractional Brownian motion series and a data set generated by the Poisson process were chosen as the reference of long-range dependent and independent process. The level shift, linear trend, and parabolic trend were then added to these series. A series of ATM cell arrivals obtained from a real-time traffic measurements on the Swedish University NETwork was also analyzed to demonstrate the practical side of the problem.

- I have shown that in general the presence of non-stationarity results in unreliable detection of long-range dependence and poor estimation of the Hurst parameter by long-range dependence tests (variance-time plot, R/S analysis, periodogram plot). It is easy to confuse long-range dependence with non-stationary short-range dependent processes. I have suggested that long-range dependence testing should not be used without a preceding stationary analysis.

The estimation of the Hurst parameter is not an easy task since long-range dependence is an asymptotic property. Moreover, it is made more difficult by the appearance of non-stationarity which is often observed in the real data traffic. Unfortunately, these effects sometimes cannot be detected and/or removed from the data, particularly from bursty network traffic. The presented study is far from being complete but it may provide some reference points to avoid pitfalls in long-range dependence traffic modeling.

The results presented in Chapter 2 are published in [J3, C3].

## 6.2   Characterization of IP traffic components

In Chapter 3 the aim is to investigate the impact of the components in the overall IP traffic from the correlation and scaling point of view. I have carried out a detailed analysis on some selected IP traffic traces measured at the Department of Telecommunications and Telematics, Budapest University of Technology and Economics.

First the correlation study was performed. It is known that the aggregation of long-range dependent streams is also long-range dependent with the highest Hurst parameter.

- I have shown that in practice the correlation structure of the component with highest variance dominates the correlation structure of the aggregated stream.

This finding is verified in long-range dependence analysis of the IP traffic components at the transport layers and of the TCP components at the application layers. The autocorrelation function of the IP traffic inherits its form from the correlation structure of the TCP traffic as well as the TCP from the HTTP traffic although at the application layer the FTPdata traffic was found to have the highest Hurst parameter.

In scaling analysis I have found that the multifractal aggregation is composed of parts with very different scaling behavior (no scaling, monoscaling, multiscaling).

- I have shown that multifractal properties of network traffic can also be present at large time scales, not only at small times scales.

Some authors [18, 19, 22] argue that the scaling properties of the WAN traffic can be categorized into two regions: a large time scaling phenomenon with self-similarity and a small time scale phenomenon multifractal scaling. Possible physical explanations of scaling phenomena should be found to fit these statements. The presented findings show that the characteristics of the WAN traffic should be carefully analyzed and further studies are needed to understand the large scale multiscaling behavior of the traffic.

The results of Chapter 3 provide some contributions to a deeper understanding of network characteristics. The results were published in [C4, C5, J4].

## 6.3   Queuing performance of multifractal traffic

In Chapter 4 a mathematical formula was provided for the estimation of queue tail probabilities of an infinite capacity single server queue serviced at a constant rate and driven by a general multifractal input process. I have proven the approximation formula for the queue tail asymptotics and shown different applications of the formula. I have also proposed a practical methodology for queue tail estimation of real traffic cases.

Fractal traffic research is a new, alternative direction of network traffic modeling. There are few results concerning the queuing behavior of data traffic with scaling properties. Actually, there are only some results which are presented regarding the proposed concrete scaling model like fractional Brownian motion [42, 14] or the multifractal wavelet model [43].

- I have derived a general asymptotic approximation for the queue tail probabilities of a queuing system fed by an input traffic with scaling property. It involves the cases of self-similar, monofractal, and multifractal processes. I also shown that the so-called moment factor of multifractality is needed besides of the scaling function.

Since the formula is proven for the general scaling cases, it can be applied for self-similar traffic like fractional Brownian motion. However, there are needs of both the moment factor and the scaling function of this traffic.

- I have derived the multifractal characteristic functions for the fractional Brownian motion and shown that the approximation provides exactly the Weibullian queuing formula which had been proven using the Large Deviation Technique [14].

A very interesting question for network researchers is that how multifractal traffic impact differ from monofractal case. I have shown some highlights for this problem in a simulation study.

- I have shown that having the same moment factor, a process with multiscaling property can produce worse queuing behavior than that of the process with monoscaling property. Moreover, the queuing behavior of such a system is also very sensitive to changes of the moment factor.

One of the most useful feature of the queuing approximation is that it forms the ideal to construct a methodology for estimation of multifractal queuing systems. I have proposed a numerical calculation method for queue tail probabilities estimation of network traffic with scaling property. The method was found to be very effective in evaluation analysis of real measured traffic traces.

- I have proposed a methodology for queue tail estimation of a queuing system driven by multifractal traffic input knowing its characteristics functions. I also provided a modified method for estimation of these functions from the measured traffic trace.

The results of Chapter 4 are published in [J2, J1, C2].

## 6.4   A multifractal traffic model

In Chapter 5 the aim is to construct a simple multifractal of the traffic network. The model should be able to capture the complete characteristics of multifractals containing both the moment factor and the scaling function. It could be more useful and easy to manage if it has less parameters.

- I have proposed an new model for multifractal traffic based on the multiplicative cascades. The model is the combination of a multiplicative cascade with an independent lognormal process and it has only three parameters.

A full description of a model should contain its detailed statistical properties which show how it can fit the traffic to be modeled.

- I have extended the properties of the multiplicative cascade to the proposed model. I have shown that it has all the important properties observed in data traffic including long-range dependence, multifractality, and lognormality.

Once the model is chosen the obvious task is to set the parameters of the model to fit the traffic data. This operation is shown in simulation example of several measured traffic traces.

- I have proposed some practical guidelines for parameter setting of the model from the estimated characteristic functions of the traffic data.

In Chapter 5 there are also some ideals and opportunities for further developments of the model. The results in Chapter 5 are published in [J1, C1].

# Appendix A

# Appendices of Chapter 4

## A.1   Proof of Lemma 4.3.1

Denote by $X(t)$ the Gaussian process. Since $X(t)$ has scaling property it satisfies the general definition for multifractal process, i.e., $\mathbb{E}[|X(t)|^q] = c(q)t^{\tau(q)+1}$. Thus the variance of the $X(t)$ process should be $\sigma_t^2 = c(2)t^{\tau(2)+1}$. The Gaussian process $X(t) \sim N\left(0, c(2)t^{\tau(2)+1}\right)$ has the normal distribution and we have

$$f(x) = \frac{1}{\sqrt{2\pi c(2)t^{\tau(2)+1}}} \exp\left(-\frac{x^2}{2c(2)t^{\tau(2)+1}}\right).$$

The $q^{th}$ moment of $X(t)$ can be calculated by the definition:

$$
\begin{aligned}
\mathbf{E}[|X(t)|^q] &= \int_{-\infty}^{+\infty} |x|^q f(x)\mathrm{d}x \\
&= 2\int_0^{+\infty} x^q \frac{1}{\sqrt{2\pi c(2)t^{\tau(2)+1}}} \exp\left(-\frac{x^2}{2c(2)t^{\tau(2)+1}}\right)\mathrm{d}x.
\end{aligned}
$$

Introduce $y := \frac{x^2}{2c(2)t^{\tau(2)+1}}$. The formula above can be rewritten as follows:

$$
\begin{aligned}
\mathbf{E}[|X(t)|^q] &= \frac{2^{q/2}}{\sqrt{\pi}} \left[c(2)t^{\tau(2)+1}\right]^{q/2} \int_0^{+\infty} y^{\frac{q-1}{2}} \exp(-y)\mathrm{d}y \\
&= \frac{[2c(2)]^{q/2}}{\sqrt{\pi}} \Gamma\left(\frac{q+1}{2}\right) t^{\frac{q}{2}[\tau(2)+1]},
\end{aligned} \tag{A.1}
$$

which concludes our proof.  $\square$

## A.2 Proof of Proposition 4.3.2

The approximation in Proposition 2 states that

$$\frac{1}{\sqrt{\pi}}\frac{\Gamma\left[\Psi^{-1}(\log x)\right]}{x^{\Psi^{-1}(\log x)-1/2}} \approx \exp(-x), \qquad x \text{ large}$$

$$\Leftrightarrow \quad \log\Gamma\left[\Psi^{-1}(\log x)\right] \approx \left[\Psi^{-1}(\log x)-1/2\right]\log x - x + \log\sqrt{\pi}, \qquad (A.2)$$

By the *Stirling*'s formula we have

$$\log\Gamma(z+1) - (z+1/2)\log z + z \approx \log\sqrt{2\pi} \qquad \text{as } z \to \infty. \qquad (A.3)$$

Put $z + 1 = \Psi^{-1}(\log x)$, hence $x = \exp\Psi(z+1) \to \infty$ as $z \to \infty$ by the monotonicity of $\Psi(\cdot)$. We obtain

$$\log\Gamma\left[\Psi^{-1}(\log x)\right] - \left[\Psi^{-1}(\log x)-1/2\right]\log\left[\Psi^{-1}(\log x)-1\right] + \left[\Psi^{-1}(\log x)-1\right] \approx$$
$$\approx \log\sqrt{2\pi} \qquad \text{as } x \to \infty. \quad (A.4)$$

In [11] it is derived that

$$\lim_{z\to\infty}\frac{\Psi(z+1)}{\log z} = 1, \qquad (A.5)$$

hence $x = \Psi^{-1}\left[\omega(x)\log x\right]-1$ where $\lim_{x\to\infty}\omega(x) = 1$. Using the approximation $\Psi^{-1}(\log x)-1 \approx x$ for large $x$, we get the equation

$$\log\Gamma\left[\Psi^{-1}(\log x)\right] - \left[\Psi^{-1}(\log x)-1/2\right]\log x + x \approx \log\sqrt{2\pi}, \qquad (A.6)$$

which is a good approximation as numerical computations also demonstrate.

Then the approximation in Eq. A.2 follows if we change the constant $\log\sqrt{2\pi}$ by $\log\sqrt{\pi}$.

$\square$

# Bibliography

[1] *The internet traffic archive*, http://ita.ee.lbl.gov.

[2] P. Abry, P. Flandrin, M. S. Taqqu, and D. Veitch, *Wavelets for the analysis, estimation and synthesis of scaling data*, Self-Similar Network Traffic Analysis and Performance Evaluation (K. Park and W. Willinger, eds.), 1999.

[3] P. Abry and D. Veitch, *Wavelet analysis of long range dependent traffic*, IEEE Trans. Inform. Theory **44** (1998), no. 1, 2–15.

[4] J. Beran, *Statistics for long-memory processes*, Chapman & Hall, One Penn Plaza, New York, NY 10119, 1995.

[5] V. Bolotin, J. Coombs-Reyes, D. Heyman, Y. Levy, and D. Liu, *IP traffic characterization for planning and control*, Proc. ITC 16 (P. Key and D. Smith, eds.), Elsevier Science B. V., 1999, pp. 425–436.

[6] F. Brichet, J. Roberts, A. Simonian, and D. Veitch, *Heavy traffic analysis of a storage model with long range dependent on/off sources*, Queueing Systems **23** (1996), 197–215.

[7] P. J. Brockwell and R. A. Davis, *Time series: Theory and methods*, Springer, 1996.

[8] L. Calvet, A. Fisher, and B. B. Mandelbrot, *Large deviations and the distribution of price changes*, Yale University, 1997, Working Paper.

[9] D. R. Cox and P. A. W. Lewis, *The statistical analysis of series of events*, Menthuen, 1966.

[10] N. Desaulniers-Soucy and A. Iuoras, *Traffic modeling with universal multifractals*, Proc., GLOBECOM '99, 1999.

[11] L. Devroye, *Random variate generation for the digamma and trigamma distributions*, J. of Statistical Computation and Simulation **43** (1992), 197–216.

[12] N. G. Duffield, J. T. Lewis, N. O'Connell, R. Russel, and F. Toomey, *Statistical issues raised by the Bellcore data*, 11th Teletraffic Symposium (Cambridge), 23-25 March 1994.

[13] N. G. Duffield, W. A. Massey, and W. Whitt, *A nonstationary offered-load model for packet networks*, Sel. Proc. of the 4th INFORMS Telecomm. Conf., 1999.

[14] N. G. Duffield and N. O'Connell, *Large deviations and overflow probabilities for the general single-server queue, with applications*, Proc., Cam. Phil. Soc., vol. 118, 1994, pp. 363–374.

[15] R. Ellis, *Large deviations for a general class of random vectors*, Ann. Prob. **12** (1984), 1–12.

[16] T. Éltető and S. Molnár, *On the distribution of round-trip delays in TCP/IP networks*, The 24th Annual Conference on Local Computer Networks (LCN'99) (Lowell, Boston, MA), October 1999.

[17] A. Erramilli, P. Pruthi, and W. Willinger, *Self-similarity in high speed network traffic measurements: Fact or artifact?*, Proc. of the 12th Nordic Teletraffic Seminar, NTS12 (Espoo, Finland), 22-24 Augustus 1995.

[18] A. Feldmann, A. C. Gilbert, and W. Willinger, *Data networks as cascades: Investigating the multifractal nature of Internet WAN traffic*, ACM Computer Communication Review **28** (1998), 42–55.

[19] A. Feldmann, A. C. Gilbert, W. Willinger, and T. G. Kurtz, *The changing nature of network traffic: Scaling phenomena*, ACM Computer Communication Review **28** (1998), 5–29.

[20] A. Fisher, L. Calvet, and B. B. Mandelbrot, *Multifractality of Deutschmark/US Dollar exchanges rates*, Yale University, 1997, Working Paper.

[21] J. Gao and I. Rubin, *Multiplicative multifractal modelling of long-range dependent network traffic*, International Journal of Telecommucication Systems **14** (2001), 783–801.

[22] A. C. Gilbert, W. Willinger, and A. Feldmann, *Scaling analysis of conservative cascades, with applications to network traffic*, IEEE Trans. Inform. Theory **45** (1999), no. 3, 971–991.

[23] S. Giordano, N. O'Connell, M. Pagano, and G. Procissi, *A variational approach to the queueing analysis with fractional brownian motion input traffic*, 7th IFIP Workshop on Performance Modelling and Evaluation of ATM Networks (Antwerp, Belgium), June 1999.

[24] M. Grasse, M. R. Frater, and J. F. Arnold, *Implications of non-stationarity of MPEG2 video traffic*, Tech. report, COST 257 TD(97)01, January 1997.

[25] H. E. Hurst, *Long-term storage capacity of reservoirs*, Proc. Amer. Soc. Civil Eng. **76(11)** (1950).

[26] J. Hüsler and V. Piterbarg, *Extremes of a certain class of Gaussian processes*, Stochastic Process. Appl. **83** (1999), 257–271.

[27] J. Jormakka, *On self-similar models for ATM traffic*, ITC Specialist seminar on Control in Communications, 1996, pp. 277–288.

[28] V. Klemes, *The hurst phenomenon: A puzzle?*, Water Resources Research 10 (1974), 675–688.

[29] H. Kunsch, *Discrimination between monotonic trends and long-range dependence*, J. Appl. Prob. **23** (1986), 1025–1030.

[30] J. W. Lamperti, *Semi-stable stochastic processes*, Trans. Am. Math. Soc. **104** (1962), 62–78.

[31] W. E. Leland, M. S. Taqqu, W. Willinger, and D. V. Wilson, *On the self-similar nature of Ethernet traffic (extended version)*, IEEE/ACM Transactions on Networking **2** (1993), no. 1, 1–15.

[32] J. Lévi-Véhel and R. Riedi, *Fractional Brownian motion and data traffic modeling: The other end of the spectrum*, Fractals in Engineering (J. Lévi-Véhel, E. Lutton, and C. Tricot, eds.), Springer, 1997, pp. 185–202.

[33] ———, *Fractional brownian motion and data traffic modeling: The other end of the spectrum*, Fractals in Engineering (Berlin) (J. Lévi-Véhel, E. Lutton, and C. Tricot, eds.), Springer-Verlag, 1997, pp. 185–202.

[34] J. Lévy-Véhel and B. Sikdar, *A multiplicative multifractal model for TCP traffic*, Proc., IEEE ISCC (Hammamet, Tunisia), July 2001, pp. 714–719.

[35] Z. Lui, P. Nain, D. Towsley, and Z. L. Zhang, *Asymptotic behavior of a multiplexer fed by a long-range dependent process*, J. Appl. Prob. **36** (1999), 105–118.

[36] B. B. Mandelbrot and J. W. Van Ness, *Fractional brownian motions, fractional noises and applications*, SIAM Rev. **10** (1968), 422–437.

[37] P. Mannersalo and I. Norros, *Multifractal analysis of real ATM traffic: A first look*, Tech. report, VTT Information Technology, January 1997, COST257TD(97)19.

[38] M. B. Marcus and L. A. Shepp, *Sample behaviour of Gaussian processes*, Proc., Sixth Berkeley Symp. Math. Statist. Prob. (Berkeley), vol. 2, Univ. of Calif. Press, 1972, pp. 423–442.

[39] S. Molnár and I. Maricza eds., *Source characterization in broadband networks*, Interim report, COST 257, Vilamoura, Portugal, January 1999.

[40] S. Molnár and A. Gefferth, *On the scaling and burst structure of data traffic*, 8th Int. Conference on Telecommunication Systems, Modelling and Analysis (Nashville, Tennessee), 9-12 March 2000.

[41] S. Molnár, A. Vidács, and A. A. Nilsson, *Bottlenecks on the way towards fractal characterization of network traffic: Estimation and interpretation of the Hurst parameter*, Int. Conf. of the Performance and Management of Complex Communication Networks, November 1997.

[42] I. Norros, *A storage model with self-similar input*, Queueing Systems **16** (1994), 387–396.

[43] V. J. Ribeiro, R. H. Riedi, M. S. Crouse, and R. G. Baraniuk, *Multiscale queuing analysis of long-range dependent network traffic*, Proc., IEEE INFOCOM 2000 (Tel Aviv, Israel), March 2000, pp. 1026–1035.

[44] R. H. Riedi, *Multifractal processes*, Theory and Applications of Long Range Dependence (P. Doukhan, G. Oppenheim, and M. S. Taqqu, eds.), Birkhäuser, Boston, 2002.

[45] R. H. Riedi, M. S. Crouse, V. J. Ribeiro, and R. G. Baraniuk, *A multifractal wavelet model with application to network traffic*, IEEE Trans. Inform. Theory **45** (1999), no. 3, 992–1018.

[46] R. H. Riedi and J. Lévy-Véhel, *Multifractal properties of TCP traffic: a numerical study*, INRIA research report 3129, Rice University, February 1997.

[47] R. H. Riedi and W. Willinger, *Toward an improved understanding of network traffic dynamics*, Self-Similar Network Traffic and Performance Evaluation (K. Park and W. Willinger, eds.), Wiley, June 1999.

[48] M. Roughan and D. Veitch, *Measuring long-range dependence under changing traffic conditions*, Proc., INFOCOM '99 (New York, NY), April 1999, pp. 1513–1521.

[49] H. Saito, T. Tsuchia, Gy. Marosi, Gy. Horváth, P. Tatai, and S. Asano, *Real-time simulation with traffic monitoring tool*, ICCCN99 (Natick, Boston, MA), October 11-13, 1999.

[50] G. Samorodnitsky and M. S. Taqqu, *Stable non-Gaussian processes: Stochastic models with infinite variance*, Chapman & Hall, New York, One Penn Plaza, New York, NY 10119, 1994.

[51] M. S. Taqqu, V. Teverovsky, and W. Willinger, *Is network traffic self-similar or multifractal?*, Fractals **5** (1997), 63–73.

[52] V. Teverovski and M. S. Taqqu, *Testing for long-range dependence in the presence of shifting means or a slowly declining trends, using variance type estimator*, J. of Time Series analysis **18** (1997), no. 3, 279–304.

[53] B. Tsybakov and N. D. Georganas, *On self-similar traffic in ATM queue: Definitions, overflow probability bound, and cell delay distribution*, IEEE/ACM Trans. on Networking **5** (1997), no. 3, 397–409.

[54] S. Vaton and E. Moulines, *A locally stationary semi-markovian representation for ethernet LAN traffic data*, IFIP TC6/WG6.2 4th Int. Conference on Broadband Communications (Stuttgart, Germany), April 1-3 1998.

[55] S. Vaton, E. Moulines, H. Korezlioglu, and D. Kofman, *Statistical identification of LAN traffic data*, ATM97, 5th IFIP Workshop on Performance Modelling and Evaluation of ATM Networks (Ilkley, UK), July 21-23 1997.

[56] E. Waymire and S. Williams, *Multiplicative cascades: Dimension spectra and dependence*, Jour. Fourier Anal. and Appl. (1995), 589–609.

[57] W. Willinger, M. S. Taqqu, and A. Erramilli, *A bibliographical guide to self-similar traffic and performance modeling for modern high-speed networks*, Stochastic Networks: Theory and Applications (Oxford) (F. P. Kelly, S. Zachary, and I. Ziedins, eds.), Royal Statistical Society Lecture Notes Series, vol. 4, Oxford University Press, 1996, pp. 339–366.

# Publications

**Journal papers**

[J1] **T. D. Dang**, S. Molnár, I. Maricza. A Framework for Multifractal Performance Analysis. Submitted to *European Transactions on Telecommunications*, 2002.

[J2] **T. D. Dang**, S. Molnár, I. Maricza. Queueing Performance Estimation for General Multifractal Traffic. *Int. Journal of Communication Systems*, Vol. 16, No. 2, pp. 117–136, 2003.

[J3] **T. D. Dang**, S. Molnár. On the Effects of Non-Stationarity in Long-Range Dependence Tests. *Periodica Polytechnica, Electrical Engineering*, Vol. 43, No. 4, pp. 227–250, 1999.

[J4] **T. D. Dang**, S. Molnár, and A. Vidács. Investigation of Fractal Properties in Data Traffic. *Journal on Communications*, XLIX:12–18, November-December 1998.

**Conference papers**

[C1] **T. D. Dang**, S. Molnár, I. Maricza. Some Results on Multiscale Queueing Analysis. *10th International Conference on Telecommunications ICT'2003*, Tahiti, Papeete, French Polynesia, February 2003.

[C2] **T. D. Dang**, S. Molnár, I. Maricza. Capturing the Complete Multifractal Characteristics of Network Traffic. In *Proc., GLOBECOM 2002*, Taipei, Taiwan, November 2002.

[C3] S. Molnár, **T. D. Dang**, I. Maricza. On the Queue Tail Asymptotics for General Multifractal Traffic. In *Proc., IFIP Networking 2002*, pp. 105–116, Pisa, Italy, May 2002.

[C4] S. Molnár, **T. D. Dang**. Pitfalls in Long-Range Dependence Testing and Estimation. In *Proc., GLOBECOM 2000*, San Francisco, CA, November 2000.

[C5] S. Molnár, **T. D. Dang**. Scaling Analysis of IP Traffic Components. In *Proc., ITC Specialist Seminar on IP Traffic Measurement, Modeling and Management*, Monterey, CA, September 2000.

[C6] S. Molnár, **T. D. Dang**, and A. Vidács. Heavy-tailedness, Long-Range Dependence and Self-similarity in Data Traffic. In *Proc., 7th Int. Conf. on Telecommunication Systems, Modeling and Analysis*, pp. 10–21, Nashville, Tennessee, March 1999.

[C7] **T. D. Dang**. On the Analysis of Long-Range Dependence and Self-similarity. *Student Scientific Conference*, Budapest Univ. of Technology and Economics, Budapest, Hungary, November 1999.